Effects of transformations of Ag and CuO nanoparticles on their fate in freshwater wetland sediments and plants

Submitted in partial fulfillment of the requirements for

the degree of

Doctor of Philosophy

in

Civil and Environmental Engineering

John Peter Stegemeier

B.S., Chemistry, Chapman University

M.S., Civil Engineering, Carnegie Mellon University

Carnegie Mellon University

Pittsburgh, PA

September, 2016

Acknowledgements

The research presented in this dissertation and my progress through the Ph.D. program at Carnegie Mellon University would not have been possible without the support of many professors, colleagues, friends and family. I am extremely grateful for all the time, energy and motivation they have provided to develop my research skills and encourage me throughout the process.

Primarily, I would like to thank my advisor, Greg Lowry, for his endless encouragement and motivation even in the most challenging times. His ability to always have a positive outlook on my research, ask the most important and relevant questions and provide his students with incredible opportunities has inspired me to become a better scientist. I am truly grateful for all the time he spent prioritizing the needs of his students among all his work and travel. His perfect balance between always being available to offer advice and allowing his students freedom to pursue their own direction in projects is more than I could have asked for in an advisor.

I would like to thank my co-advisor, Jeanne VanBriesen, for her interest in my research and her ability to ask the most challenging questions which required me to put my research into greater context and summarize why people should care about my research. I am grateful for her willingness to provide support for and improve my research. I would also like to thank my committee members, Dave Dzombak and Elizabeth Casman, for their interest in my research as well as the time and effort they have provided to improve the quality of my work. Dave has provided important advice on my research, particularly insights into the water chemistry aspects

of my project. Elizabeth has provided essential insight into how my research may impact the public policy governing the regulation of nanomaterials.

I would not be where I am today without my undergraduate advisor, Christopher Kim, for providing me with invaluable opportunities to explore synchrotron science. Conducting research in the Environmental Geochemistry laboratory at Chapman University was my first exposure to scientific research and it has sparked a true passion for research. The dedication Chris provides to his students and the opportunities he gives undergraduate researchers is truly remarkable.

Many collaborators and colleagues have provided helpful feedback, advice and encouragement throughout my journey at CMU. My colleagues from Duke University, Ben Colman and Fabienne Schwab, provided valuable planning, experimental and writing assistance as well as shedding much needed light onto the physiologic and ecological aspects of this work. Although they both have moved onto other positions, their help and support will not be forgotten. My fellow lab-mates, Joe Moore and Eleanor Spielman-Sun, provided much needed support and encouragement during my many trips to the Duke Mesocosms and Synchrotrons, respectively. I want to thank my colleagues in France, Clement Levard and Nathan Bossa, for their friendship and support during my stay in Aix-en-Provence.

I thank many researchers for providing advice, laboratory assistance and planning. I thank Ron Ripper for his laboratory support needed to get anything done. All the members of the CEINT meetings, the journal club and all the researchers in 207C, you all provided me with advice, criticism and friendship.

Outside of CMU, I am eternally grateful to my parents, David and Susan, for their love, support and instilling me with a love of learning; my grandparents, Richard and Marjorie, for

providing support, encouragement and inspiration to achieve greatness; and my brothers, Paul and David, for being supporting and lending an ear when needed. Finally, I thank my loving wife, Krystin, for providing the much needed motivation, our daughter Marie, to finish this thesis and move on to the next phase of my life.

Funding for this work was provided by the US National Science Foundation (NSF) and the Environmental Protection Agency (EPA) under NSF Cooperative Agreement EF 0830093, Center for the Environmental Implications of NanoTechnology (CEINT) and TINE, and from the NSF Nanotechnology Environmental Effects and Policy Integrated Graduate Education and Research Traineeship (NEEP-IGERT) (DGE-0966227). Portions of this research were carried out at the Stanford Synchrotron Radiation Lightsource (SSRL) and University of Chicago's Advanced Photon Source (APS). Both are national user facilities of the Department of Energy, Office of Basic Energy Sciences and I would like to thank all the beamline scientists for all support. Clément Levard contributed to the planning of these experiments, and Michael F. Hochella Jr. is acknowledged for instrument sharing and helpful discussion about TEM-EDS.

Abstract

Engineered nanomaterials (ENMs) are increasing becoming incorporated into consumer products to imbue remarkable physical and chemical properties. The increased use of these ENMs leads to a growing need to understand the environmental fate of ENMs after release. Many ENMs, including Ag and Cu ENMs, have the potential to undergo complex physical and chemical transformations which impact their toxicity, solubility and fate in the environment. There is a lack of research characterizing the transformation rate and understanding how these transformations affect interactions with organisms and the ultimate environmental fate.

The first objective of this thesis was to understand how transformations of Ag ENMs affect the uptake, distribution and speciation of these materials in plants. Terrestrial (alfalfa, *Medicago sativa*) and an aquatic (duckweed, *Landoltia punctate*) plant species were exposed hydroponically to as manufactured ("pristine") Ag^0-NPs and more environmentally relevant ("transformed") Ag_2S NPs. The uptake, spatial distribution and speciation of Ag were analyzed using synchrotron based X-ray Absorption Spectroscopy (XAS) techniques to provide mechanistic insights into the uptake of these ENMs. The reduced solubility and reactivity of Ag_2S ENMs was expected to prevent plants from solubilizing these particles and only allow for direct uptake of particles. For the more soluble Ag species, the absorption of Ag^+ ions was expected to be primarily the mechanism of Ag uptake. Although the total Ag associated with the plants was similar, the Ag distribution in the roots was dramatically different. The transformed ENMs (Ag_2S) appeared to be taken into the plant tissue as sulfidized ENMs. The pristine Ag^0 ENMs were found to partially dissolve and incorporate into the plant tissue as both dissolved Ag and Ag^0-NPs. The fact that ENMs readily attach onto plant tissue regardless of speciation and

solubility suggests that exposure to ENMs may be controlled by factors affecting attachment to root surfaces. However, internalization of Ag appears to be affected by solubility.

The second objective was to characterize the impact of transformations of Ag and Cu-based ENMs on the distribution, speciation and fate of these materials in subaquatic sediments and the aquatic plant, *E. Densa* in a simulated emergent freshwater wetland using large-scale mesocosms. The exposure of pristine (Ag^0 and CuO) ENMs and their transformed analogues (Ag_2S and CuS) was compared to an ionic control ($Cu(NO_3)_2$) to determine if nanoparticulate species of metals were distributed differently than their dissolved counterparts. The metal speciation was determined using XAS to elucidate relative timescales of transformations. The pristine ENMs were expected to rapidly transform into their more stable sulfidized species and the uptake of Ag and Cu were expected to depend on the solubility of the ENMs. Transformations of the pristine ENMs were found to be rapid (weeks) in the surficial sediment, but slower (months) in the aquatic plant tissue. The uptake of ENMs coupled with the slow transformation in the aquatic plant tissue suggests ENMs persist longer than the timescales measured in sediments. This knowledge enables better risk forecasting for ENMs exposed to aquatic organisms and informs toxicity testing to ensure correct forms of ENMs are examined.

This thesis provided several novel contributions to the understanding of how transformations of ENMs affect their interactions with plants and their fate in real complex environments. Mechanistic insights into the attachment and uptake of ENMs into plant tissues were identified suggesting two predominant uptake pathways. Relative timescales of ENM transformations in freshwater wetland sediments and plant tissue provided suggests plants can slow transformations and allow labile ENMs to persist longer than assumed.

This work is dedicated to my grandparents,

Richard and Marjorie Stegemeier,

for providing the support and inspiration to pursue

a doctoral degree in engineering

Table of Contents

List of Tables

List of Figures

Chapter 1

Introduction

Engineered nanomaterials (ENMs) are materials manufactured to have at least one dimension on the nanoscale (less than 0.1μm). Their small size can imbue products with novel properties compared to their larger sized counterparts having the same chemical composition. As such, they are increasingly being incorporated into consumer products to enhanced product performance.[1] Silver-based ENMs are currently being utilized in a vast array of products (lotions, textiles, plastics) primarily for their antimicrobial properties.[2-4] Their inevitable release into waste water streams results in these materials becoming an emerging class of environmental pollutant.[5,6] ENMs incorporated into both industrial and consumer products can be released into the environment through many routes including waste water treatment plant (WWTP) effluents being discharged directly into freshwater ecosystems,[7-9] application of nano-contaminated WWTP biosolids onto agricultural crops or direct input of ENMs through the application of nano-enabled pesticides, fungicides and bactericides on crops.[10-16] Copper-based ENM (Certis™ Kocide 3000) are currently being applied directly onto agricultural crops for anti-microbial and anti-fungal benefits. Runoff from these agricultural fields contaminated with ENM are projected to contaminate fresh water wetlands.[17] If enough copper accumulates in freshwater wetlands, it may become toxic to aquatic organisms including fish and plants.[18-20] It is also unclear if the nanoparticulate forms of these metals will behave differently than soluble forms of the metals, leading to unanticipated environmental effects.

Engineered nanomaterials undergo a number of complex processes in the environment including physical (aggregation, attachment, adsorption and transport) and chemical (dissolution, sulfidation and speciation changes) transformations, and interactions with organisms (cellular attachment, uptake and trophic transfer).[21-26] Better understanding of these processes, and how these transformations affect the interactions between ENMs and the ecosystem is needed to accurately predict the ultimate fate and effects of ENMs in the environment.

Interactions between ENMs and plants, especially aquatic macrophytes, are particularly important because of their critical role in terrestrial and aquatic ecosystem health and function. They are energy producers, food sources and provide shelter and dissolved oxygen for many other organisms. Terrestrial plants are exposed to biosolids and nano-fertilizers when they are applied to agricultural crops, and aquatic plants are exposed through the runoff of agricultural fields into freshwater ecosystems. ENMs can enter plant tissues and are reported to exhibit a variety of different ecological responses such as reduced biomass, inhibition of growth rate, decreased leaf cover and inhibition of root nodulation.[11,27,28] Additionally, these plant-ENM interactions are important because there is a significant potential for trophic transfer and bioaccumulation, which will contaminate the human food web in the case of terrestrial plants and ecological food webs with contaminated aquatic plants.

The majority of current research focuses primarily on the interactions between as-manufactured or "pristine" ENM with plants and on their behavior in ecosystems, although ENMs are known to readily transform in the environment.[21,29] Many of the exposure routes

discussed above will induce transformations in ENMs before these materials enter the environment and interact with plants.[30] These transformations can affect the physical and chemical properties of the ENMs relevant to exposure and effects, e.g. solubility and aggregation state, but it is still unclear on what timescale these transformations take place and the magnitude of their effect on the physiological interactions and the potential to upset the ecosystem.[31] Sulfidation of soft metal cationic metals are known to be an important and potentially rapid transformation leading to the production of stable metal sulfides.[32] Metal sulfides are generally less soluble and less reactive than their metal or metal oxide counterparts suggesting they will behave differently in the environment.[33] Although many recent studies have investigated the interactions between plants and pristine ENM, there remain significant knowledge gaps concerning the rate of transformations and the effects certain transformations, like sulfidation, will have on the interactions of ENM with plants.

This thesis evaluates a number of hypotheses and the following chapters provide evidence to determine their validity.

- Due to many physical barriers in plant tissues, metal ions will more readily associate with and become incorporated into plant tissue than either pristine or transformed ENMs.

- Because metal sulfide analogs of metal ENMs generally have lower solubility and reactivity, they will less readily associate with and incorporate into plant tissue than their pristine metal and metal oxide counterparts.

- The metal distribution in plant roots will be affected by the sulfidation of ENMs. The decreased solubility of the transformed ENMs will result in reduced nanoparticle dissolution and less uniform metal distribution.

- Metal sulfide ENMs, being less soluble and less reactive than their pristine counterparts, will resist solubilization and persist as metal sulfide in the plant tissue.

- Timescales of transformation (e.g. sulfidation) for metallic silver and copper oxide will be relatively rapid (weeks to months) while the metal sulfides are expected to persist as metal sulfides.

Research Objectives and Motivation

The ultimate goal of this research was to determine how transformed ENMs, mainly less soluble sulfidized analogues of pristine metal and metal oxide ENMs, interact with plants and distribute in a freshwater wetland environment. This requires exposing ENMs and their transformed products to plants (hydroponically) and simulated freshwater wetlands, and identifying the key differences in plant uptake, metal distribution, speciation and fate. The specific objectives of this research were to:

1. Quantify the differences in metal uptake between Ag^0 and Ag_2S NPs into plant tissue, compare this uptake to an ionic control ($AgNO_3$) and determine any effects of the initial characteristics of the ENMs on the overall uptake and distribution in the plants.

Silver ENMs have been shown to associate with plant tissues in laboratory and mesocosm studies. Metallic silver ENMs can undergo oxidative dissolution and release Ag+ ions when in the presence of dissolved oxygen. Silver ions are expected to be more available to plant root tissues than ENMs due to size restrictions of the root pores. Since the Ag_2S NPs are much less soluble than the Ag^0 NPs, the Ag_2S NPs are expected to only be able to attach onto the root surface and be absorbed directly as NPs while the Ag^0 NPs can attached and dissolve into ions which are taken up more readily internalized than the NPs.

2. Investigate the spatial distribution of silver in plant roots exposed to Ag^0 and Ag_2S NPs, compare this distribution to the ionic ($AgNO_3$) treatment and provide mechanistic insights into the binding and uptake of ENM to terrestrial and aquatic plants.

The physical barriers at the root surface, such as mucilage and the pores in cell walls, can facilitate NP attachment and prevent internalization into the root's vasculature system. Ionic silver easily enters the vasculature system of plant roots and distributes relatively uniformly throughout the root tissue. The less soluble ENMs are expected to attach onto the root surface and display a significantly different distribution pattern (less uniform with discrete clusters) than the ionic or more soluble metal ENMs. The more soluble ENMs (Ag^0) will likely show a combination of the Ag_2S and the ionic Ag distributions, displaying both discrete clusters and uniform distribution. The Ag distributions can provide mechanistic insights into the uptake of

ENMs into plants indicating whether adsorption followed by direct NP uptake or dissolution followed by ionic uptake are the predominant mechanism of silver uptake into plants.

3. Determine the relative timescales of change in the speciation of metals in the surficial sediment layer of realistic mesocosm exposed to Ag^0, Ag_2S, CuO and CuS ENMs and determine the impact of the initial form of metal ENM had on these timescales and overall metal speciation in this layer.

Transformations in sediments are important parameters in environmental fate models used to forecast risk of ENM exposed to the environment. The transformation of Ag^0 and CuO into their corresponding metal sulfides is expected to be the major transformation in the surficial sediments due to the likely presence of reduced sulfur. The metal sulfide ENMs are expected to be significantly less labile and either not transform or have a very slow rate of transformation. Obtaining an accurate and realistic timescale of transformations in the sediment and in plant tissues are essential to inform these models.

4. Identify timescales of changes in the speciation of metals in plant tissue after being exposed to Ag^0, Ag_2S, CuO and CuS ENMs, and determine the effect of initial metal speciation on the transformation in plant tissues.

Plant defense mechanisms transform metals mainly through complexation with proteins and amino acids. Metal complexation with glutathione and other sulfur containing physiologic molecules are expected to play a major role in the fate of metals internalized by plants. Metal

sulfides may be so stable and inert that the plant responses cannot alter the sulfidized ENMs leading to very little change in the speciation. The stability and low solubility of metal sulfides are expected to remain as metal sulfides or employ a very slow transformation rate compared to the more labile pristine counterparts.

Approach

In order to characterize the differences between the interactions of pristine and transformed ENM in terrestrial plants likely to be exposed to ENMs, alfalfa were grown and exposed hydroponically to silver, silver sulfide and ionic silver (as silver nitrate). Total silver metal concentrations were investigated in the roots and shoots of the plants to determine the extent of translocation of silver from the roots to the above ground tissues. The roots were also investigated using X-ray fluorescence (XRF) spectroscopy to spatially map the silver distribution in the roots after exposure. Roots were thin-sectioned, fixed, and investigated using transmission electron microscopy (TEM) to determine the presence of nanomaterials in the root cells as well as any physiological differences.

In order to characterize the interactions between aquatic plants and ENMs (both pristine and transformed), a common plant found in freshwater ecosystems, duckweed plants, were hydroponically exposed to silver, silver sulfide and ionic silver (as silver nitrate). Total silver metal concentrations were measured in the dried plant tissue to determine differences in the uptake of silver between treatments. The roots were mapped using XRF spectroscopy to determine the spatial distribution of silver in the roots. Finally, dried plant tissue was

investigated using X-ray absorption spectroscopy (XAS) to determine the speciation of silver associated with the plants and identify any changes induced by the plants.

Once the uptake mechanism was observed in well-controlled laboratory systems more realistic exposures were examined. In order to identify the key differences between pristine and transformed ENMs and their interactions in realistic freshwater ecosystems, five large scale mesocosms were dosed with Ag, Ag_2S, CuO or CuS NPs to assess if initial speciation of metal NP entering the wetland affects their fate and behaviors. Total silver and copper metal concentrations were determined in an aquatic plant (*Egeria densa*) and the surficial sediment layer to determine the relative amount of metal associated with each compartment. The speciation was investigated using XAS techniques at multiple time points to determine a relative timescale of transformation in each compartment and compare between treatments.

Dissertation Overview

This dissertation consists of five chapters and an appendix. The experimental work, which has either been published or submitted to the peer review journal *Environmental Science and Technology* is presented in chapters two, three and four.

Chapter 1 introduces the research, provides a brief background and context of the research, outlines the major objectives and general approaches to achieve these objectives and provides a summary of the additional chapters.

Chapter 2 presents research conducted on the hydroponic uptake of metallic silver and silver sulfide nanomaterials into the terrestrial plant alfalfa (*Medicago sativa*). The spatial distribution of silver is investigated and insights into the mechanism of metal uptake are provided. Direct evidence of cellular uptake of nanoparticles along with microscale physiologic responses of the plants is observed.

Chapter 3 presents research concerning the uptake and distribution of metallic silver and silver sulfide ENMs into a common aquatic plant, duckweed (*Landoltia punctata*). The silver distribution in the roots is compared with dissolved silver and differences in the silver distribution are shown as a function of solubility. The silver speciation and distribution in the plant tissue is shown to be affected by the species of ENM dosed suggesting direct uptake, dissolution and transformations are taking place.

Chapter 4 presents research exposing copper oxide, copper sulfide, metallic silver and silver sulfide nanomaterials to realistic simulated freshwater mesocosms containing an aquatic plant, *Egeria densa*. The silver and copper speciation was investigated in both the plant tissue and the surficial sediment layer and compared between treatments. Relative timescales of transformations for each treatment were identified and differences between the speciation of metal in sediment and plant tissues are discussed.

Chapter 5 provides the conclusions of the research and discusses the implications of this research on the overall scientific field. This chapter also discusses significant knowledge gaps which still remaining and suggests potential directions of future research.

The appendices provide additional experimental data published in the supporting information of chapters 2, 3 and 4.

References

1. Vance, M. E.; Kuiken, T.; Vejerano, E. P.; McGinnis, S. P.; Hochella, M. F., Jr.; Rejeski, D.; Hull, M. S., Nanotechnology in the real world: Redeveloping the nanomaterial consumer products inventory. *Beilstein Journal of Nanotechnology* **2015,** *6*, 1769-1780.

2. Impellitteri, C. A.; Tolaymat, T. M.; Scheckel, K. G., The speciation of silver nanoparticles in antimicrobial fabric before and after exposure to a hypochlorite/detergent solution. *J. Environ. Qual.* **2009,** *38*, (4), 1528-1530.

3. Sondi, I.; Salopek-Sondi, B., Silver nanoparticles as antimicrobial agent: a case study on E-coli as a model for Gram-negative bacteria. *J. Colloid Interf. Sci.* **2004,** *275*, (1), 177-182.

4. Marambio-Jones, C.; Hoek, E. M. V., A review of the antibacterial effects of silver nanomaterials and potential implications for human health and the environment. *J. Nanopart. Res.* **2010,** *12*, (5), 1531-1551.

5. Luoma, S. N. *Silver nanotechnologies and the environment: old problems or new challenges?*; Woodrow Wilson International Center for Scholars: Washington, DC, 2008.

6. Yu, S.-j.; Yin, Y.-g.; Liu, J.-f., Silver nanoparticles in the environment. *Environmental Science: Processes & Impacts* **2013,** *15*, (1), 78-92.

7. Adams, N. W. H.; Kramer, J. R., Silver speciation in wastewater effluent, surface waters, and pore waters. *Environ. Toxicol. Chem.* **1999,** *18*, (12), 2667-2673.

8. Hendren, C. O.; Badireddy, A. R.; Casman, E.; Wiesner, M. R., Modeling nanomaterial fate in wastewater treatment: Monte Carlo simulation of silver nanoparticles (nano-Ag). *Sci. Total Environ.* **2013,** *449*, 418-425.

9. Brar, S. K.; Verma, M.; Tyagi, R. D.; Surampalli, R. Y., Engineered nanoparticles in wastewater and wastewater sludge – Evidence and impacts. *Waste Management* **2010,** *30*, (3), 504-520.

10. Ma, R.; Levard, C.; Judy, J. D.; Unrine, J. M.; Durenkamp, M.; Martin, B.; Jefferson, B.; Lowry, G. V., Fate of Zinc Oxide and Silver Nanoparticles in a Pilot Wastewater Treatment Plant and in Processed Biosolids. *Environ. Sci. Technol.* **2013,** *48*, (1), 104-112.

11. Judy, J. D.; McNear, D. H.; Chen, C.; Lewis, R. W.; Tsyusko, O. V.; Bertsch, P. M.; Rao, W.; Stegemeier, J.; Lowry, G. V.; McGrath, S. P.; Durenkamp, M.; Unrine, J. M., Nanomaterials in Biosolids Inhibit Nodulation, Shift Microbial Community Composition, and Result in Increased Metal Uptake Relative to Bulk/Dissolved Metals. *Environ. Sci. Technol.* **2015,** *49*, (14), 8751-8758.

12. Lombi, E.; Donner, E.; Taheri, S.; Tavakkoli, E.; Jämting, Å. K.; McClure, S.; Naidu, R.; Miller, B. W.; Scheckel, K. G.; Vasilev, K., Transformation of four silver/silver chloride nanoparticles during anaerobic treatment of wastewater and post-processing of sewage sludge. *Environ. Pollut.* **2013,** *176*, (0), 193-197.

13. Kaegi, R.; Voegelin, A.; Sinnet, B.; Zuleeg, S.; Hagendorfer, H.; Burkhardt, M.; Siegrist, H., Behavior of metallic silver nanoparticles in a pilot wastewater treatment plant. *Environ. Sci. Technol.* **2011,** *45*, (9), 3902-3908.

14. Pradas del Real, A. E.; Castillo-Michel, H.; Kaegi, R.; Sinnet, B.; Magnin, V.; Findling, N.; Villanova, J.; Carrière, M.; Santaella, C.; Fernández-Martínez, A.; Levard, C.; Sarret, G., Fate of Ag-NPs in Sewage Sludge after Application on Agricultural Soils. *Environ. Sci. Technol.* **2016,** *50*, (4), 1759-1768.

15. Mehrazar, E.; Rahaie, M.; Rahaie, S., Application of nanoparticles for pesticides, herbicides, fertilisers and animals feed management. *International Journal of Nanoparticles* **2015,** *8*, (1), 1-19.

16. Larue, C.; Castillo-Michel, H.; Sobanska, S.; Cécillon, L.; Bureau, S.; Barthès, V.; Ouerdane, L.; Carrière, M.; Sarret, G., Foliar exposure of the crop Lactuca sativa to silver nanoparticles: Evidence for internalization and changes in Ag speciation. *J. Hazard. Mater.* **2014,** *264*, 98-106.

17. Yang, Y.-Y.; Gray, J. L.; Furlong, E. T.; Davis, J. G.; ReVello, R. C.; Borch, T., Steroid Hormone Runoff from Agricultural Test Plots Applied with Municipal Biosolids. *Environ. Sci. Technol.* **2012,** *46*, (5), 2746-2754.

18. Lalau, C.; Mohedano, R.; Schmidt, É.; Bouzon, Z.; Ouriques, L.; dos Santos, R.; da Costa, C.; Vicentini, D.; Matias, W., Toxicological effects of copper oxide nanoparticles on the growth rate, photosynthetic pigment content, and cell morphology of the duckweed Landoltia punctata. *Protoplasma* **2015,** *252*, (1), 221-229.

19. Gunawan, C.; Teoh, W. Y.; Marquis, C. P.; Amal, R., Cytotoxic Origin of Copper(II) Oxide Nanoparticles: Comparative Studies with Micron-Sized Particles, Leachate, and Metal Salts. *ACS Nano.* **2011,** *5*, (9), 7214-7225.

20. Lee, W.-M.; An, Y.-J.; Yoon, H.; Kweon, H.-S., Toxicity and bioavailability of copper nanoparticles to the terrestrial plants mung bean (Phaseolus radiatus) and wheat (Triticum

aestivum): Plant agar test for water-insoluble nanoparticles. *Environ. Toxicol. Chem.* **2008,** *27*, (9), 1915-1921.

21. Wang, Z.; von dem Bussche, A.; Kabadi, P. K.; Kane, A. B.; Hurt, R. H., Biological and Environmental Transformations of Copper-Based Nanomaterials. *ACS Nano.* **2013,** *7*, (10), 8715-8727.

22. Liu, J.; Wang, Z.; Liu, F. D.; Kane, A. B.; Hurt, R. H., Chemical transformations of nanosilver in biological environments. *ACS Nano.* **2012,** *6*, (11), 9887-9899.

23. Lowry, G. V.; Espinasse, B. P.; Badireddy, A. R.; Richardson, C. J.; Reinsch, B. C.; Bryant, L. D.; Bone, A. J.; Deonarine, A.; Chae, S.; Therezien, M.; Colman, B. P.; Hsu-Kim, H.; Bernhardt, E. S.; Matson, C. W.; Wiesner, M. R., Long-Term Transformation and Fate of Manufactured Ag Nanoparticles in a Simulated Large Scale Freshwater Emergent Wetland. *Environ. Sci. Technol.* **2012,** *46*, (13), 7027-7036.

24. Levard, C.; Hotze, E. M.; Lowry, G. V.; Brown, G. E., Environmental Transformations of Silver Nanoparticles: Impact on Stability and Toxicity. *Environ. Sci. Technol.* **2012,** *46*, (13), 6900-6914.

25. Gardea-Torresdey, J. L.; Rico, C. M.; White, J. C., Trophic Transfer, Transformation, and Impact of Engineered Nanomaterials in Terrestrial Environments. *Environ. Sci. Technol.* **2014,** *48*, (5), 2526-2540.

26. Lowry, G. V.; Gregory, K. B.; Apte, S. C.; Lead, J. R., Transformations of Nanomaterials in the Environment. *Environ. Sci. Technol.* **2012,** *46*, (13), 6893-6899.

27. Thwala, M.; Klaine, S. J.; Musee, N., Interactions of metal-based engineered nanoparticles with aquatic higher plants: A review of the state of current knowledge. *Environ. Toxicol. Chem.* **2016**, n/a-n/a.

28. Ma, C.; White, J. C.; Dhankher, O. P.; Xing, B., Metal-Based Nanotoxicity and Detoxification Pathways in Higher Plants. *Environ. Sci. Technol.* **2015,** *49*, (12), 7109-7122.

29. Reidy, B.; Haase, A.; Luch, A.; Dawson, A. K.; Lynch, I., Mechanisms of Silver Nanoparticle Release, Transformation and Toxicity: A Critical Review of Current Knowledge and Recommendations for Future Studies and Applications. *Materials* **2013,** *6*, (6).

30. Kaegi, R.; Voegelin, A.; Sinnet, B.; Zuleeg, S.; Siegrist, H.; Burkhardt, M., Transformation of AgCl nanoparticles in a sewer system — A field study. *Sci. Total Environ.* **2015,** *535*, 20-27.

31. Thalmann, B.; Voegelin, A.; Sinnet, B.; Morgenroth, E.; Kaegi, R., Sulfidation Kinetics of Silver Nanoparticles Reacted with Metal Sulfides. *Environ. Sci. Technol.* **2014,** *48*, (9), 4885-4892.

32. Ma, R.; Stegemeier, J.; Levard, C.; Dale, J. G.; Noack, C. W.; Yang, T.; Brown, G. E.; Lowry, G. V., Sulfidation of copper oxide nanoparticles and properties of resulting copper sulfide. *Environmental Science: Nano* **2014,** *1*, (4), 347-357.

33. Levard, C.; Hotze, E. M.; Colman, B. P.; Dale, A. L.; Truong, L.; Yang, X. Y.; Bone, A. J.; Brown, G. E.; Tanguay, R. L.; Di Giulio, R. T.; Bernhardt, E. S.; Meyer, J. N.; Wiesner, M. R.; Lowry, G. V., Sulfidation of Silver Nanoparticles: Natural Antidote to Their Toxicity. *Environ. Sci. Technol.* **2013,** *47*, (23), 13440-13448.

Chapter 2

Speciation Matters: Bioavailability of Silver and Silver Sulfide Nanoparticles to Alfalfa (*Medicago sativa*)[1]

2.0 Abstract

Terrestrial crops are directly exposed to silver nanoparticles (Ag-NPs) and their environmentally-transformed analog silver sulfide nanoparticles (Ag_2S-NPs) when wastewater treatment biosolids are applied as fertilizer to agricultural soils. This leads to a need to understand their bioavailability to plants. In the present study, the mechanisms of uptake and distribution of silver in alfalfa (*Medicago sativa*) were quantified and visualized upon hydroponic exposure to Ag-NPs, Ag_2S-NPs, and $AgNO_3$ at 3 mg total Ag/L. Total silver uptake was measured in dried roots and shoots, and the spatial distribution of silver was investigated using transmission electron microscopy (TEM) and synchrotron-based X-ray imaging techniques. Despite large differences in release of Ag^+ ions from the particles, Ag-NPs, Ag_2S-NPs, and Ag^+ became associated with plant roots to a similar degree, and exhibited similarly limited (<1%) amounts of translocation of silver into the shoot system. X-Ray fluorescence (XRF) mapping revealed differences in the distribution of Ag into roots for each treatment. Silver nanoparticles mainly accumulated in the (columella) border cells and elongation zone, whereas Ag^+ accumulated more uniformly throughout the root. In contrast, Ag_2S-NPs remained largely adhered to the root exterior, and the presence of cytoplasmic nano-Si_xO_y aggregates was

[1] Originally appeared in June 2015 issue of *Environmental Science and Technology.* Coauthors include Fabienne Schwab, Benjamin P. Colman, Samuel M. Webb, Matthew Newville, Antonio Lanzirotti, Christopher Winkler, Mark R. Wiesner, and Gregory V. Lowry.

observed. Exclusively in roots exposed to particulate silver, NPs smaller than the originally dosed NPs were identified by TEM in the cell walls. The apparent accumulation of Ag in the root apoplast determined by XRF, and the presence of small NPs in root cell walls suggests uptake of partially dissolved NPs and translocation along the apoplast.

2.1. Introduction

Silver nanoparticles (Ag-NPs) are used in many commercial products due to their anti-microbial properties. Inevitably, a portion of these nanomaterials, often in the form of the sulfidized transformation product Ag_2S-NPs, flows into wastewater treatment plants[1-4] and ultimately exits with the biosolids leaving the treatment plants.[1,2,5] In many countries, biosolids are applied to agricultural feed crops as fertilizer, providing a potential entry point into animal and human food chains.[3,6-8]

Current research has focused on the bioavailability and toxicity of Ag^+ ions and/or Ag-NPs to many types of organisms including bacteria,[9] animals,[10,11] and plants.[12-14] Ag-NPs have been observed in plant tissue[15,16] accompanied by effects such as growth inhibition,[17] cell erosion[18] and growth stimulus (hormesis) at subacute concentrations.[19] Distinguishing the mechanisms of Ag uptake and assessing the biodistribution of Ag in plants are confounded by the ability of some plants, including agriculturally important legumes such as *Medicago sativa* (alfalfa), to produce metallic Ag-NPs in their tissue via a natural reduction process after being exposed to elevated concentrations of Ag^+ ions.[20-23]

The uptake of bulk or particle Ag^0 or Ag_2S by plants may be a result of (active) dissolution and Ag ion uptake. Many plant species are known to exude organic ligands into the acidic rhizosphere to solubilize metals used as essential nutrients for plant growth.[24,25] These and other root exudates, particularly thiols, can alter the NPs before direct uptake due to changes in

pH and/or metal complex formation. On one hand, NPs that are normally insoluble, including Ag_2S-NPs, can potentially dissolve in the rhizosphere.[26,27] On the other hand, interactions between plant root exudates and NPs may reduce the metal bioavailability, as has been shown for ZnO, CeO_2 and TiO_2, where large NP concentrations adsorbed onto the root surface are associated with limited NP uptake and translocation.[28-33] Elucidating the mechanism of Ag-NPs and Ag_2S-NPs uptake by plants remains challenging because, among other things, it requires mapping of elements at μm- to nm-resolution.

Although Ag_2S-NPs are more environmentally relevant than Ag-NPs, there remains little research devoted to the uptake of Ag_2S-NPs by plants.[7,34] Relative to Ag-NPs, Ag_2S-NPs possesses an increased thermodynamic stability and release less Ag^+ ions ($Ag_2S_{(s)} \rightarrow 2Ag^+ + S^{2-}$, $K_{sp}=6\text{-}8\times10^{-51}$).[35,36] Because the mechanism of Ag uptake by plants may in part be governed by the solubility of the silver compound,[35] Ag_2S-NPs can be hypothesized to exhibit lower bioavailability and toxicity. Indeed, Ag_2S-NPs are less toxic than Ag-NPs to many organisms.[36-39] However, despite the transformation of Ag-NPs into Ag_2S in wetland sediments, silver remained bioavailable to invertebrates, fish, and aquatic and terrestrial plant roots and, to a lesser extent, plant shoots.[40,41] For plants, this suggests that Ag_2S-NPs may either be taken up directly by plants as intact nanoparticles (NPs), or by Ag_2S-NP oxidation, dissolution, and subsequent silver ion uptake. Alternatively, much of the silver associated with those plant roots may simply be Ag_2S-NPs adsorbed to the root surfaces, as the distribution of Ag in root tissue was not determined.

The main goals of the present study were to a) quantify the differences in uptake of Ag^+, Ag-NPs, and Ag_2S-NPs in alfalfa (*Medicago sativa*) grown hydroponically, and then b) qualitatively elucidate and compare the mechanisms of uptake of these three forms of silver. We

used electron microscopic and X-ray fluorescence techniques to investigate the uptake, distribution, and speciation of silver in alfalfa.

2.2. Methods

2.2.1 Silver Nanoparticle Synthesis

Two batches of Ag-NPs coated with polyvinylpyrrolidone (PVP) were synthesized using a protocol adapted from previously published methods.[10] Briefly, 1.5 g of PVP (1000 g/mol) was added to 280 mL of deionized water. Nine milliliters of 0.10 M $AgNO_3$ was added and stirred for five minutes. Eleven milliliters of ice-cold, 0.08 M $NaBH_4$ was added rapidly while mixing. This suspension was then split into two aliquots, one for the Ag-NPs treatment and the other to be sulfidized to produce Ag_2S-NPs. One aliquot of the Ag-NPs was washed three times by removing the NPs from solution using an ultracentrifuge operating at 50,000 ×g for 30 min, decanting the supernatant and re-suspending the NPs in deionized water via a sonicating probe (Branson Model 250 at power level 3 for one minute). The decanted supernatant was retained for comparative purposes and to rule out toxicity of soluble reaction byproducts or PVP in hydroponic dosing of a subset of plants. The second aliquot of Ag-NPs was directly sulfidized with Na_2S to create Ag_2S NPs in the presence of PVP as described next.

2.2.2 Sulfidation of Silver NPs

The Ag-NPs were sulfidized using a direct sulfidation process as described in detail elsewhere.[38] The Ag-NPs were exposed to dissolved oxygen and reduced sulfur simultaneously. Nine milliliters of 0.1 M Na_2S were added to one of the batches of fresh Ag-NPs to provide a S:Ag molar ratio of 2:1. This four times stoichiometric excess of S was used to ensure complete sulfidation and to account for inevitable sulfide loss due to H_2S outgassing and oxidation to

sulfate. Aquarium air pumps fastened with pipet tips provided the source of dissolved oxygen required for Ag dissolution and sulfidation.[42] These particles were allowed to react for one week at room temperature while maintaining a constant volume via daily additions of deionized water. These Ag_2S NPs were then washed using the same procedure as for the Ag-NPs, and the supernatant was collected from the final wash and retained for subsequent dosing of a subset of plants.

2.2.3 Characterization of Nanomaterials

Aliquots from each batch (i.e. Ag-NPs and Ag_2S-NPs) were separated and characterized. Particle hydrodynamic diameter was determined by dynamic light scattering (DLS) in 3 ppm nano-Ag dispersions in deionized water directly after washing using a Zetasizer Nano ZS (Malvern, UK). Dried samples of the washed NP suspensions were analyzed using an X-Radia XRD (X'Pert Pro MPD X-ray diffractometer operating with a Cu K-α X-ray source) and the crystal structure determined through peak matching using X'pert Highscore Plus. Aliquots of the fresh samples were dried on formvar coated copper grids and imaged on a TECNAI G^2 Twin (FEI, Hillsboro OR, USA) transmission electron microscope (TEM). Dissolution of the Ag-NPs and Ag_2S-NPs was determined by suspending the NPs at 3 ppm Ag in plant growth medium (half strength Hoagland's medium[43]) that was aerated using an aquarium pump for 5 days. The fraction of silver passing a 0.025 μm nitrocellulose filter paper was quantified by adding concentrated nitric acid to the filtrates, and measuring the total silver in the resulting solutions using inductively coupled plasma - mass spectroscopy (ICP-MS). This kind of ultrafiltration does not necessarily result in complete removal of the nanoparticles.[44,45] The "filterable silver" measured in this study only served for comparative purposes between the two particles in a complex medium.

2.2.4 Exposure to *Medicago sativa*

Alfalfa seeds (*Medicago sativa*) were cleaned, sprouted, and transferred into specially designed hydroponic growth containers as shown in Figure A.1 (Appendix A) to prevent unintentional exposure of the stems and the leaves to the dosed growth medium. The root compartment containing the NP suspensions was protected from light irradiation by an aluminum foil cover. Glass marbles were added to the root compartments to reduce the required volume of NP suspension and to provide a structure to promote root stability. The silver solution or suspension of NPs was added to the growth medium in the containers and was not renewed for the duration of the experiment. Aquarium air diffusers were used in all cases with the goal of supplying dissolved oxygen to the medium and maintaining NPs in suspension. Four replicate containers per treatment, each containing five alfalfa sprouts (i.e. 20 sprouts/treatment), were exposed to six treatments including a control with only the growth medium, silver ions added as $AgNO_3$, Ag-NPs, or Ag_2S-NPs (each containing 3 mg total Ag/L), and two treatments exposed to the supernatants (last washing step) of the NP suspensions to assess the potential toxicity of particle leachate or reaction byproducts. This exposure concentration was selected to ensure sufficient Ag in the roots for X-ray mapping without being acutely toxic to the plants. Samples were grown in a growth chamber illuminated by continuous cool fluorescent light (150 μmol photons m^{-2} s^{-1}) at 25 °C. The plants were harvested after six days of exposure and rinsed thoroughly with deionized water prior to preparation for elemental analysis.

2.2.5 Sample Preparation for Silver Content, XRF, and TEM Analysis

The harvested alfalfa plants were immediately sectioned for TEM analysis. A portion of the roots and shoots from each treatment was dried, weighed and digested with hydrogen peroxide, concentrated nitric acid and concentrated hydrochloric acid for analysis[40] of the total

silver content using a PerkinElmer 3100 flame atomic absorption spectrometer (PerkinElmer, Waltham, Massachusetts, USA).

Roots of fresh alfalfa plants were also prepared for low-energy (Ag L-edge) and high-energy (Ag K-edge) XRF mapping and TEM imaging following standard procedures.[46,47] Briefly, specimens were cut off the living plant while immersed in a 0.1 M phosphate buffered 3.0% glutaraldehyde pre-fixative solution (pH 7.0) Inter- and intracellular gas bubbles were eliminated by applying a gentle vacuum to the immersed specimens.[47] Subsequently, the specimens were allowed to sit in the pre-fixative at room temperature for 2 hrs, and then at 4 °C overnight. Next, they were fixed in 1% OsO_4 for 2 hrs, washed using 0.1 M phosphate buffer (2×10 min), and dehydrated using a 30, 50, 70, 90, 95, 4×100% EtOH series (15-20 min each). Finally, the specimens were embedded in a series of mixtures of EtOH and Spurr's resin[48] progressing from EtOH:resin ratios of 2:1, 1:1, 1:2, and then 3×100% Spurr resin (each step 5-14 h, last step overnight), then cured at 60 °C for 24 h, and sectioned using an ultramicrotome. The thin sections obtained were placed on hexagonal copper grids for TEM analysis on a TECNAI G^2 Twin (FEI, Hillsboro OR, USA). The same grids were used to study elemental composition of selected electron dense particles in cells by TEM combined with energy-dispersive X-ray spectroscopy (TEM-EDS) at 200 kV on a JEOL 2100 S/TEM (JEOL Inc., Peabody MA, USA).

Roots for XRF mapping were chemically fixed as described above, except that the EtOH series was stopped at 70%,[47] and the samples were stored in 70% ethanol in darkness until analysis to ensure preservation of the cell structure during storage (<4 d). For K-edge XRF mapping, all specimens were sealed inside a polyimide tape window in the presence of storage

solution to prevent drying. The samples for L-edge XRF mapping were mounted in air adhered on a polyimide tape due to the shallow penetration depth of softer X-rays.

2.2.6 XRF Measurements

Silver K-edge (25,514 eV) XRF mapping was conducted to spatially determine the silver distribution in the root. Ethanol preserved samples were analyzed at room temperature at the Advanced Photon Source (APS)'s beamline IDE-13, which provided a 1×2 μm spot size X-ray microprobe. The roots were mounted at a 45-degree angle relative to the incident beam, and a four-element fluorescence detector was positioned normal to the incident beam. The samples were rastered across the incident X-ray beam (28,000 eV) with a 2 μm stepsize and 100 ms dwell time per pixel. This loss of dimensional information implies that variations in root thickness may cause the Ag signal from the center of the root to appear artificially high. We considered this in the interpretation of the maps of the present study. The silver $K\alpha_1$ fluorescence peak (22,163 eV) was used to generate the silver specific maps.

Lower energy X-ray mapping was used to spatially resolve any correlations between silver and lighter elements (primarily sulfur). Samples stored in ethanol were immediately run at Stanford Synchrotron Radiation Lightsource's (SSRL) beamline 14-3 at room temperature, which provided a 5×5 μm spot size at 3400 eV, sufficient to excite silver's L(III) edge (3351 eV). The samples were analyzed using the 45-degree geometry and a single fluorescence detector (Vortex model) normal to the incident beam housed in a sample chamber under a He atmosphere. The silver Lα fluorescence peak (2,984 eV) was used to generate the Ag maps, while the sulfur Kα fluorescence peak was used to generate sulfur maps. The correlation between number of counts associated with silver versus sulfur (Figure A.2) were used to generate masked regions associated with relatively high, medium, and low Ag:S count ratios.

Lower energy X-rays are more easily absorbed and have a very short X-ray penetration depth. The root samples analyzed were significantly thicker than the penetration depth of the beam (~75 μm of water and ~50 μm in ethanol at 3400 eV), which is much shorter than the root samples analyzed. The fluoresced photons, having lower energy and even shorter penetration length thus primarily mapped elements near the root surface. Due to the thickness of the roots and the 45-degree geometry, a minor shadowing effect was noticed on the tape background immediately to the side of each root. Additionally, due to the relatively narrow energy range between fluorescence peaks of light elements, overlap of fluorescence signals results in some degree of autocorrelation between near elements. Neither shadowing nor correlation of adjacent elements in fluorescence energy was found to notably affect the results. Argon traces (2,957 eV) in the helium caused a uniform background signal of one hundred silver (2,984 eV) counts (Appendix A, Figure A.5).

2.3. Results and Discussion

2.3.1 Characterization of Ag-NPs and Ag_2S-NPs

The median primary particle size of the synthesized NPs as determined by TEM was 6.3 and 7.8 nm for Ag-NPs and Ag_2S-NPs respectively (TEM micrographs and size distribution histograms are shown in Figure A.3 in Appendix A). Dynamic light scattering measurements in the growth medium showed that the particles were well dispersed in the growth medium, as the hydrodynamic diameter for the Ag-NPs and Ag_2S-NPs was 11.6±2.9 nm and 16±13 nm, respectively (Appendix A, Table A.1). X-Ray diffraction (XRD) measurements confirm the crystalline structure as metallic silver for the Ag-NPs and acanthite for the Ag_2S-NPs (Appendix A, Figure A.4).[49] Significant peak broadening in the Ag_2S-NPs suggests that the Ag_2S

formed is polycrystalline with very small crystallite size, which is a common phenomenon for Ag nanoparticles in this size range.[49] The electrophoretic mobility of the particles in growth medium was -1.526±0.024 and -1.73±0.10 μm $cmV^{-1}s^{-1}$ for Ag-NPs and Ag_2S-NPs, respectively. This corresponds to a zeta potential of -19.50 ±0.29 and -22.1 ±1.3 mV, respectively, as calculated from the Henry equation. The relatively high charge is consistent with the stability of the particle suspensions against aggregation After five days in aerated growth medium, 0.65 mg Ag/L (~22% of the 2.9 mg/L total) was found to be filterable for Ag-NPs, and 0.07 mg Ag/L (~2% of the 2.8 mg/L total) was filterable for Ag_2S-NPs. This is in agreement with Levard et al., who found almost one order of magnitude more dissolved silver in Ag-NPs than in Ag_2S-NPs suspensions. [37]

2.3.2 Silver Concentrations in Roots and Shoots

The silver concentrations associated with the alfalfa roots and shoots from the four treatments (control, $AgNO_3$, Ag-NPs, Ag_2S-NPs) are shown in Figure 2.1. These values include all Ag that was associated with the plants (internalized and external) after collection and rinsing with deionized water as described in the methods section.

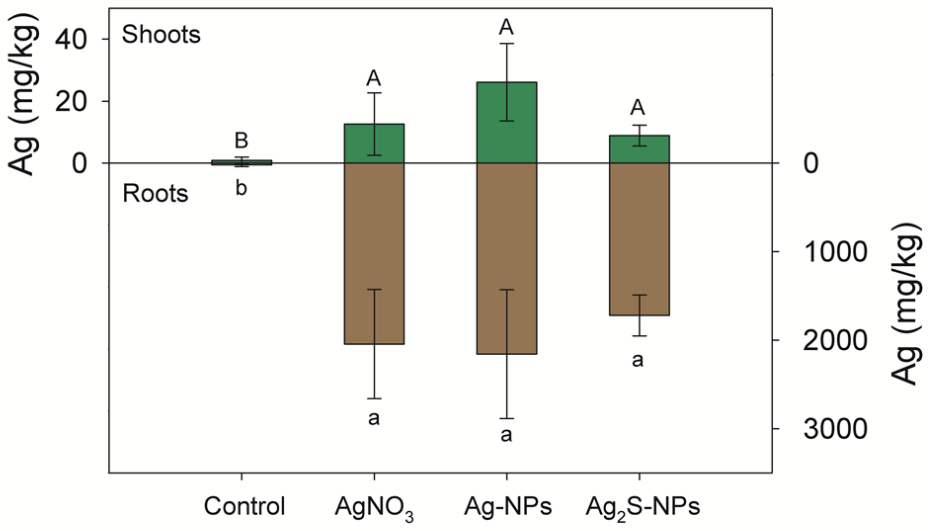

Figure 2.1: Total silver concentrations in dried alfalfa plants roots (bottom) and shoots (top) after six days of hydroponic exposure. Note the y-axis values are two orders of magnitude higher for the roots (bottom) compared to the shoots (top). The data are presented as averages ± standard deviation. Significant differences (based on ANOVA and Tukey HSD post-hoc tests on log transformed data) are indicated by different letters with shoots indicated by uppercase letters and roots by lowercase letters.

A majority (~99%) of the plant-associated silver was sequestered on/in the roots of alfalfa irrespective of the form of silver introduced. The silver concentrations associated with the roots exposed to Ag_2S-NPs (1,720±231 mg kg^{-1} dry weight), Ag-NPs (2,157±727 mg kg^{-1}) and the soluble $AgNO_3$ (2,043±615 mg kg^{-1}) were not significantly different from one anther but were significantly higher than the controls (ANOVA with Tukey HSD post-hoc test). These root measurements included both sorbed and internalized NPs or Ag^+. The accumulation of silver in plant tissue many fold times higher than the exposure solution has been observed.[50] Other studies using elevated Ag concentrations have shown a lower silver concentration in the plant tissue than the exposure solution for alfalfa and zucchini.[51,52] The alfalfa shoots contained ~1% or less of the

total plant associated Ag, indicating that little of the root associated Ag was translocated into the shoots regardless of the form of the Ag presented to the plants. This is consistent with prior studies with short exposures showing higher recoveries in roots compared to shoots.[12] In long term studies, plants can accumulate more of the total silver in the aboveground tissue.[40,41] Differences in shoot Ag concentrations between NP-exposed treatments and the $AgNO_3$ control were not statistically significant, but were all significantly higher than the unexposed control plant (ANOVA with Tukey-HSD post-hoc test). It is noteworthy that the concentration of silver translocated into the aboveground tissue for Ag_2S-NPs was comparable to $AgNO_3$ despite the low solubility of Ag_2S-NPs. The presence of Ag in plant shoots for low solubility Ag_2S-NP could indicate direct uptake and translocation of Ag_2S NPs as has been recently shown for cowpea and wheat.[53] However, it is also possible that plant root exudates partially dissolve the Ag_2S-NPs, making them more bioavailable. Evidence for both of these mechanisms were found with XRF mapping and TEM as discussed later.

2.3.3 XRF Maps of Roots

High-resolution Ag $K\alpha_1$ XRF maps of the root tips exposed to Ag-NPs and Ag_2S-NPs for six days are shown in Figure 2.2. The low silver concentration (<25 ppm) rendered XRF microprobe analysis in the shoots unfeasible. The Ag-NPs exposed root (Figure 2.2A) contained Ag associated primarily with the root cap (columella cell)s. The net-like distribution of Ag, especially in between the root cap cells, suggests that Ag entered the root preferentially through the intracellular spaces along the apoplast. Silver was also present in the rest of the root tip (blue coloration throughout the tip), which clearly demonstrates silver uptake into the root, but in lower concentrations than into the root cap. In contrast, the root exposed to Ag_2S-NPs (Figure 2.2B) revealed dense clusters of silver enriched material, adhered onto the exterior of the root,

apparently bound to mucilage and sloughed root (border) cells. The Ag abundance inside of the Ag_2S-NP exposed root tip was also much lower compared to the Ag-NPs exposed root tip, suggesting less uptake in this root. Likely, this is a result of the low solubility of Ag_2S-NPs compared to Ag-NPs. Despite these differences in the distribution of silver in the root tips, similar amounts of Ag translocated to the shoots for both the Ag_2S-NPs exposed roots and the Ag-NP exposed roots. This suggests that Ag must have been taken up elsewhere, potentially as Ag_2S NPs.[53] Ag was indeed found in the elongation zone of the root, the region of the root between the meristematic zone and the zone of differentiation, as discussed below (Figure 2.3).

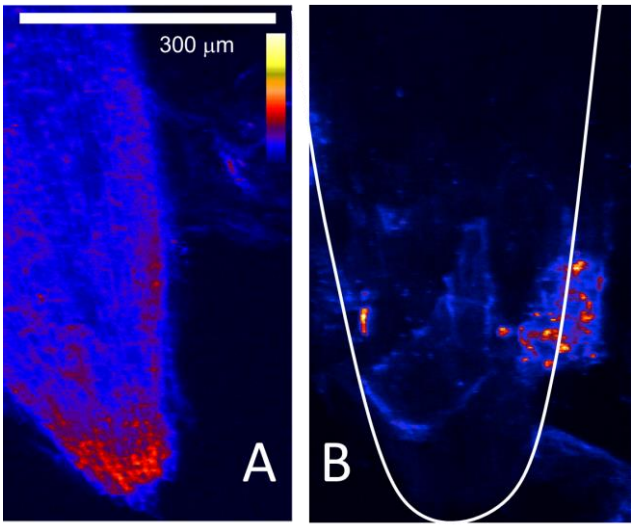

Figure 2.2: Silver Kα1 specific elemental maps of alfalfa root tips exposed to Ag-NPs (A) and Ag_2S-NPs (B) with a white outline of the root structure for reference. Note that the color scale of the XRF maps was calibrated internally.

The lower resolution Ag L(III) maps, corrected for argon fluorescence using the control (Appendix A, Figure A.5), show the distribution of Ag in a larger region of the root (Figure 2.3). This mapping also provides correlations (based on counts) between Ag and S in the root, and provides qualitative assessment of the Ag speciation. The maps (Figure 2.3) showed a similar

silver distribution for the Ag-NPs and Ag_2S-NPs to those observed in the Ag $K\alpha_1$ maps (Figure 2.2). Much of the silver in Ag-NP exposed roots was concentrated near or in the root cap (Figure 2.3, middle, first column). Further, the maps suggest that silver from the Ag-NPs was internalized and distributed within the root tip less uniformly than the dissolved silver from the silver nitrate salt (Figure 2..3, top, first column). We hypothesize that this is due to accumulation of Ag-NPs on the root surface, and on or in the root border cells. In agreement with the results of the high resolution maps, the root exposed to Ag_2S-NPs has relatively little silver associated with the root cap (Figure 2.3, bottom, first column), but although the high-resolution maps suggest little uptake, the lower resolution maps show considerable amounts of internalized silver, especially in the root elongation zone above the root tip. The high Ag concentration seen in the elongation zone of the Ag_2S-NP exposed root suggests internalization of Ag_2S-NP during growth.

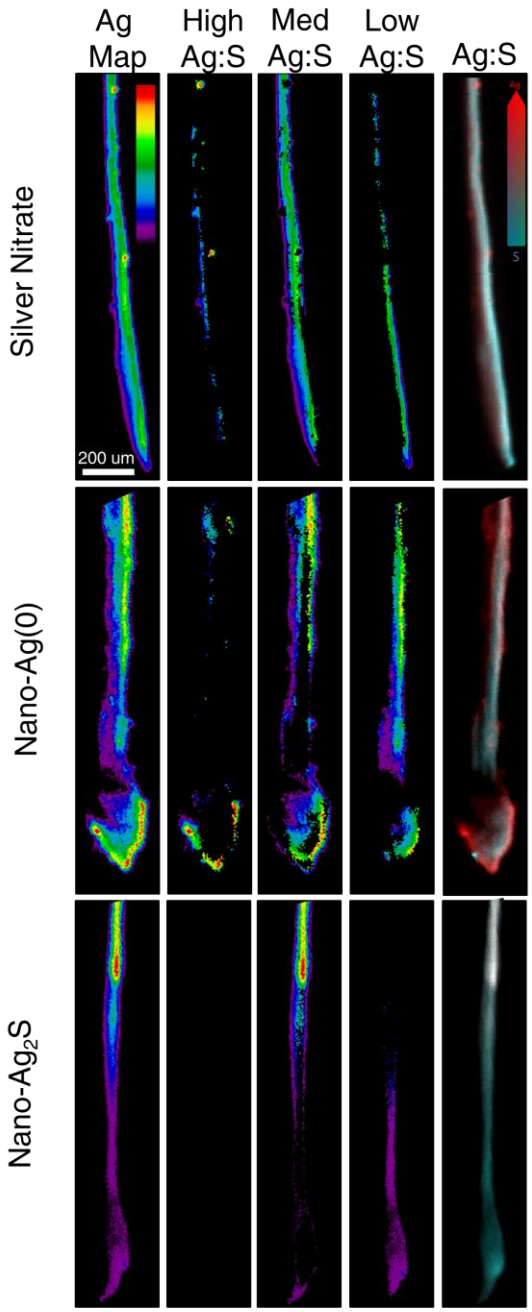

Figure 2.3: Silver:Sulfur fluorescence count correlations for $AgNO_3$ (top), Ag-NP (middle), and Ag_2S-NP (bottom) exposed alfalfa roots with bi-color maps (Ag = Red and S = Cyan) – Masked regions is shown in Figure A.4 for the relatively high, medium and low Ag:S correlations. Elemental specific μ-X-ray fluorescence maps of alfalfa root tips generated using windows around Ag Lα1 (2 984 eV) and S Kα1 (2 308 eV). Please note: Length scale bars are valid for all samples while color scale bars are unique to each sample and element. The range of counts used in each scale bar is shown in Table A.3.

Maps of the ratio of the Ag:S fluorescence signal (Figure 2.3, right columns) give qualitative evidence of the presence of (a) thiol associated Ag (Ag < S), a possible plant response to metal exposure); (b) intact Ag_2S-NPs in the Ag_2S-NP treatment (Ag > S); (c) presence of silver in excess of S (Ag >> S). The regions associated with high Ag:S in the root exposed to $AgNO_3$ shows discrete silver accumulations near bumps in the root resembling emerging lateral roots (red dots in map in Figure 2.3 top, right column; Ag:S correlation plots in Appendix A, Figure A.2) The lowest Ag:S ratios were located at the root tips suggesting silver associated with thiols, which may have been generated in response to the Ag.

The root exposed to Ag-NPs showed high Ag:S ratios near the root cap cells of the root tip, pointing to accumulation of Ag in/on these cells, which is in agreement with the results of the high energy X-ray maps (Figure 2.2). High Ag:S ratios were found at the exterior of the root suggesting nanoparticles attached to the root surface before uptake. As a whole, the Ag:S ratios of the Ag-NPs exposed root were less uniformly distributed along the root than those of $AgNO_3$. Ag-NPs must have either undergone (partial) dissolution limiting internalization, or Ag-NPs were taken up directly. Uptake of Ag-NPs via partial Ag dissolution is supported by the TEM results discussed in the sections below, the high solubility of Ag-NPs, and the similar, albeit spatially less uniform, uptake profile of Ag-NPs and $AgNO_3$ in Figure 2.3 and in the correlation plots of Figure A.2 (Appendix A).

The silver in the root exposed to Ag_2S-NPs was highly correlated with the signal of sulfur (Figure 2.3 and Figure A.2). Regions exhibiting a high Ag:S ratio were nonexistent, demonstrating that silver remained colocated with sulfur. This means that Ag_2S-NPs either was almost exclusively taken up in nanoparticulate form or the plants strongly responded to the NP exposure by generation of thiols, such as glutathione, for subsequent biotransformation.

Glutathione is known to play an important role in the detoxification of heavy metals by plants.[54,55] Dimkpa et al. has shown elevated levels of the oxidized form of glutathione in the roots of wheat grown in the presence of silver ions and NPs.[56] Accumulation of intact Ag_2S-NPs in the root tip was minimal given the absence of an appreciable Ag signal. Silver from the Ag_2S-NPs exposed samples was primarily located at the elongation zone of the root, highlighting a clear difference in the uptake mechanisms (but not the mobility) of silver between the pristine and sulfidized silver nanoparticles. Overall, the silver from the Ag_2S-NPs was less uniformly internalized and less prevalent in the root tip than for Ag-NPs or $AgNO_3$, likely a result of two factors: the lower filterable silver concentration associated with Ag_2S-NPs; and the sorption of Ag_2S-NP with cells at the root tip that are readily sloughed off by the root (Figure 2.2).

2.3.4 Microscopic Analysis of NPs in Plant Tissues

Two types of particles were exclusively found on or in the NP-exposed roots: Large particles with low electron density adsorbed to border cells, and small electron dense particles in the cell walls and channels. There were thousands of very low electron density particles adhered to the border cells of the Ag-NP and Ag_2S-NP treatments with diameters of 74 ± 14 and 84 ± 34 nm, respectively (Figure 2.4N,S, Figure 2.5, Table A.2). Some of these particles were also found in the intracellular spaces (data not shown). The smaller particles were found in the intercellular spaces and interfibrillar channels of the cell wall and had diameters of 2.52 ± 0.83 and 2.54 ± 0.77 nm in the Ag-NPs and Ag_2S-NPs treatments, respectively (insets in Figure 2.4M,R), which is consistent with previous observations of uptake pathways.[12,57] Although alfalfa has been shown to generate silver NPs of similar size following exposure to silver nitrate in agar,[58] no such NPs were present in the control cell wall and the cell walls of plants exposed to $AgNO_3$ (Figure 2.4C,H). The spatial resolution and sensitivity of TEM/EDX was insufficient to identify

the elemental composition of these few nm-sized particles within the cell wall matrix. Nevertheless, the location of the particles in the cell wall and interfibrillar channels (Figure 2.4M,R), and the lack of these particles in the control and the $AgNO_3$ treatment (Figure 2.4C,H) suggests that Ag-NPs and Ag_2S-NPs at least partially dissolved in the acidic environment of the root border cells, and then diffused into the intercellular spaces and subsequently translocated along the apoplast.

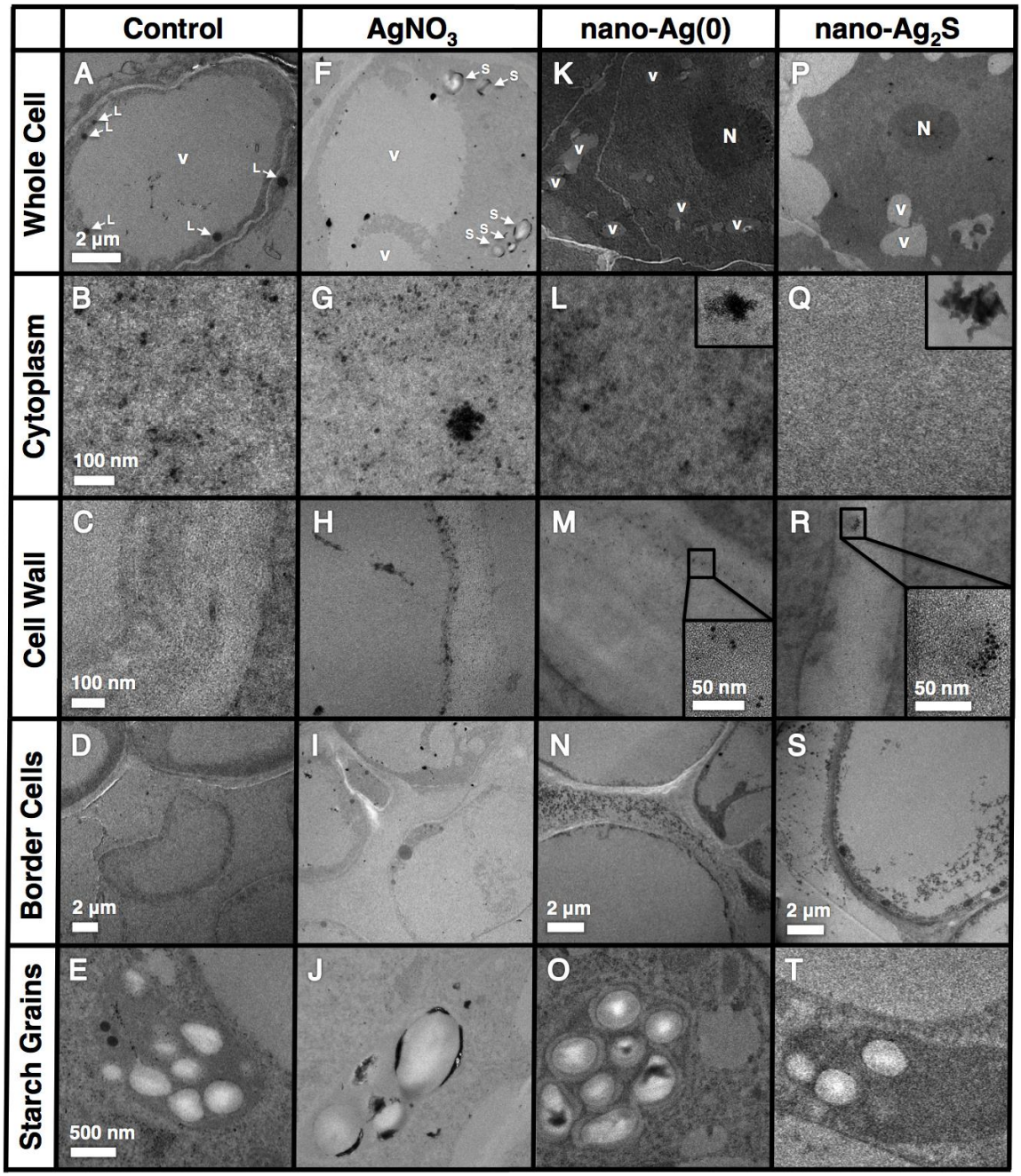

Figure 2.4: Transmission electron microscopic images of control and exposed root cells of *Medicago sativa* (alfalfa). A, F, K, P: Root cortex cells. B, G, L, Q: An area in the cytoplasm of cortex cells. C, H, M, R: Border cell walls. D, I, N, S: Border cells and extracellular space; E, J, O, T: Starch grains. Rulers are valid for entire rows, if no other ruler is shown. Recommended screen resolution to view at least 1280 × 800 pixel. L: Lipid bodies, stained by OsO_4 due to the high content of polyunsaturated fatty acids (see Figure A.7 for close-up); V: Vacuole; N: Nucleolus; S: Starch grain. See Table A.2 and Figure 2.4 for a detailed description of the electron dense particles visible in B, F-I, L-N, and P-S.

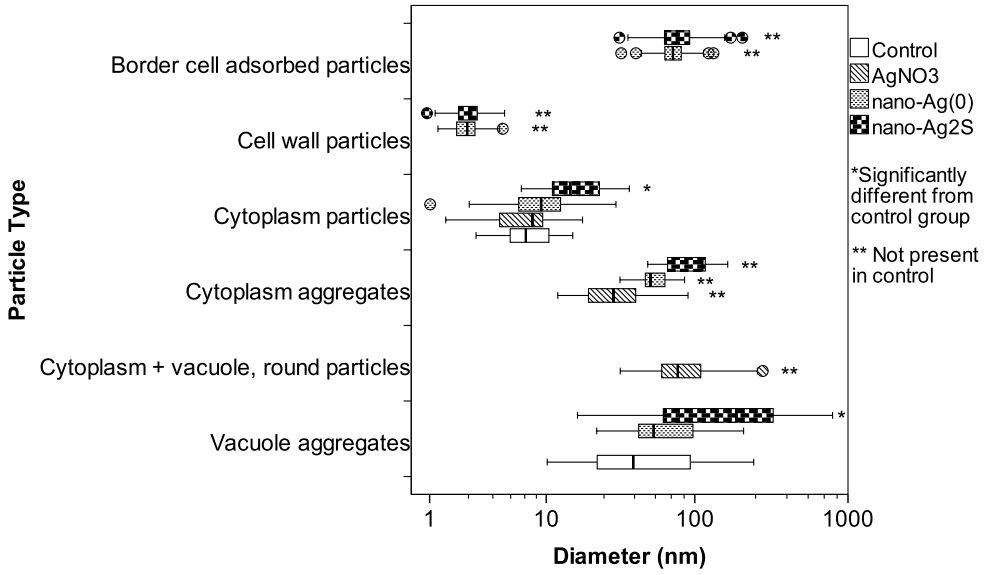

Figure 2.5: Diameters of electron dense nanoparticles (NPs) and aggregates measured by transmission electron microscopy (TEM) in different cell compartments of alfalfa root tips exposed to four treatments: Background growth medium only; dissolved $AgNO_3$; dispersed Ag-NPs; or Ag_2S-NPs respectively. Corresponding micrographs of the NPs are shown in Figure 2.4 and Figure A.7, and the numerical values are provided in Table A.2. Note that only two types of NPs were present in the control, whereas two additional types of NPs were exclusively observed in the NP-exposed roots: The particles adsorbed to the border cells (Figure 2.4N,S) and the particles in the cell wall (Figure 2.4M,R) or in channels in the cell wall (Figure 2.4R, insert).

Analysis of many transmission electron microscope images revealed a variety of electron-dense particles of different sizes and shapes in and on the alfalfa roots (Figure 2.5 and Figures A.6 and A.7 in Appendix A). The types, sizes, and shapes of these particles (Figure 2.5 and Table A.2) depended on the form of silver used to expose the plants, providing useful insights into how the plant responded physiologically to each form of silver at a microscopic (cellular) level. In all treatments (control, $AgNO_3$, Ag-NPs, and Ag_2S-NPs), the cytoplasm in the cells of the root cortex contained abundant small particles (Figure 2.4B,G,L, in the inset of Q, and Figure A.6). In control roots, these cytoplasmic particles (average diameter 7.9–9.9 nm)

were evenly distributed or loosely grouped (Figure 2.4B, Figure A.6). In the $AgNO_3$ and Ag-NP roots, there were also larger aggregates of these cytoplasmic particles of 33 ± 18 and 55 ± 17 nm in diameter, respectively (average ± standard deviation; Figure 2.4G, and inset in panel L). In contrast to the control, $AgNO_3$, and Ag-NP exposed roots, the cytoplasm of A_g2S-NP exposed roots was mostly bare of the small cytoplasm particles as shown in Figure 2.4Q. Instead, the cytoplasm contained large 96 ± 35 nm aggregates of smaller primary particles (17.2 ± 7.8 nm in diameter, Figure 2.4P and inset in Figure 2.4Q, Figures A.6 and A.7A in Appendix A). These primary particles were significantly larger than the cytoplasm particles observed in the other treatments (ANOVA assuming unequal variances, Dunnett-C posthoc test; Figure 2.5, Table A.2). Hotspots of colocated Si and O in maps generated using S/TEM (Figure A.7) suggest that the small cytoplasm particles and their aggregates mainly consisted of silicates. In the present hydroponic setup, the plants apparently formed Si_xO_y particles in their cytoplasm. Potential sources for Si are dissolved Si species (i.e., orthosilicic acid) mobilized by the root exudates interacting with the glass marbles or the seed coats, replacing natural silicate-containing rocks.

Differences in the aggregation state of the naturally formed cytoplasmic silicate particles in plants exposed to different forms of silver suggest that they are part of the defense mechanisms against silver toxicity. In the control, the natural cytoplasmic silicate particles are not aggregated, whereas these particles are partially aggregated ($AgNO_3$ and Ag-NPs) or completely aggregated (nano-Ag_2S) in plants exposed to silver. The degree of flocculation achieved ($AgNO_3$ < Ag-NPs < Ag_2S) was inversely proportional with the availability of filterable Ag ($AgNO_3$ > Ag-NPs > Ag_2S). This suggests that production of silicate aggregates was hampered under the condition of heavy stress by Ag^+ exposure ($AgNO_3$ and Ag-NP), but was fully operational when exposed to lower levels of filterable silver (Ag_2S-NPs). More

evidence for higher exposure to dissolved Ag^+ are the stunted growth and structural damages of the root epidermis as observed by electron microscopy (data not shown) of plants exposed to $AgNO_3$ and Ag-NPs compared to nano-Ag_2S (Figure A.1). We speculate that the naturally formed silicate aggregates in the roots of alfalfa may have served the plants to adsorb Ag^+ or Ag_2S-NPs and thus alleviated their toxicity and potential to translocate. This defense mechanism is common in plants against heavy metals or pests.[59,60] Coprecipitation of heavy metal ions on/in highly sorptive naturally formed silicate aggregates (also called phytoliths) or silicate colloids in plant cells is already well-known, e.g., for Cd in rice.[59,61,62] In rice and other plants, silicate aggregates or colloids in roots can reduce translocation of heavy metals into shoots.

The XRF Ag element maps in Figure 2.3 confirm that in the Ag_2S-NPs treatment little Ag was present in the root tip, the Ag:S ratio was low, and most Ag concentrated in the elongation zone above the root tip, indicating that the root tip itself containing the sensitive apical meristem was exposed to less toxic Ag^+ ions than in other treatments. The question remains whether the individual cytoplasm particles or aggregates would show traces of Ag^+ or even intact Ag_2S-NPs at higher resolution. Such analysis is currently not feasible for NPs of this size in biological samples.

2.4. Environmental Implications

Overall, the present study suggests that nanoparticles of silver, even when transformed to low solubility Ag_2S-NPs, strongly accumulate on and in the roots of alfalfa, an agriculturally important legume relevant for the human food chain (1,608–2,019 ppm dry weight, corresponding to a 536- to 673-fold increase from the nominal dose). Surprisingly, different Ag distributions were present in the roots despite similar Ag uptake concentrations for different kinds of Ag NPs and ionic Ag^+.

This work suggests different uptake mechanisms for $AgNO_3$, Ag-NPs, and Ag_2S-NPs in alfalfa. Silver in the $AgNO_3$ (i.e., Ag^+ ion control) exposed sample was highly concentrated and uniformly distributed throughout the root tip cells. In contrast, the root tip exposed to Ag_2S-NPs accumulated very little Ag inside the root tip cells. Instead, Ag aggregates adsorbed on the exterior of the root, and small particles <4.94 nm were found in the apoplast. Notably, the Ag_2S-NP exposed roots contained abundant natural SiO_2-NPs aggregates in the cytoplasm, which we hypothesize to be a defense reaction of the plant that was absent in the treatments with higher intracellular Ag concentrations (and which appeared less healthy). These SiO_2-NPs aggregates may immobilize the toxic Ag ions released from the NPs. Similar biomineralization of sorptive mineral phases in roots exposed to heavy metals has been known for decades, but is reported here for NPs for the first time. Overall, these observations suggest very limited Ag^+ ion uptake for Ag_2S-NPs, and that the primary mechanism of Ag uptake includes NP attachment, and migration of partially dissolved NPs into the root apoplast. Silver in Ag-NP exposed roots was found accumulated in the root cap, in discrete clusters of silver attached to the upper regions of the root tip (probably near emerging lateral roots), and silver distributed throughout the root tip cells. Again, particles <4.48 nm were found in the root apoplast. These results suggest that the mechanism of Ag uptake from Ag-NPs is a combination of both NP attachment to the root surface followed by direct uptake of small or partially dissolved NPs into the root apoplast, as well as dissolution and Ag ion uptake. Although much of the silver is associated with sulfur suggesting thiol-complexes or Ag_2S, long-term transformations may be likely during harvesting and drying process to prepare alfalfa for livestock feed.

This study suggests that pristine and transformed NPs as well as ionic phases of silver associate and interact with plant roots in a different manner, and although the total amount of Ag

associated with the root may remain similar, the mechanisms of uptake are not the same. A better understanding of how different NP phases interact with plant roots helps to predict more accurately the fate of these materials in environmental and agricultural scenarios.

References

1. Kaegi, R.; Voegelin, A.; Sinnet, B.; Zuleeg, S.; Hagendorfer, H.; Burkhardt, M.; Siegrist, H., Behavior of metallic silver nanoparticles in a pilot wastewater treatment plant. *Environ. Sci. Technol.* **2011,** *45*, (9), 3902-3908.

2. Lombi, E.; Donner, E.; Taheri, S.; Tavakkoli, E.; Jämting, Å. K.; McClure, S.; Naidu, R.; Miller, B. W.; Scheckel, K. G.; Vasilev, K., Transformation of four silver/silver chloride nanoparticles during anaerobic treatment of wastewater and post-processing of sewage sludge. *Environ. Pollut.* **2013,** *176*, (0), 193-197.

3. Ma, R.; Levard, C.; Judy, J. D.; Unrine, J. M.; Durenkamp, M.; Martin, B.; Jefferson, B.; Lowry, G. V., Fate of Zinc Oxide and Silver Nanoparticles in a Pilot Wastewater Treatment Plant and in Processed Biosolids. *Environ. Sci. Technol.* **2013,** *48*, (1), 104-112.

4. Choi, O.; Deng, K. K.; Kim, N.-J.; Ross, L.; Surampalli, R. Y.; Hu, Z., The inhibitory effects of silver nanoparticles, silver ions, and silver chloride colloids on microbial growth. *Water Res.* **2008,** *42*, (12), 3066-3074.

5. Kim, B.; Park, C.-S.; Murayama, M.; Hochella, M. F., Discovery and characterization of silver sulfide nanoparticles in final sewage sludge products. *Environ. Sci. Technol.* **2010,** *44*, (19), 7509-7514.

6. EPA, Standards for the Use or Disposal of Sewage Sludge; Final Rules In *40 CFR Part 257*, Agency, E. P., Ed. Code of Federal Regulations, 1993.

7. Gardea-Torresdey, J. L.; Rico, C. M.; White, J. C., Trophic Transfer, Transformation, and Impact of Engineered Nanomaterials in Terrestrial Environments. *Environ. Sci. Technol.* **2014,** *48*, (5), 2526-2540.

8. Hirsch, M. P., Availability of sludge-borne silver to agricultural crops. *Environ. Toxicol. Chem.* **1998,** *17*, (4), 610-616.

9. Fabrega, J.; Fawcett, S. R.; Renshaw, J. C.; Lead, J. R., Silver Nanoparticle Impact on Bacterial Growth: Effect of pH, Concentration, and Organic Matter. *Environ. Sci. Technol.* **2009,** *43*, (19), 7285-7290.

10. Yang, X.; Gondikas, A. P.; Marinakos, S. M.; Auffan, M.; Liu, J.; Hsu-Kim, H.; Meyer, J. N., Mechanism of Silver Nanoparticle Toxicity Is Dependent on Dissolved Silver and Surface Coating in *Caenorhabditis elegans*. *Environ. Sci. Technol.* **2012,** *46*, (2), 1119-1127.

11. Kim, Y. S.; Kim, J. S.; Cho, H. S.; Rha, D. S.; Kim, J. M.; Park, J. D.; Choi, B. S.; Lim, R.; Chang, H. K.; Chung, Y. H.; Kwon, I. H.; Jeong, J.; Han, B. S.; Yu, I. J., Twenty-Eight-Day Oral Toxicity, Genotoxicity, and Gender-Related Tissue Distribution of Silver Nanoparticles in Sprague-Dawley Rats. *Inhal. Toxicol.* **2008,** *20*, (6), 575-583.

12. Ma, X.; Geisler-Lee, J.; Deng, Y.; Kolmakov, A., Interactions between engineered nanoparticles (ENPs) and plants: phytotoxicity, uptake and accumulation. *Sci. Total Environ.* **2010,** *408*, (16), 3053-61.

13. Yin, L.; Cheng, Y.; Espinasse, B.; Colman, B. P.; Auffan, M.; Wiesner, M.; Rose, J.; Liu, J.; Bernhardt, E. S., More than the ions: the effects of silver nanoparticles on Lolium Multiflorum. *Environ. Sci. Technol.* **2011,** *45*, (6), 2360-2367.

14. Dimkpa, C. O.; McLean, J. E.; Martineau, N.; Britt, D. W.; Haverkamp, R.; Anderson, A. J., Silver Nanoparticles Disrupt Wheat (*Triticum aestivum* L.) Growth in a Sand Matrix. *Environ. Sci. Technol.* **2013,** *47*, (2), 1082-1090.

15. Lee, W.-M.; Kwak, J. I.; An, Y.-J., Effect of silver nanoparticles in crop plants Phaseolus radiatus and Sorghum bicolor: Media effect on phytotoxicity. *Chemosphere* **2012,** *86*, (5), 491-499.

16. Nam, D.-H.; Lee, B.-c.; Eom, I.-c.; Kim, P.; Yeo, M.-K., Uptake and bioaccumulation of titanium- and silver-nanoparticles in aquatic ecosystems. *Mol. Cell. Toxicol.* **2014,** *10*, (1), 9-17.

17. Musante, C.; White, J. C., Toxicity of silver and copper to Cucurbita pepo: Differential effects of nano and bulk-size particles. *Environ. Toxicol.* **2012,** *27*, (9), 510-517.

18. Pokhrel, L. R.; Dubey, B., Evaluation of developmental responses of two crop plants exposed to silver and zinc oxide nanoparticles. *Sci. Total Environ.* **2013,** *452–453*, (0), 321-332.

19. Wang, J.; Koo, Y.; Alexander, A.; Yang, Y.; Westerhof, S.; Zhang, Q.; Schnoor, J. L.; Colvin, V. L.; Braam, J.; Alvarez, P. J. J., Phytostimulation of Poplars and Arabidopsis Exposed to Silver Nanoparticles and Ag+ at Sublethal Concentrations. *Environ. Sci. Technol.* **2013,** *47*, (10), 5442-5449.

20. Gardea-Torresdey, J. L.; Gomez, E.; Peralta-Videa, J. R.; Parsons, J. G.; Troiani, H.; Jose-Yacaman, M., Alfalfa sprouts: A natural source for the synthesis of silver nanoparticles. *Langmuir* **2003,** *19*, (4), 1357-1361.

21. Gardea-Torresdey, J. L.; Parsons, J. G.; Gomez, E.; Peralta-Videa, J.; Troiani, H. E.; Santiago, P.; Yacaman, M. J., Formation and Growth of Au Nanoparticles inside Live Alfalfa Plants. *Nano Letters* **2002,** *2*, (4), 397-401.

22. Marchiol, L.; Mattiello, A.; Poscic, F.; Giordano, C.; Musetti, R., In vivo synthesis of nanomaterials in plants: location of silver nanoparticles and plant metabolism. *Nanoscale Res. Lett.* **2014,** *9*, (1), 101.

23. Lukman, A. I.; Gong, B.; Marjo, C. E.; Roessner, U.; Harris, A. T., Facile synthesis, stabilization, and anti-bacterial performance of discrete Ag nanoparticles using Medicago sativa seed exudates. *J. Colloid Interf. Sci.* **2011,** *353*, (2), 433-444.

24. Prasad, M. N. V.; Sajwan, K. S.; Naidu, R., *Trace elements in the environment : biogeochemistry, biotechnology, and bioremediation*. Boca Raton: CRC/Taylor and Francis, 2006.

25. Huang, X.; Chaparro, J. M.; Reardon, K. F.; Zhang, R.; Shen, Q.; Vivanco, J. M., Rhizosphere interactions: root exudates, microbes and microbial communities. *Botany* **2014**.

26. Zhang, P.; Ma, Y. H.; Zhang, Z. Y.; He, X.; Guo, Z.; Tai, R. Z.; Ding, Y. Y.; Zhao, Y. L.; Chai, Z. F., Comparative toxicity of nanoparticulate/bulk Yb_2O_3 and $YbCl_3$ to cucumber (*Cucumis sativus*). *Environ. Sci. Technol.* **2012,** *46*, (3), 1834-1841.

27. Battke, F.; Leopold, K.; Maier, M.; Schmidhalter, U.; Schuster, M., Palladium exposure of barley: Uptake and effects. *Plant Biol.* **2008,** *10*, (2), 272-276.

28. Wang, P.; Menzies, N. W.; Lombi, E.; McKenna, B. A.; Johannessen, B.; Glover, C. J.; Kappen, P.; Kopittke, P. M., Fate of ZnO Nanoparticles in Soils and Cowpea (Vigna unguiculata). *Environ. Sci. Technol.* **2013,** *47*, (23), 13822-13830.

29. Zhao, L.; Peralta-Videa, J. R.; Ren, M.; Varela-Ramirez, A.; Li, C.; Hernandez-Viezcas, J. A.; Aguilera, R. J.; Gardea-Torresdey, J. L., Transport of Zn in a sandy loam soil treated with ZnO NPs and uptake by corn plants: Electron microprobe and confocal microscopy studies. *Chem. Eng. J.* **2012,** *184*, (0), 1-8.

30. Zhao, L.; Peralta-Videa, J. R.; Varela-Ramirez, A.; Castillo-Michel, H.; Li, C.; Zhang, J.; Aguilera, R. J.; Keller, A. A.; Gardea-Torresdey, J. L., Effect of surface coating and organic matter on the uptake of CeO2 NPs by corn plants grown in soil: Insight into the uptake mechanism. *J. Hazard. Mater.* **2012,** *225–226*, (0), 131-138.

31. Servin, A. D.; Castillo-Michel, H.; Hernandez-Viezcas, J. A.; Diaz, B. C.; Peralta-Videa, J. R.; Gardea-Torresdey, J. L., Synchrotron Micro-XRF and Micro-XANES Confirmation of the Uptake and Translocation of TiO2 Nanoparticles in Cucumber (Cucumis sativus) Plants. *Environ. Sci. Technol.* **2012,** *46*, (14), 7637-7643.

32. Lin, D.; Xing, B., Root Uptake and Phytotoxicity of ZnO Nanoparticles. *Environ. Sci. Technol.* **2008,** *42*, (15), 5580-5585.

33. Dimkpa, C. O.; McLean, J. E.; Britt, D. W.; Anderson, A. J., CuO and ZnO nanoparticles differently affect the secretion of fluorescent siderophores in the beneficial root colonizer, *Pseudomonas chlororaphis* O6. *Nanotoxicology* **2012,** *6*, (6), 635-642.

34. Cornelis, G.; Hund-Rinke, K.; Kuhlbusch, T.; Van den Brink, N.; Nickel, C., Fate and Bioavailability of Engineered Nanoparticles in Soils: A Review. *Crit. Rev. Environ. Sci. Technol.* **2014,** *44*, (24), 2720-2764.

35. Ratte, H. T., Bioaccumulation and toxicity of silver compounds: A review. *Environ. Toxicol. Chem.* **1999,** *18*, (1), 89-108.

36. Liu, J.; Wang, Z.; Liu, F. D.; Kane, A. B.; Hurt, R. H., Chemical transformations of nanosilver in biological environments. *ACS Nano.* **2012,** *6*, (11), 9887-9899.

37. Levard, C.; Hotze, E. M.; Colman, B. P.; Dale, A. L.; Truong, L.; Yang, X. Y.; Bone, A. J.; Brown, G. E.; Tanguay, R. L.; Di Giulio, R. T.; Bernhardt, E. S.; Meyer, J. N.; Wiesner, M. R.; Lowry, G. V., Sulfidation of Silver Nanoparticles: Natural Antidote to Their Toxicity. *Environ. Sci. Technol.* **2013,** *47*, (23), 13440-13448.

38. Reinsch, B. C.; Levard, C.; Li, Z.; Ma, R.; Wise, A.; Gregory, K. B.; Brown, G. E.; Lowry, G. V., Sulfidation of Silver Nanoparticles Decreases Escherichia coli Growth Inhibition. *Environ. Sci. Technol.* **2012,** *46*, (13), 6992-7000.

39. Levard, C.; Hotze, E. M.; Lowry, G. V.; Brown, G. E., Environmental Transformations of Silver Nanoparticles: Impact on Stability and Toxicity. *Environ. Sci. Technol.* **2012,** *46*, (13), 6900-6914.

40. Colman, B. P.; Arnaout, C. L.; Anciaux, S.; Gunsch, C. K.; Hochella, M. F., Jr.; Kim, B.; Lowry, G. V.; McGill, B. M.; Reinsch, B. C.; Richardson, C. J.; Unrine, J. M.; Wright, J. P.; Yin, L.; Bernhardt, E. S., Low Concentrations of Silver Nanoparticles in Biosolids Cause Adverse Ecosystem Responses under Realistic Field Scenario. *PLoS ONE* **2013,** *8*, (2), e57189.

41. Lowry, G. V.; Espinasse, B. P.; Badireddy, A. R.; Richardson, C. J.; Reinsch, B. C.; Bryant, L. D.; Bone, A. J.; Deonarine, A.; Chae, S.; Therezien, M.; Colman, B. P.; Hsu-Kim, H.; Bernhardt, E. S.; Matson, C. W.; Wiesner, M. R., Long-Term Transformation and Fate of Manufactured Ag Nanoparticles in a Simulated Large Scale Freshwater Emergent Wetland. *Environ. Sci. Technol.* **2012,** *46*, (13), 7027-7036.

42. Liu, J.; Pennell, K. G.; Hurt, R. H., Kinetics and mechanisms of nanosilver oxysulfidation. *Environ. Sci. Technol.* **2011,** *45*, (17), 7345-7353.

43. Hoagland, D. R.; Arnon, D. I., The water-culture method for growing plants without soil. . *Circular. California Agricultural Experiment Station* **1950,** *347*, 3.

44. Umeda, Y.; Kojima, C.; Harada, A.; Horinaka, H.; Kono, K., PEG-Attached PAMAM Dendrimers Encapsulating Gold Nanoparticles: Growing Gold Nanoparticles in the Dendrimers for Improvement of Their Photothermal Properties. *Bioconjugate Chemistry* **2010,** *21*, (8), 1559-1564.

45. Nghiem, L. D.; Schäfer, A. I.; Elimelech, M., Pharmaceutical Retention Mechanisms by Nanofiltration Membranes. *Environ. Sci. Technol.* **2005,** *39*, (19), 7698-7705.

46. Hall, J. L.; Hawes, C. R., *Electron Microscopy of Plant Cells*. Academic Press: London, UK & San Diego CS, USA, 1991.

47. Paiva, É.; Pinho, S.; Oliveira, D., Large Plant Samples: How to Process for GMA Embedding? In *Light Microscopy*, Chiarini-Garcia, H.; Melo, R. C. N., Eds. Humana Press: 2011; Vol. 689, pp 37-49.

48. Hülskamp, M.; Schwab, B.; Grini, P.; Schwarz, H., Transmission Electron Microscopy (TEM) of Plant Tissues. *Cold Spring Harbor protocols* **2010,** *2010*, (7), pdb.prot4958.

49. Wang, X.; Zhang, S.; Zhang, Z., Synthesis of hexagonal nanosized silver sulfide at room temperature. *Mater. Chem. Phys.* **2008,** *107*, (1), 9-12.

50. Colman, B. P.; Espinasse, B.; Richardson, C. J.; Matson, C. W.; Lowry, G. V.; Hunt, D. E.; Wiesner, M. R.; Bernhardt, E. S., Emerging Contaminant or an Old Toxin in Disguise? Silver Nanoparticle Impacts on Ecosystems. *Environ. Sci. Technol.* **2014,** *48*, (9), 5229-5236.

51. Harris, A.; Bali, R., On the formation and extent of uptake of silver nanoparticles by live plants. *J. Nanopart. Res.* **2008,** *10*, (4), 691-695.

52. Stampoulis, D.; Sinha, S. K.; White, J. C., Assay-Dependent Phytotoxicity of Nanoparticles to Plants. *Environ. Sci. Technol.* **2009,** *43*, (24), 9473-9479.

53. Wang, P.; Menzies, N. W.; Lombi, E.; Sekine, R.; Blamey, F. P.; Hernandez-Soriano, M. C.; Cheng, M.; Kappen, P.; Peijnenburg, W. J.; Tang, C.; Kopittke, P. M., Silver sulfide nanoparticles (AgS-NPs) are taken up by plants and are phytotoxic. *Nanotoxicology* **2015**, 1-9.

54. Collin, B.; Doelsch, E.; Keller, C.; Cazevieille, P.; Tella, M.; Chaurand, P.; Panfili, F.; Hazemann, J.-L.; Meunier, J.-D., Evidence of sulfur-bound reduced copper in bamboo exposed to high silicon and copper concentrations. *Environ. Pollut.* **2014,** *187*, 22-30.

55. Jozefczak, M.; Keunen, E.; Schat, H.; Bliek, M.; Hernández, L. E.; Carleer, R.; Remans, T.; Bohler, S.; Vangronsveld, J.; Cuypers, A., Differential response of Arabidopsis leaves and

roots to cadmium: Glutathione-related chelating capacity vs antioxidant capacity. *Plant Physiology and Biochemistry* **2014,** *83*, 1-9.

56. Dimkpa, C. O.; McLean, J. E.; Martineau, N.; Britt, D. W.; Haverkamp, R.; Anderson, A. J., Silver Nanoparticles Disrupt Wheat (Triticum aestivum L.) Growth in a Sand Matrix. *Environ. Sci. Technol.* **2012,** *47*, (2), 1082-1090.

57. Gaff, D.; Chamllers, T.; Maekus, K., Studies of Extrafascicular Movement of Water in the Leaf. *Aust. J. Biol. Sci.* **1964,** *17*, (3), 581-586.

58. Gardea-Torresdey, J. L.; Gomez, E.; Peralta-Videa, J. R.; Parsons, J. G.; Troiani, H.; Jose-Yacaman, M., Alfalfa Sprouts: A Natural Source for the Synthesis of Silver Nanoparticles. *Langmuir* **2003,** *19*, (4), 1357-1361.

59. Wu, J.-W.; Shi, Y.; Zhu, Y.-X.; Wang, Y.-C.; Gong, H.-J., Mechanisms of Enhanced Heavy Metal Tolerance in Plants by Silicon: A Review. *Pedosphere* **2013,** *23*, (6), 815-825.

60. Ma, J. F.; Yamaji, N., Silicon uptake and accumulation in higher plants. *Trends Plant Sci.* **2006,** *11*, (8), 392-397.

61. Zhang, C.; Wang, L.; Nie, Q.; Zhang, W.; Zhang, F., Long–term effects of exogenous silicon on cadmium translocation and toxicity in rice (*Oryza sativa* L.). *Environ. Exp. Bot.* **2008,** *62*, (3), 300-307.

62. Schaller, J.; Brackhage, C.; Paasch, S.; Brunner, E.; Baucker, E.; Dudel, E. G., Silica uptake from nanoparticles and silica condensation state in different tissues of *Phragmites australis*. *Sci. Total Environ.* **2013,** *442*, 6-9.

Chapter 3

Uptake and Distribution of Silver in the Aquatic Plant *Landoltia punctata* (Duckweed) Exposed to Silver and Silver Sulfide Nanoparticles[1]

3.0 Abstract

Wetland ecosystems are exposed to Ag^0 and Ag_2S nanoparticles (NPs) through waste streams such as run-off from crops grown in soils amended with NP contaminated biosolids. Interactions between engineered nanoparticles and aquatic plants in wetlands can affect their fate in fresh water ecosystems, but there is limited data available on these interactions. This study investigates the speciation and distribution of silver in duckweed (*Landoltia punctata*) exposed to silver and silver sulfide NPs at 10 mg/L total silver. The silver distribution in the root tissue was visualized using synchrotron-based micro X-ray fluorescence (XRF) mapping. The Ag speciation was determined using extended X-ray absorption fine structure (EXAFS) spectroscopy. The mass of silver measured in roots exposed to Ag_2S-NPs was the same at for roots exposed to Ag^0-NPs despite an order of magnitude lower solubility of Ag_2S-NPs compared to Ag^0-NPs. Moreover, the distribution of silver in NP exposed plants was more heterogeneous compared to the silver ion control. This indicates that attachment of NPs to the root surface controlled silver exposure rather than dissolution. Silver NPs were partially transformed into silver sulfide and silver thiol species, suggesting that dissolution at the root interface occurs.

[1] To be submitted to *Environmental Science and Technology*. Coauthors include Benjamin P. Colman, Fabienne Schwab, Mark R. Wiesner, and Gregory V. Lowry

Ag_2S-NPs were more resistant to change, and remained primarily as Ag_2S, while Ag ion exposure led to creation of both Ag^0-NPs and Ag_2S in plant tissues. These findings indicate that the form of the Ag NP exposed to plants, and exposure time affects its distribution in aquatic plants, and that Ag is labile and available to duckweed, even when added as relatively insoluble Ag_2S-NPs.

3.1. Introduction

Engineered nanomaterials (ENMs) are an emerging class of pollutants in aquatic ecosystems. These ENMs can be released to ecosystems either directly, *e.g.* in waste water effluent, or indirectly, *e.g.* through the erosion of land-applied biosolids.[1-3] Especially nanosilver (Ag^0-NPs)—used as an antibiotic in many commercial nano-enabled products—that can be toxic to aquatic[4] and terrestrial organisms.[5,6] Understanding the environmental fate of these ENMs is needed to better characterize environmental exposures to Ag^0-NPs. However, most ENMs including Ag^0-NPs are subject to a complex range of transformations, which can influence their toxicity, solubility, fate, and transport, and which is currently not fully understood.[2,3,7-12] While Ag_2S-NPs are much less toxic and soluble[6,13,14] than metallic silver ENMs, transformations between Ag_2S, Ag^+ and Ag^0, and formation of new Ag^0-NPs can occur under environmentally relevant conditions.[15,16] In terrestrial environments in contact with treated wastewater and biosolids, most of the Ag^0-NPs, much alike other metal nanoparticles, *e.g.* ZnO-NPs, can be transformed into their less reactive metal sulfide equivalents (Ag_2S-NPs, ZnS-NPs, etc.).[17-20] In the case of silver, Ag_2S can account for more than 90% of the Ag in the wastewater treatment plant biosolids.[13,20] In aquatic environments such as wetlands, the dissolution and precipitation

dynamics of Ag^0-NPs is highly complex,[15] and the factors that influence ENM interactions with aquatic plants remain poorly characterized.[21]

Plants have central functions in aquatic ecosystems. Plants provide food, moderate flow regimes, drive ecosystem biogeochemistry through production of oxygen, remove (excess) nutrients, and they are strongly involved in metal and ENM cycling.[21-24] In aquatic plants, ENMs are expected to adsorb onto the surface as well as be taken up into tissues of exposed plants.[25,26] Although smaller particles are generally more rapidly internalized by plants, the type of plant, ENM composition, exposure conditions and many other factors can influence if and how readily ENMs are incorporated into plant tissues.[21,25,27,28] For example, plants are known to take up both dissolved metals and nanoparticles, with some evidence of dissolved metals entering more readily.[29] This suggests that the solubility of a metal or metal oxide nanomaterial could greatly affect the amount, pathway, and rate of metal uptake. Highly soluble ENMs are expected to dissolve, yielding greater uptake and translocation than less soluble ENMs that tend to attach to the outsides of the roots, or be taken up as intact nanoparticles, much alike it was observed in a terrestrial plant (alfalfa) exposed to soluble and insoluble Ag-NP species.[27]

Individual species in several different genera of small floating aquatic plants (*Lemna*, *Landoltia*, and *Spirodella*; also termed "duckweeds") are common model organisms to assess the toxicity of contaminants,[30] and they have been used to assess the toxicity of Ag^0-NPs.[31] Their small size, rapid growth rate, and propensity for accumulating large concentrations of metals also make them ideal for both studies on the fate and transport of metal and metal oxide ENMs. Moreover, duckweeds are promising potential tools for (ENM) phytoremediation.[32,33] With this

in mind, the goal of the present study was to elucidate the interaction mechanism of duckweed with ENMs, adding to the limited data available on the interactions of ENMs with aquatic plants. We assessed the pathway and extent of uptake of silver NP species by the aquatic plant *Landoltia punctata* (termed duckweed throughout the rest of the text). The specific goals were to a) determine the differences in uptake of Ag^{+}, Ag^{0}-NPs and Ag_2S-NPs in the duckweed species *Landoltia punctata*, and b) qualitatively elucidate and compare the speciation and route of uptake of these forms into the tissues of exposed plants. We used X-ray based mapping and speciation techniques to investigate the Ag uptake, distribution and speciation of silver associated with duckweed tissue.

3.2. Materials and Methods

3.2.1 Synthesis

Polyvinylpyrrolidone (PVP) coated Ag^{0}-NPs were synthesized based on a protocol of Yang and co-workers,[34] and a part of these Ag^{0}-NPs was oxidized to Ag_2S-NPs as described by Reinsch and co-workers,[35] and adapted elsewhere.[27] In brief, 1.5g of PVP (1000 g/mol) was dissolved in 280 mL of deionized water before stirring in 9 mL of 0.10M $AgNO_3$ for 5 minutes. Under constant stirring, 11 mL of ice-cold 0.08M $NaBH_4$ was added, allowed to react for 1 hour, and washed as described below, resulting in the final stock suspension of Ag^{0}-NPs.[27] The Ag_2S-NPs were synthesized from a second batch of Ag^{0}-NPs by adding 9 mL of 0.10 M Na_2S into an aqueous suspension of Ag^{0}-NPs bubbled with aquarium air pumps (AP 200, Tetratec, China) to provide dissolved oxygen, and allowed to react for one week before washing. Both NP suspensions were washed three times using ultracentrifugation (50,000× g for 30 min) and

resuspension in deionized water using a sonicating probe (Sonic Dismembrator Model 550, Fisher Scientific, USA, power level 3, 1 min). Washed suspensions were stored at 4 ºC until use.

3.2.2 Characterization

Two batches of each type of NP (Ag^0 and Ag_2S) were synthesized (once for each exposure corresponding to the synchrotron schedule). Only the first batch of washed Ag^0-NPs and Ag_2S-NPs were sampled for TEM and XRD characterization of the NPs, while the second batch was analyzed via DLS to ensure similarity between batches. The crystalline phase was verified by X-ray diffraction (XRD) of an air-dried sample using an X-Radia XRD (X'Pert Pro MPD X-ray diffractometer with a Cu X-ray source). The XRD spectra were background-subtracted and peak-matched using X'pert Highscore Plus software. The morphology and diameter of the NPs were determined by Transmission Electron Microscopy (TEM) imaging of samples dried on formvar coated copper grids using a TECNAI G^2 Twin (FEI, Hillsboro OR, USA). The hydrodynamic diameter and zeta potential, calculated using the Smoluchowski equation, of the NPs was also determined in 10 ppm Ag^0-NP suspension in half strength Hutner's solution using an ALV/CGS-3 (ALV, Germany) and a Zetasizer Nano ZS (Malvern, UK), respectively. The hydrodynamic diameter was measured at t=0 and again after 48 hours in the growth chamber exposed to cool fluorescent light (see below) to assess the stability of the NPs against aggregation in the growth media. Finally, the soluble fraction of silver was determined in the suspensions after 48 hours in half strength Hutner's medium using a 3 kDa centrifuge filter to separate the particles from the dissolved species.

3.2.3 Exposure of Duckweed to Ag^0 and Ag_2S Nanoparticles

Two batches of semi-sterile cultures of duckweed (*Landoltia puctata*) were stabilized in half strength Hutner's medium and exposed to the NPs using a method adapted from Brain et al. 2007,[36] one for the XRF mapping and another for the EXAFS analysis. Twenty specimens of *Landoltia punctata*, each containing 3 developed fronds (a mother and two 1st-generation daughter fronds) were exposed in 25 mL plastic petri dishes (Appendix B, Figure B.1). To prepare the exposure medium, suspensions of Ag^0-NPs, Ag_2S-NPs or $AgNO_3$ were added to 20mL of growth medium to achieve 10 ppm total silver concentration. Dishes were placed in a reflective aluminum tray and covered with another aluminum tray which had holes cut for the two cool fluorescent lights placed approximately 6 inches from the samples (Figure B.1). The cultures were harvested 24 hours after exposure, and immediately rinsed by lightly agitating the cultures in two consecutive petri dishes containing DI water using a sterile fork. This was done to remove any loosely bound particles and any ionic silver associated with the exposure media. Several specimens were collected after 24 and 60 hours of exposure, and prepared by sealing fresh plant tissue inside plastic sample holders with DI water sealed within Kapton tape to keep them hydrated during XRF mapping. Additional tissue samples were immediately frozen in liquid nitrogen and lyophilized for x-ray absorption spectroscopy (XAS) analysis to determine Ag speciation, and a portion was digested in concentrated nitric acid for 24 hours on an end-over-end rotator and was then used for total Ag analysis by ICP-MS after dilution with DI water to 5% nitric acid and analyzed using a 5-point single element (Ag) calibration standard. The exposure medium was also collected and analyzed for total silver to determine the fraction of added silver that was associated with the plant tissues and to calculate a mass balance for silver.

3.2.4 Silver Speciation

The Ag speciation in the freeze dried tissues was investigated by pressing the tissue into pellets and analyzed by Ag K-edge XAS. Extended x-ray absorption fine structure (EXAFS) spectra were collected on beamline 11-2 at Stanford Synchrotron Radiation Lightsource (SSRL). The Si(111) crystal monochromator was calibrated by setting the first inflection of the Ag K-edge of the Ag reference foil to 25,514 eV. The monochromator was detuned to 75% of its maximum to reduce harmonics and the spectra for the exposed duckweed samples were collected in fluorescence mode using a 100-element solid state Ge detector. To ensure good energy calibration, the spectra of the reference Ag foil was simultaneously collected in transmission mode between ion chambers filled with Ar.

All spectra were analyzed using the Athena software package.[37] Background was corrected and the E_0 set to 25,534 eV. The sample spectra were fitted by linear combination fitting (LCF) of averaged k^3- weighted EXAFS spectra. The EXAFS data was fitted over 3-9.5 $Å^{-1}$ K-range using a variety of Ag model compounds.[35] A complete list of the model compounds used is presented in Table B.1 (Appendix B). The fits were not constrained to 100% and utilized the cycle-fit method: finding the best 1-component fit, and adding another component if the R-factor is decreased by 10% through addition of that compound. The R-factor is a goodness-of-fit parameter and lower values indicate better fits; although this parameter depends on the fitting range, a 10% decrease is used to indicate a significant improvement to the fit when principal component analysis (PCA) and target transform (TT) are not possible due to the low number of samples.

3.2.5 Silver Distribution

To spatially resolve the silver in the duckweed plant tissue, synchrotron XRF microprobe mapping was conducted on the IDE-13 beamline at APS. The incident beam with an excitation energy of 28,000 eV to maximize the silver K-edge fluorescence signal. This produced a 2.5x2.5 μm beam which was scanned across the root tip with a 2 μm step size and 20 ms dwell time. A 4-element vortex silicon drift detector was placed normal to the incident beam with the sample mounted in the 45-degree geometry. Signals from Ag and Zn were calibrated using standards and integrated from the multiple channel analysis by fitting the K-edge fluorescence peaks. The signals from each element were normalized with I_0 to produce element specific maps. Silver specific maps were obtained using the Ag K-α emission line (22,163 eV) and processed with the X-ray Data Browser software provided by APS. Zinc specific maps are shown in the Figure B.2 in Appendix B.

3.3. Results and Discussion

3.3.1 Characterization

The NP characterization including the hydrodynamic diameters and the zetapontential measured in the half strength Hutner's growth media, the TEM diameters, and the diffraction analysis (XRD) are provided in Table 3.1. The crystalline phases identified by XRD were BCC metallic silver in the Ag^0-NP and acanthite (Ag_2S) in the Ag_2S-NP, suggesting that complete sulfidation had been achieved with the sulfidation method used. The particles were spheroidal, with primary particle sizes determined by TEM of 6.3 and 7.8 nm for the Ag^0-NPs and Ag_2S-NPs, respectively (Appendix B, Figure B.3). The number-averaged hydrodynamic diameter of

the freshly prepared and 0.2μm filtered Ag^0-NP and Ag_2S-NP in half strength Hutner's media determined by DLS was found to be 13.4±2.9 and 17.9±2.4 nm for the respectively. The hydrodynamic diameter determined in half strength Hutner's media is larger than TEM likely due to the presence of an electron transparent PVP coating invisible in TEM, and potentially also due to aggregation. However, the particle size was found to be relatively constant after two days in the growth medium 14.4±4.0 and 20.3±0.6nm for the Ag^0-NPs and Ag_2S-NPs, respectively. An example of the size distribution and autocorrelation function are provided in Figure B.4 (Appendix B). Because ion uptake is known to be a major pathway of metal uptake; the solubility of the NPs is expected to influence the uptake of silver. The soluble fraction of silver after two days in half strength Hutner's medium was 0.53 and 0.06 ppm soluble silver for the 10 ppm suspension of Ag^0-NPs and Ag_2S-NPs, respectively. This is consistent with expectations and previous finding showing that Ag_2S is the less soluble form of the silver NPs.[27,38-40] The three treatments ($AgNO_3$, Ag^0, Ag_2S) spanned three orders of magnitude of soluble silver which will highlight the differences between ion and NP uptake into the plants.

Table 3.1. Characterization of freshly prepared Ag^0 and Ag_2S nanoparticles and after exposure to half strength Hutner's medium. Soluble silver was the fraction of silver in half strength Hunter's medium without plants than passed a 3kDa filter after 2 days.

	Hydrodynamic Diameter (nm)[c]		**Zeta Potential (mV)**	**Soluble Ag (ppm)**	**TEM size (nm)[a,b]**	**XRD Phase[a]**
Media	1/2 Hutners	1/2 Hutners	1/2 Hutners	1/2 Hutners		
Exp. Time	0 day	2 day	0 day	2 day	-	-
Ag^0-NP	13.4±2.9	14.0±4.0	-11.5±4.8	5.3	6.3±6.2	Silver Metal
Ag_2S-NP	17.9±2.4	20.3±0.6	-10.2±3.8	0.6	7.8±2.2	Acanthite

[a]Data were reproduced from Stegemeier et al. 2015[27] as these are the same NPs used in that study. [b]Mean plus/minus standard deviation. [c]Number-weighted (primary peak >99% of total weight) averaged particle size distribution ± peak width from samples filtered with 0.2um cellulose filter.

3.3.2 Silver Concentrations in Tissue

Total silver concentrations associated with the bulk lyophilized duckweed tissue exposed to either Ag_2S-NPs, Ag^0-NPs or $AgNO_3$ were measured after 24 hours. Total silver is presumed to include both silver attached onto the exterior of the plants and internalized silver. The silver concentrations in the duckweed exposed to Ag_2S-NPs and Ag^0-NPs were found to be very similar, 372±6 and 389±3 ppm Ag respectively. The plants exposed to $AgNO_3$ contained nearly twice the silver concentration (685 ±6 ppm Ag) as the NP exposed samples. Clearly, the ions were more readily accessible than the particulate forms of Ag. However, the silver concentrations of roots exposed to Ag^0 and Ag_2S did not follow the trends in particle solubility: they had similar concentrations of silver despite the factor of 10 lower solubility of Ag_2S-NPs compared to Ag^0-NPs. This suggests that attachment of particles is likely the primary mode of NP association with duckweed roots. The attachment onto the root surface is expected to be

similar for these two NPs given their similar size, zeta potential and PVP coating. In all cases, only 1-2 % of the total silver added was associated with the plant tissue. The majority of the silver remained in the exposure medium given the low plant mass to medium volume used. While other studies have shown that duckweed can remove >60% of total Zn and Cu within 2 day, the total biomass to metal concentration was much higher in those studies [33]. The silver concentration in the exposed duckweed tissue is similar to the concentrations found in the roots of *Lolium Multiflorum* exposed to similar concentrations of Ag^0-NPs.[41] A total Ag recovery (including plant tissue, exposure media and an aqua regia wash of the exposure vessel) of 75-90% was achieved (data not shown). A bioconcentration factor (BCF) for the one day exposure to 10 ppm Ag was estimated by dividing the wet weight concentration by the exposure concentration, assuming 95% water weight for duckweed.[42] The BCF was ~3 for $AgNO_3$, and ~2 for the NPs, suggesting that duckweed concentrates and accumulates silver in its tissue.

3.3.3 Silver Distribution

Silver Kα XRF maps of hydrated root tips exposed to $AgNO_3$, Ag^0-NPs and Ag_2S-NPs demonstrate clear differences in the distribution of Ag for each type of Ag used (Figure 3.1). Note that each image is color-scaled internally using the highest Ag counts in the image and therefore one should not make direct comparisons between image intensities. The maximum Ag count used to calibrate each image is provided in Table B.2 (Appendix B). Very little silver was detected in the initial Ag specific maps for the fronds compared to the roots (Appendix B, Figure B.5). This conflicts with other reports of metal uptake by duckweed where most of the metal uptake is through the fronds. The difference in behavior is likely to the difference in the species being investigated. Here we are looking at uptake by *Landoltia punctata*, which is known to

uptake metals through the roots.[43,44] Other studies showing uptake primarily by the fronds used *Spirodela polyrhiza, Lemna gibba* and *Lemna minor*.[45-47] Given the absence of metal in the fronds of *Landoltia punctata*, the mapping focused mainly on the silver rich root tips.

After 24 hours of exposure to $AgNO_3$ the silver is distributed throughout the root tip potentially in the apical meristem. The root cap is visible as a blue shadow around the root tip indicating it has adsorbed a relatively smaller portion of silver. This Ag distribution pattern suggests Ag^+ ions are able to migrate into the active zone of root tip and do not appear to be restricted by the root cap. The root tip exposed to Ag^0-NPs for 24h shows a similar distribution of Ag as the silver nitrate exposed samples suggesting the NPs may be dissolving prior to entering the root tip. Additionally, there are clusters of Ag located at the end of the root cap suggesting attachment of a solid silver phase, likely Ag^0-NPs. The primary route of Ag^0-NP uptake into these plant roots appears to be through attachment onto the root surface (root cap), dissolution and internalization of dissolved silver, although direct uptake of NPs is likely also occurring. In contrast to Ag^0, the root tip exposed to Ag_2S-NPs shows a cluster of silver located at the end of the root cap suggesting the silver was not readily internalized. The root cap is visible indicating the presence of Ag throughout the cap, but the absence of silver in the apical meristem suggests that little dissolved silver was able to be internalized after 1 day. Due to the low solubility, the primary route of uptake of Ag_2S-NPs appears to be attachment onto the root surface with the potential of direct NP migration into the plant tissue.

After 60 hours of exposure to $AgNO_3$ the root tip shows many small Ag clusters throughout the root tip primarily located near the apical meristem (Figure 3.1). It is important to

note these are different root samples than the 24 hour images and not a progression from the previous images. The duckweed samples exposed to ionic silver for 60h were visually lighter (turning white) than the other samples suggesting this this level of ionic silver exposure was toxic to the duckweed. Since the reduction, precipitation and sequestration of metals in plant roots are common responses to large doses of dissolved metals, these clusters are likely biogenic silver NPs being sequestered in the plant tissue.[48,49] The root tip exposed to Ag^0-NPs for 60h appears similar to the 24h exposed with silver primarily located at the apical meristem and the presence of discrete clusters adhered to the root cap. Again, this is indicative of NP attachment onto the root surface as well as ionic uptake into the active region of the root tip. The silver associated with the root tip exposed to Ag_2S-NPs for 60h appears to have been internalized with silver in the apical meristem region. The lack of uniformity in the silver distribution suggests limited NP dissolution although the silver from Ag_2S-NPs appears to be bioavailable, which is consistent with other recent studies using different plants.[6,27] Given the limitations of two dimensional maps of three dimensional roots, these maps cannot prove NP internalization but strongly suggests the metals from the NPs are not merely attached onto the surface and have entered the vascular system. XRF maps for metal uptake by plants have previously been modeled and correlated to specific metal distribution in the plant vasculature (e.g. adhered to outside of root vs. internalize into the vasculature). The pattern in our images is consistent with metal uptake into the plant vasculature.[50]

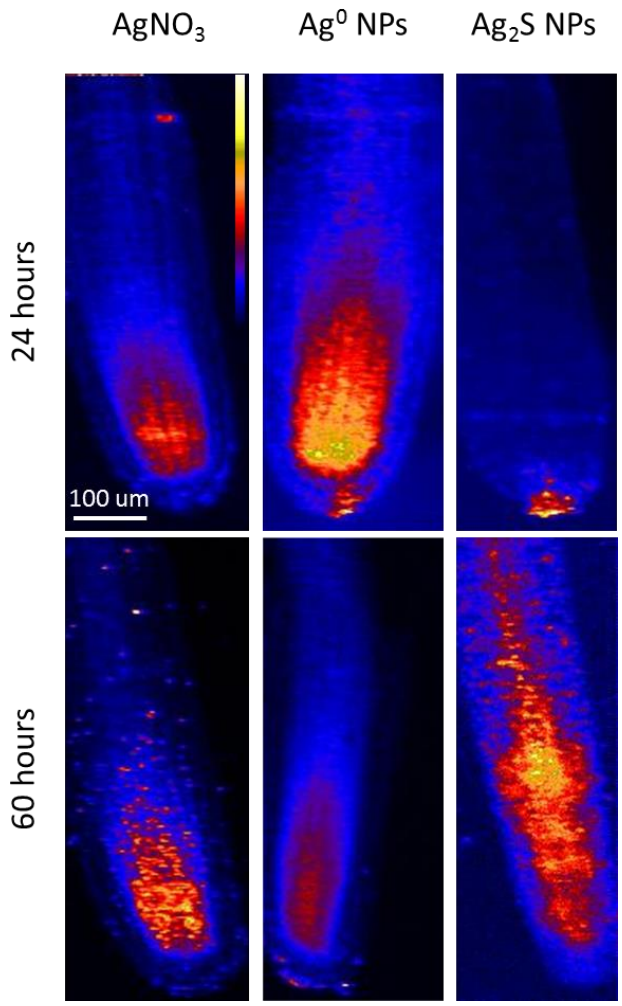

Figure 3.1. Silver Kα XRF maps of fresh duckweed root tips exposed to $AgNO_3$, Ag^0-NPs and Ag_2S-NPs for 24 and 60 hours.

3.3.4 Silver Speciation

Normalized EXAFS spectra and their corresponding fits of the three treatments ($AgNO_3$, Ag^0-NPs, Ag_2S-NPs) show clear differences in the Ag absorption spectra (Figure 3.2). The LCF results are summarized in Table 3.2. We did not force the sums of the EXAFS fits to one, as is often done for Ag EXAFS.[6,38,51] Although all sample spectra fit to combinations of above 100% of the model compounds which may be a result of background removal and normalization procedure, other studies have shown higher than 100% fits in EXAFS combination fitting.[52,53]

However, the phases and relative amplitudes for each fit match well, so it is unlikely that we are missing an important Ag species. The silver associated with the duckweed tissue exposed to silver nitrate was found to be primarily (78%) zero-valent. The EXAFS spectra from this sample is characteristic of metallic silver particles with strong Ag-Ag scattering giving rise to large oscillations k>7.[20] Photoreduction of silver during the beam exposure during the measurement is not likely due to the consistency of multiple scans, the conditions under which the measurements were collected (freeze-dried and 77K), and the absence of reduced silver in the model compounds and the Ag_2S sample. The presence of metallic silver particles is not surprising considering many species of plants have been shown to precipitate metallic Ag-NPs after exposure to ionic silver.[54] It is also possible that metallic silver NPs formed under visible light has also been observed,[15,16] although the uniformity of the silver distribution in the root tip compared to the Ag^0-NPs exposed tips suggest that the predominant for of silver in the solution exposed to the duckweed was ionic silver. The remaining silver in the silver nitrate treatment was sulfur associated; in this case silver sulfide was the best fit. The presence of Ag_2S instead of a thiolated Ag species was unexpected given the known defense mechanisms of plants against oxidative stress via metal toxicity, e.g. glutathione production.[25,55] The Ag-thiol signal may have also been present but was less than 10% of the total silver or was masked by the presence of large oscillations of metallic silver signal.

In contrast to $AgNO_3$, the majority of the silver from the Ag^0-NP treatment consisted of sulfidized species, namely a mixture of Ag_2S (64%) and Ag-thiol (53%). Metallic Ag was also present (16%), due either to direct attachment/uptake of NPs onto/into the duckweed, or due to the in-vivo reduction of ionic silver following the dissolution of the NPs. The different

speciation of Ag from $AgNO_3$ and Ag^0-NP treatments suggests that the duckweed responds to the presence of ions differently than to NPs. However, this difference could simply be a result of the higher concentration of dissolved ions in the $AgNO_3$ exposure compared to the Ag^0-NP exposure where only a fraction of the Ag is present as ions. The $AgNO_3$ exposure may overwhelm the plants ability to combat the presence of Ag (noted from the whitening of the fronds), whereas the plants can respond with glutathione and other sulfide-based defenses against toxicity for the Ag^0-NPs which provide Ag ions at a metered rate.

Based on the bulk EXAFS, silver from the Ag_2S-NP treatment remained as silver sulfide, which suggests that the plant was not able to dissolve or transform a significant amount of the Ag_2S-NPs after 24 h. This is expected for the majority of Ag_2S given its high chemical stability and low solubility. Micro-scale XANES measurements made on hot spots on the Ag_2S exposed root tip generally agree with this speciation (Appendix B, Figure B.6). But, there is also some indication of metallic silver in these most concentrated areas of the root tip. This suggests that the plants may have some capacity to solubilize Ag_2S-NPs at the root surface. However, these micro-scale XANES measurements are made at room temperature and in hydrated plant tissues so photo-reduction of silver to its metallic form cannot be ruled out.[56]

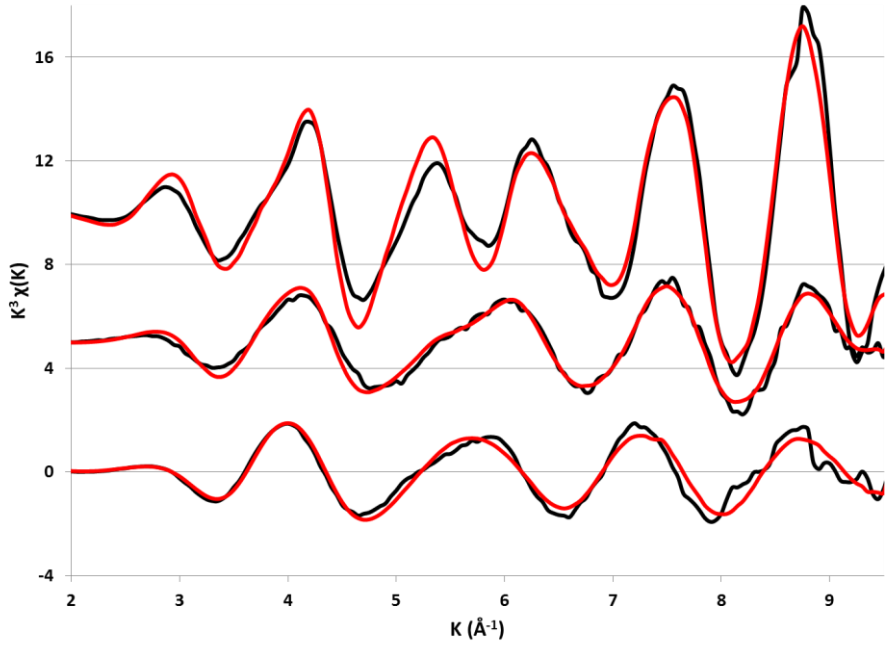

Figure 3.2. Experiential (black) and fitted (red) Ag K-edge EXAFS spectra from lyophilized duckweed tissue exposed to $AgNO_3$ (top), Ag^0-NPs (middle) or Ag_2S-NPs (bottom).

Table 3.2. EXAFS LCF fitting results fit over k of 2-9.5.

	EXAFS Fitting Results				
Treatment	**Ag^0**	**Ag_2S**	**Ag-Thiol**	**Sum**	**R factor**
$AgNO_3$	78%	39%		116%	0.035
Ag^0-NP	16%	64%	53%	132%	0.032
Ag_2S-NP		127%		127%	0.069

3.4. Implications

The findings of this study have a number of important implications regarding the interactions between metallic NPs and the aquatic plants that are essential to ecosystem function.

For hydroponic exposures used here, which is a relevant exposure scenario for floating and submerged aquatic plants, metallic NPs interact with aquatic plants differently than ions of the same metal. Ions are indeed more readily internalized than NPs. Moreover, the Duckweed response to exposures to ions and to NPs appears to be different. These responses appear to be related to the properties of the particles (i.e. dissolution rate), and lead to differences in metal speciation and distribution in the roots after 24 and 60 hours of exposures. These differences in speciation may subsequently affect the health of the plants, and their ability to respond to other chemical insults.

This study also indicates that nanoparticulate phases of metals readily attach to, and are available to aquatic plants. Silver, even in the poorly soluble Ag_2S species, readily attached to the duckweed roots. The attachment strength was more influenced by the particle properties (size, charge, and coating) than by the solubility. Adhered particles are then taken up to some degree into the plant root vasculature, either after being solubilized or as particles. Although comparable amounts of silver were associated with roots for both the Ag^0-NPs and the Ag_2S-NPs, the amount internalized will depend on the speciation. In view of the low solubility of Ag_2S-NPs, this finding suggests that particle uptake is occurring to some extent, and is consistent with other reports of uptake of NPs by duckweed species.[46,57,58] Overall, this confirms that poorly soluble NPs can be internalized into the plant tissue (bioavailable) to some extent.

The use of duckweed for phytoremediation of metals has been proposed.[33] To assess the potential of phytoremediation to remove metal and metal oxide NPs, follow-up studies should focus on more accurate determination of the attachment strength, and attachment and

internalization rate of NPs to duckweed. Studies are also needed to better understand the long term fate of particles as plants continue to grow.

References

1. Gottschalk, F.; Sonderer, T.; Scholz, R. W.; Nowack, B., Modeled environmental concentrations of engineered nanomaterials (TiO_2, ZnO, Ag, CNT, fullerenes) for different regions. *Environ. Sci. Technol.* **2009,** *43*, (24), 9216-9222.

2. Lowry, G. V.; Espinasse, B. P.; Badireddy, A. R.; Richardson, C. J.; Reinsch, B. C.; Bryant, L. D.; Bone, A. J.; Deonarine, A.; Chae, S.; Therezien, M.; Colman, B. P.; Hsu-Kim, H.; Bernhardt, E. S.; Matson, C. W.; Wiesner, M. R., Long-Term Transformation and Fate of Manufactured Ag Nanoparticles in a Simulated Large Scale Freshwater Emergent Wetland. *Environ. Sci. Technol.* **2012,** *46*, (13), 7027-7036.

3. Pradas del Real, A. E.; Castillo-Michel, H.; Kaegi, R.; Sinnet, B.; Magnin, V.; Findling, N.; Villanova, J.; Carrière, M.; Santaella, C.; Fernández-Martínez, A.; Levard, C.; Sarret, G., Fate of Ag-NPs in Sewage Sludge after Application on Agricultural Soils. *Environ. Sci. Technol.* **2016,** *50*, (4), 1759-1768.

4. Navarro, E.; Piccapietra, F.; Wagner, B.; Marconi, F.; Kaegi, R.; Odzak, N.; Sigg, L.; Behra, R., Toxicity of silver nanoparticles to Chlamydomonas reinhardtii. *Environ. Sci. Technol.* **2008,** *42*, (23), 8959-8964.

5. Ratte, H. T., Bioaccumulation and toxicity of silver compounds: A review. *Environ. Toxicol. Chem.* **1999,** *18*, (1), 89-108.

6. Wang, P.; Menzies, N. W.; Lombi, E.; Sekine, R.; Blamey, F. P.; Hernandez-Soriano, M. C.; Cheng, M.; Kappen, P.; Peijnenburg, W. J.; Tang, C.; Kopittke, P. M., Silver sulfide nanoparticles (AgS-NPs) are taken up by plants and are phytotoxic. *Nanotoxicology* **2015**, 1-9.

7. Reidy, B.; Haase, A.; Luch, A.; Dawson, A. K.; Lynch, I., Mechanisms of Silver Nanoparticle Release, Transformation and Toxicity: A Critical Review of Current Knowledge and Recommendations for Future Studies and Applications. *Materials* **2013,** *6*, (6).

8. Starnes, D. L.; Unrine, J. M.; Starnes, C. P.; Collin, B. E.; Oostveen, E. K.; Ma, R.; Lowry, G. V.; Bertsch, P. M.; Tsyusko, O. V., Impact of sulfidation on the bioavailability and toxicity of silver nanoparticles to Caenorhabditis elegans. *Environ. Pollut.* **2015,** *196*, 239-246.

9. Levard, C.; Hotze, E. M.; Colman, B. P.; Dale, A. L.; Truong, L.; Yang, X. Y.; Bone, A. J.; Brown, G. E.; Tanguay, R. L.; Di Giulio, R. T.; Bernhardt, E. S.; Meyer, J. N.; Wiesner, M. R.; Lowry, G. V., Sulfidation of Silver Nanoparticles: Natural Antidote to Their Toxicity. *Environ. Sci. Technol.* **2013,** *47*, (23), 13440-13448.

10. Cornelis, G.; Hund-Rinke, K.; Kuhlbusch, T.; Van den Brink, N.; Nickel, C., Fate and Bioavailability of Engineered Nanoparticles in Soils: A Review. *Crit. Rev. Environ. Sci. Technol.* **2014,** *44*, (24), 2720-2764.

11. Yu, S.-j.; Yin, Y.-g.; Liu, J.-f., Silver nanoparticles in the environment. *Environmental Science: Processes & Impacts* **2013,** *15*, (1), 78-92.

12. Levard, C.; Hotze, E. M.; Lowry, G. V.; Brown, G. E., Environmental Transformations of Silver Nanoparticles: Impact on Stability and Toxicity. *Environ. Sci. Technol.* **2012,** *46*, (13), 6900-6914.

13. Nowack, B., Nanosilver Revisited Downstream. *Science* **2010,** *330*, (6007), 1054-1055.

14. Devi, G. P.; Ahmed, K. B. A.; Varsha, M. K. N. S.; Shrijha, B. S.; Lal, K. K. S.; Anbazhagan, V.; Thiagarajan, R., Sulfidation of silver nanoparticle reduces its toxicity in zebrafish. *Aquat. Toxicol.* **2015,** *158*, 149-156.

15. Badireddy, A. R.; Farner Budarz, J.; Marinakos, S. M.; Chellam, S.; Wiesner, M. R., Formation of Silver Nanoparticles in Visible Light-Illuminated Waters: Mechanism and Possible Impacts on the Persistence of AgNPs and Bacterial Lysis. *Environmental Engineering Science* **2014,** *31*, (7), 338-349.

16. Yu, S.; Yin, Y.; Zhou, X.; Dong, L.; Liu, J., Transformation kinetics of silver nanoparticles and silver ions in aquatic environments revealed by double stable isotope labeling. *Environmental Science: Nano* **2016,** *3*, (4), 883-893.

17. Kim, B.; Park, C.-S.; Murayama, M.; Hochella, M. F., Discovery and characterization of silver sulfide nanoparticles in final sewage sludge products. *Environ. Sci. Technol.* **2010,** *44*, (19), 7509-7514.

18. Brunetti, G.; Donner, E.; Laera, G.; Sekine, R.; Scheckel, K. G.; Khaksar, M.; Vasilev, K.; De Mastro, G.; Lombi, E., Fate of zinc and silver engineered nanoparticles in sewerage networks. *Water Res.* **2015,** *77*, 72-84.

19. Kaegi, R.; Voegelin, A.; Sinnet, B.; Zuleeg, S.; Hagendorfer, H.; Burkhardt, M.; Siegrist, H., Behavior of metallic silver nanoparticles in a pilot wastewater treatment plant. *Environ. Sci. Technol.* **2011,** *45*, (9), 3902-3908.

20. Ma, R.; Levard, C.; Judy, J. D.; Unrine, J. M.; Durenkamp, M.; Martin, B.; Jefferson, B.; Lowry, G. V., Fate of Zinc Oxide and Silver Nanoparticles in a Pilot Wastewater Treatment Plant and in Processed Biosolids. *Environ. Sci. Technol.* **2013,** *48*, (1), 104-112.

21. Thwala, M.; Klaine, S. J.; Musee, N., Interactions of metal-based engineered nanoparticles with aquatic higher plants: A review of the state of current knowledge. *Environ. Toxicol. Chem.* **2016**, n/a-n/a.

22. McNear Jr., D. H., The rhizosphere—roots, soil and everything in between. *Nature Education Knowledge* **2013,** *4*, (3), 1.

23. Vymazal, J., *Algae and Element Cycling in Wetlands*. Lewis Publishers: Boca Raton, USA, 1995.

24. Janauer, G. A.; Schmidt-Mumm, U.; Schmidt, B., Aquatic macrophytes and water current velocity in the Danube River. *Ecological Engineering* **2010,** *36*, (9), 1138-1145.

25. Schwab, F.; Zhai, G.; Kern, M.; Turner, A.; Schnoor, J. L.; Wiesner, M. R., Barriers, Pathways and Processes for Uptake, Translocation, and Accumulation of Nanomaterials in Plants—Critical Review. *Nanotoxicology* **2016,** *10*, (3), 257-278.

26. Glenn, J. B.; White, S. A.; Klaine, S. J., Interactions of gold nanoparticles with freshwater aquatic macrophytes are size and species dependent. *Environ. Toxicol. Chem.* **2012,** *31*, (1), 194-201.

27. Stegemeier, J. P.; Schwab, F.; Colman, B. P.; Webb, S. M.; Newville, M.; Lanzirotti, A.; Winkler, C.; Wiesner, M. R.; Lowry, G. V., Speciation Matters: Bioavailability of Silver and Silver Sulfide Nanoparticles to Alfalfa (*Medicago sativa*). *Environ. Sci. Technol.* **2015,** *49*, (14), 8451-8460.

28. Judy, J. D.; McNear, D. H.; Chen, C.; Lewis, R. W.; Tsyusko, O. V.; Bertsch, P. M.; Rao, W.; Stegemeier, J.; Lowry, G. V.; McGrath, S. P.; Durenkamp, M.; Unrine, J. M., Nanomaterials in Biosolids Inhibit Nodulation, Shift Microbial Community Composition, and Result in Increased Metal Uptake Relative to Bulk/Dissolved Metals. *Environ. Sci. Technol.* **2015,** *49*, (14), 8751-8758.

29. Ebbs, S. D.; Bradfield, S. J.; Kumar, P.; White, J. C.; Musante, C.; Ma, X., Accumulation of zinc, copper, or cerium in carrot (Daucus carota) exposed to metal oxide nanoparticles and metal ions. *Environmental Science: Nano* **2016**.

30. OECD, *Test No. 221: Lemna sp. Growth Inhibition Test*. OECD Publishing.

31. Kim, E.; Kim, S.-H.; Kim, H.-C.; Lee, S.; Lee, S.; Jeong, S., Growth inhibition of aquatic plant caused by silver and titanium oxide nanoparticles. *Toxicol. Environ. Health Sci.* **2011,** *3*, (1), 1-6.

32. Colman, B. P.; Espinasse, B.; Richardson, C. J.; Matson, C. W.; Lowry, G. V.; Hunt, D. E.; Wiesner, M. R.; Bernhardt, E. S., Emerging Contaminant or an Old Toxin in Disguise? Silver Nanoparticle Impacts on Ecosystems. *Environ. Sci. Technol.* **2014,** *48*, (9), 5229-5236.

33. Landesman, L.; Fedler, C.; Duan, R., Plant Nutrient Phytoremediation Using Duckweed. In *Eutrophication: causes, consequences and control*, Ansari, A. A.; Singh Gill, S.; Lanza, R. G.; Rast, W., Eds. Springer Netherlands: Dordrecht, 2011; pp 341-354.

34. Yang, X.; Gondikas, A. P.; Marinakos, S. M.; Auffan, M.; Liu, J.; Hsu-Kim, H.; Meyer, J. N., Mechanism of Silver Nanoparticle Toxicity Is Dependent on Dissolved Silver and Surface Coating in *Caenorhabditis elegans*. *Environ. Sci. Technol.* **2012,** *46*, (2), 1119-1127.

35. Reinsch, B. C.; Levard, C.; Li, Z.; Ma, R.; Wise, A.; Gregory, K. B.; Brown, G. E.; Lowry, G. V., Sulfidation of Silver Nanoparticles Decreases Escherichia coli Growth Inhibition. *Environ. Sci. Technol.* **2012,** *46*, (13), 6992-7000.

36. Brain, R. A.; Solomon, K. R., A protocol for conducting 7-day daily renewal tests with Lemna gibba. *Nat. Protocols* **2007,** *2*, (4), 979-987.

37. Ravel, B.; Newville, M., ATHENA, ARTEMIS, HEPHAESTUS: data analysis for X-ray absorption spectroscopy using IFEFFIT. *J. Synchrotron Radiat.* **2005,** *12*, (4), 537-541.

38. Levard, C.; Reinsch, B. C.; Michel, F. M.; Oumahi, C.; Lowry, G. V.; Brown, G. E., Sulfidation processes of PVP-coated silver nanoparticles in aqueous solution: impact on dissolution rate. *Environ. Sci. Technol.* **2011,** *45*, (12), 5260-5266.

39. Judy, J. D.; Kirby, J. K.; Creamer, C.; McLaughlin, M. J.; Fiebiger, C.; Wright, C.; Cavagnaro, T. R.; Bertsch, P. M., Effects of silver sulfide nanomaterials on mycorrhizal colonization of tomato plants and soil microbial communities in biosolid-amended soil. *Environ. Pollut.* **2015,** *206*, 256-263.

40. Sekine, R.; Brunetti, G.; Donner, E.; Khaksar, M.; Vasilev, K.; Jämting, Å.; Scheckel, K. G.; Kappen, P.; Zhang, H.; Lombi, E., Speciation and lability of Ag-, AgCl- and Ag2S-nanoparticles in soil determined by X-ray absorption spectroscopy and Diffusive Gradients in Thin Films. *Environ. Sci. Technol.* **2014**.

41. Yin, L.; Cheng, Y.; Espinasse, B.; Colman, B. P.; Auffan, M.; Wiesner, M.; Rose, J.; Liu, J.; Bernhardt, E. S., More than the ions: the effects of silver nanoparticles on Lolium Multiflorum. *Environ. Sci. Technol.* **2011,** *45*, (6), 2360-2367.

42. Bonomo, L.; Pastorelli, G.; Zambon, N., Advantages and limitations of duckweed-based wastewater treatment systems. *Water Sci. Technol.* **1997,** *35*, (5), 239-246.

43. Lalau, C.; Mohedano, R.; Schmidt, É.; Bouzon, Z.; Ouriques, L.; dos Santos, R.; da Costa, C.; Vicentini, D.; Matias, W., Toxicological effects of copper oxide nanoparticles on the growth rate, photosynthetic pigment content, and cell morphology of the duckweed Landoltia punctata. *Protoplasma* **2015,** *252*, (1), 221-229.

44. Lahive, E.; O'Halloran, J.; Jansen, M. A. K., Frond development gradients are a determinant of the impact of zinc on photosynthesis in three species of Lemnaceae. *Aquatic Botany* **2012,** *101*, (0), 55-63.

45. Upadhyay, R.; Panda, S. K., Zinc reduces copper toxicity induced oxidative stress by promoting antioxidant defense in freshly grown aquatic duckweed Spirodela polyrhiza L. *J. Hazard. Mater.* **2010,** *175*, (1–3), 1081-1084.

46. Farrag, H. F., Evaluation of the Growth Responses of Lemna gibba L. (Duckweed) Exposed to Silver and Zinc Oxide Nanoparticles. *World Applied Sciences Journal* **2015,** *33*, (2), 190-202.

47. Uysal, Y., Removal of chromium ions from wastewater by duckweed, Lemna minor L. by using a pilot system with continuous flow. *J. Hazard. Mater.* **2013,** *263, Part 2*, 486-492.

48. Marchiol, L.; Mattiello, A.; Poscic, F.; Giordano, C.; Musetti, R., In vivo synthesis of nanomaterials in plants: location of silver nanoparticles and plant metabolism. *Nanoscale Res. Lett.* **2014,** *9*, (1), 101.

49. Prasad, B. S. N.; Padmesh, T., Common duckweed (Lemna minor) assisted green synthesis of silver nanoparticles as potent anti-fungal nanomaterial. *Research Journal of Pharmacy and Technology* **2015,** *7*, (9), 955-958.

50. Wang, P.; Menzies, N. W.; Lombi, E.; McKenna, B. A.; de Jonge, M. D.; Donner, E.; Blamey, F. P. C.; Ryan, C. G.; Paterson, D. J.; Howard, D. L.; James, S. A.; Kopittke, P. M., Quantitative determination of metal and metalloid spatial distribution in hydrated and fresh roots of cowpea using synchrotron-based X-ray fluorescence microscopy. *Sci. Total Environ.* **2013,** *463–464*, (0), 131-139.

51. Veronesi, G.; Aude-Garcia, C.; Kieffer, I.; Gallon, T.; Delangle, P.; Herlin-Boime, N.; Rabilloud, T.; Carriere, M., Exposure-dependent Ag+ release from silver nanoparticles and its complexation in AgS2 sites in primary murine macrophages. *Nanoscale* **2015,** *7*, (16), 7323-7330.

52. Voegelin, A.; Weber, F.-A.; Kretzschmar, R., Distribution and speciation of arsenic around roots in a contaminated riparian floodplain soil: Micro-XRF element mapping and EXAFS spectroscopy. *Geochim. Cosmochim. Acta* **2007,** *71*, (23), 5804-5820.

53. Fulda, B.; Voegelin, A.; Ehlert, K.; Kretzschmar, R., Redox transformation, solid phase speciation and solution dynamics of copper during soil reduction and reoxidation as affected by sulfate availability. *Geochim. Cosmochim. Acta* **2013,** *123*, 385-402.

54. Gardea-Torresdey, J. L.; Gomez, E.; Peralta-Videa, J. R.; Parsons, J. G.; Troiani, H.; Jose-Yacaman, M., Alfalfa sprouts: A natural source for the synthesis of silver nanoparticles. *Langmuir* **2003,** *19*, (4), 1357-1361.

55. Remans, T.; Opdenakker, K.; Guisez, Y.; Carleer, R.; Schat, H.; Vangronsveld, J.; Cuypers, A., Exposure of Arabidopsis thaliana to excess Zn reveals a Zn-specific oxidative stress signature. *Environ. Exp. Bot.* **2012,** *84*, (0), 61-71.

56. Harada, M.; Katagiri, E., Mechanism of Silver Particle Formation during Photoreduction Using In Situ Time-Resolved SAXS Analysis. *Langmuir* **2010,** *26*, (23), 17896-17905.

57. Oukarroum, A.; Barhoumi, L.; Pirastru, L.; Dewez, D., Silver nanoparticle toxicity effect on growth and cellular viability of the aquatic plant Lemna gibba. *Environ. Toxicol. Chem.* **2013,** *32*, (4), 902-907.

58. Shi, J.; Abid, A. D.; Kennedy, I. M.; Hristova, K. R.; Silk, W. K., To duckweeds (Landoltia punctata), nanoparticulate copper oxide is more inhibitory than the soluble copper in the bulk solution. *Environ. Pollut.* **2011,** *159*, (5), 1277-1282.

Chapter 4

Effect of Speciation of Copper and Silver Engineered Nanoparticles on their Fate in Simulated Freshwater Mesocosms[1]

4.0 Abstract

Ag^0 and CuO nanoparticles and their sulfidized counterparts are introduced into freshwater wetlands through wastewater effluent and agricultural runoff. There are limited data available concerning the rates of transformations of these particles, and their bioavailability and biogeochemical cycling in realistic environments. In this study five large-scale freshwater wetland mesocosms were exposed to 3g of total metal as either CuO, CuS, Ag^0 or Ag_2S nanoparticles, and soluble $CuNO_3$ for comparison. Both copper and silver from all doses were found in the top centimeter of sediment and in *Egeria densa* plant tissue over nine months, although a general decreasing concentration was observed over time after dosing. X-ray Absorption Near Edge Structure (XANES) fitting was performed on sediment and plant samples collected one, three, six and nine months after dosing. Fitting of the surficial sediment samples shows rapid transformations of both Ag^0 and CuO, with no evidence of CuO NPs in sediments one week after dosing and only ~4% of silver present as Ag^0 NPs one week after dosing. XANES fitting of the dried plant tissues revealed the presence of the initial Ag^0 and CuO NPs for much longer, up to 6 months for CuO NPs and 9 months for Ag^0 NPs. Both the metal/metal oxide and metal sulfide forms of the NPs are labile and bioavailable to aquatic plants. In contrast, Ag speciation showed no temperature dependence. These findings provide important

[1] To be submitted to *Environmental Science and Technology.* Coauthors include Greg Lowry.

information concerning the fate of CuO and Ag NPs in natural freshwater ecosystems. Transformations of nanomaterials may be much slower when associated with plant tissues. This suggests that organisms living in sediments may be primarily exposed to the transformed nanomaterials, whereas aquatic plants like *Egeria densa* and organisms that feed on them may be exposed to the initially dosed NPs for extended periods.

4.1. Introduction

Engineered nanomaterials (ENM) may be inadvertently released into fresh water ecosystems from a variety of sources,[1] e.g. in waste water treatment plant (WWTP) effluent[2,3] or run-off from agricultural fields containing nano-enabled fertilizers and pesticides.[4-6] Understanding the fate of these ENMs in freshwater ecosystems is essential for remediation efforts, fate modeling and forecasting risk.[7-9]

Aquatic macrophytes, especially submerged vascular plants, may be negatively impacted from exposures to ENMs.[10-12] These macrophytes serve an important role in ecosystems as they are known to influence many important characteristics of freshwater ecosystems including physical (light penetration, temperature and hydrodynamics), chemical (dissolved oxygen, organic carbon and nutrient levels) and physiological aspects of freshwater systems.[13] Although some studies have investigated the interactions between selected ENMs and aquatic plants,[10-12,14-16] there are a number of knowledge gaps about the interactions between ENM and aquatic plants. Although transformations of ENM are known to occur in natural waters,[17,18] the effects of these transformations on their uptake into aquatic plants and ultimately the fate in natural freshwater systems is not well characterized.[15,19] The mechanisms by which aquatic plants internalize ENM

into their tissues remains poorly understood.[10] Furthermore, in-vivo transformations of internalized ENM may occur and would impact the long-term fate of ENM.[20-23]

Pristine or transformed ENMs may enter wetlands. ENMs in biosolids applied as fertilizer will likely contain metal sulfides or metal phosphates rather than the initial metallic or metal oxide forms used in products.[24-26] In contrast, agrochemicals such as CuO NPs used as fungicides may enter wetlands in their "as applied" form in agricultural run-off. Therefore, it is important to understand the fate of both "as applied" and transformed nanomaterials in wetlands. The transformations of ENMs entering into fresh water wetlands remains poorly understood, although sulfidation is expected to be an important transformation for copper and silver nanoparticles.[3,27,28] Transformations of ENMs in sediments and plant tissues (e.g. formation of Ag^0 NPs in plant tissue or sulfidation) have not been thoroughly investigated and will likely impact their fate in fresh water ecosystems.

Silver and copper based nanoparticles are among the most common soluble ENM in consumer products (lotions, soaps etc.) and nano-enabled agricultural amendments (fertilizers, fungicides and pesticides).[4,6,29] Unlike their more insoluble and chemically stable ENM counterparts (TiO_2, CeO_x, SiO_2, AlO_x and Au), silver and copper based ENMs will transform.[30-32] The speciation of the transformed materials will depend on the environmental conditions, e.g. redox state, pH, chemical composition, organic carbon content, etc.[33-35] The speciation or form of the metal nanoparticles ultimately governs the solubility, reactivity, and environmental fate of ENMs.[19,36,37] The speciation will also determine the bioavailability and toxicity potential of the particles. For example, silver sulfide nanoparticles were shown to be less toxic than metallic silver nanoparticles to several aquatic species including bacteria, fish and the aquatic plant,

duckweed.[15,38,39] One study has shown sulfidized CuO NPs are much less cytotoxic than the CuO NPs, although the particles do produce potentially toxic reactive oxygen species.[40] Conversely, the sulfidation of CuO NPs appeared to increase their toxicity to zebrafish due to the formation of very small (~a few nm) CuS particles.[32] Despite the low solubility of silver sulfide, these NPs have been found to be bioavailable to plants.[19,36]

Mesocosm experiments are a bridge between "clean" laboratory experiments and real environmental exposures. They incorporate the complexity of aquatic plants and microbial activity while providing realistic environmental exposure conditions (sunlight, seasonal and daily temperature cycling) and therefore provide insights into behaviors expected in natural systems. Recently, we demonstrated that metallic Cu and Ag NPs affected sediment microorganisms differently than CuS and Ag_2S NPs in the first three months, but by 300 days after dosing there was little difference in the microbial community structure between treatments. This suggests that ENM transformation had occurred over several months.[41] In the present study we identify the transformation products and timescales over which they take place. We also investigate uptake of metal and metal NPs by the aquatic plant, *Egeria densa*, present in the mesocosms.

The main goals of the present study are to (a) determine the persistence of the introduced nanomaterial and timescales of their transformations, (b) characterize the uptake of ENMs by the aquatic plant, E. densa by determining the metal speciation in the plants over time, and (c) identify the impact of the initial chemical form of ENM dosed on the final metal speciation after nine months. Five mesocosms were dosed with Ag, Ag_2S, CuO or CuS NPs to assess if initial speciation affects fate and behaviors. X-ray methods are used to track the rates of change of the different NPs over a nine month time period in both sediments and plants.

4.2. Materials and Methods

4.2.1 Synthesis of NPs

Gum arabic coated silver and silver sulfide nanoparticles were obtained from CEINT's NP synthesis center, and dosed to the mesocosms located in the Duke Forest. The synthesis and characterization of these particles are provided in Yin et al., 2011.[42] Briefly, 1.365 L of water, 45 mL of 10g/L gum arabic, and 45 mL of 0.1 M silver nitrate were added to an Erlenmeyer flask, and the solution was stirred for 5 min. All at once, 45 mL of 0.1 M ice-cold sodium borohydride was added, and stirring was continued for 10 min. Multiple batches were combined, and the nanoparticles were purified and concentrated by dialysis (Optiflux F200NR Fresenius Polysulfone Dialyzer, Fresenius Medical Care). The suspension was diluted with water and concentrated two additional times in order to obtain the final washed product.

Additionally, gum arabic coated copper oxide and copper sulfide NPs were prepared for the mesocosm exposure experiments. Copper oxide NPs (<50nm) were purchased from Sigma Aldrich. One gram of the NPs were suspended and stabilized with 2.5g of gum arabic in 900mL of DI water via a sonicating probe (Branson Model 250 at power level 3 for one minute). The suspension was centrifuged, washed with DI water and re-suspended with the sonicating probe three times to obtain the stabilized CuO final product. Multiple batches were combined and concentrated by centrifugation and suspension in reduced volume.

4.2.2 Sulfidation of NPs

Gum arabic coated Ag_2S particles were prepared using a modified published procedure.[43] First, Ag^0 nanoparticles were synthesized as described above. Then, 25 mL of 0.2M

thioacetamide was added to the unpurified AgGA, and the suspension was covered and stirred for 24 h. Multiple batches were combined, and the nanoparticles were purified and concentrated by dialysis (Optiflux F200NR Fresenius Polysulfone Dialyzer, Fresenius Medical Care). The suspension was diluted with water and concentrated two additional times in order to obtain the final product.

The copper oxide NPs were sulfidized using a direct sulfidation process adapted from a process described elsewhere[33,44] and described in Moore et. al. 2016.[41] First the CuO NPs were stabilized with gum arabic and suspended as described above. One hundred mL of 0.1M Na_2S was added directly to the 900mL under constant stirring and allowed to react for one week. Multiple batches of the final product were centrifuged, washed and re-suspended three times, as descried above, to remove any Na_2S and combined and concentrated to achieve the final CuS NPs.

4.2.3 Characterization of NPs

To obtain hydrodynamic diameters and electrophoretic mobility, suspensions of the Ag and Cu NPs were suspended in filtered mesocosm porewater and analyzed using a Malvern Zetasizer Nano at 10 mg/L. Aliquots of NP suspensions were diluted and deposited onto copper TEM grids containing Formvar coating before imaging on a Technai TEM. The crystalline structure of the NPs was determined using synchrotron based XRD at Stanford's 11-3 XRD beamline. In short, suspensions of NPs were dried and adhered onto Kapton tape before being placed into the 12,735 eV beam and the XRD pattern was collected in transmission mode using a MAR345 imaging plate located 100mm past the sample. The patterns were qualitatively fit

against published standards provided by crystallography open database (COD) using the X-pert Highscore Plus software package.

4.2.4 Mesocosm Setup and Dosing

Artificial wetlands were prepared at the Center for Environmental Implications of Nanotechnology (CEINT) facility in the Duke forest in a similar manner as previously described.[45,46] In short, CEINT prepared several large rectangular boxes, each 3.66m long, 1.22m wide and 0.8m deep, which contained a sloped (~13 degrees) sediment bed and a 2.8m run which was lined with water-tight 0.45 mm thick polypropylene. A blend of three top soils was used for this experiment and was characterized elsewhere[45] and used to produce ~22cm of sediment and soil cover. Approximately 400L of local well water was added to each mesocosm. The terrestrial and transitional portions of the mesocosms were planted with plugs of *Juncus effuses* and the aquatic portions were planted with plugs of *Egeria densa* on July 2013. The mesocosms were allowed to stabilize for one month before approximately 400L of water was cycled from one box to another (M9>M10>M11>M13>M24>M9) using a submergible aquarium pump in order to homogenize the water quality parameters and any potential algal contamination. The system was then allowed to stabilize for one week before exposure to NPs.

Suspensions of NPs were added once a week (Tuesday morning) for four weeks in an effort to prevent toxic levels of metal ion concentrations in the water column. A total of 3g $[Ag]_T$ or $[Cu]_T$ of Ag^0NPs, Ag_2S NPs, CuO NPs, CuS NPs and copper ion, respectively was added as 750 mg doses with a goal to provide an approximately 100ppm Cu or Ag increase in the top centimeter of subaquatic sediment. In each dose, 300 mL of a 2.5 g/L suspension of NPs or ions was added to 700 mL of mesocosm water in a 1L HDPE bottle before dosing evenly into the

top of the water column in the mesocosms using a method described elsewhere.[45] The first dose was applied on 10/14/13 dosing each box with 750 mg of Cu or Ag. The ~100ppm concentration is required to have sufficient signal to characterize the Ag and Cu speciation via X-ray absorption techniques. The background metal concentration of the sediment used in the mesocosm was approximately 25ppm Cu and below detection limits for silver.

One week after the final (fourth) addition of the NP suspension, i.e. one month after the initial dose, subaquatic sediment samples were collected from the top cm of the sediment. Sampling the surficial sediment layer was accomplished using a modified 50mL falcon tube, shown in Figure C.1 (Appendix C), by drilling two holes into the cap and fitting it with two 4 foot polypropylene tubes. Negative air pressure was generated using one tube while the other tube was lightly dragged across the top layer of sediment which vacuumed the sample directly into the falcon tube. An area approximately half way along the sloped section of the mesocosm box was selected for sampling and is shown in Figure C.2 (Appendix C). Each sampling event composited sediment collected over an area of approximately 250 cm^2, and the sampling sites were moved for each sampling so as to not sample the same region as before. This device was rinsed and washed with ethanol between each collection and then flushed with water from the water column of the mesocosm to be sampled. Two sections approximately 10 cm long of fresh *Egeria densa* was collected from the end of the new growth obtained in the sampling region and placed into a 50mL falcon tube. These surficial sediment and plant cuttings were collected from each box after one, three, six and nine months after the initial dose. Water samples were collected weekly for chemical and water quality analysis. All samples were immediately frozen for further analysis.

Freeze dried portions of the sediment and plant tissue were digested in hot nitric acid using a method similar to EPA 3050b. In short, for copper samples, 5mL of concentrated nitric acid was added to approximately 250mg of sediment or 75mg of dried plant tissue and heated to 95 °C for four hours. For the silver samples, 8mL of concentrated hydrochloric and 2mL of concentrated nitric acid were added to the sediment or plant tissue sample. The samples were allowed to cool and diluted to 5% acid with DI water before filtering using a 0.2 μm cellulose filter and analyzing for total metals using an ICP-MS. A 5-point calibration spanning three orders of magnitude was prepared from mixed element standards provided by Agilent.

4.2.5 X-ray Absorption Spectroscopy

In order to determine the metal speciation in the sediment samples, the sediments and plant tissues were freeze-dried and loaded into Teflon sample holders or pressed into a 7mm pellet for x-ray absorption spectroscopy (XAS). Silver (25,514 eV) and copper (8,979 eV) K-edge absorption spectra were collected in fluorescence mode using a 100 and 32 element Ge detector at Stanford synchrotron radiation light source's (SSRL) beamlines 11-2 and 4-1, respectively. Each sample was scanned four to twelve times depending on metal concentration and quality of the spectra. The spectra were energy calibrated using silver and copper metallic foils collected simultaneously with the samples. The sample spectra were averaged and normalized using SIXpack data processing software.[47] Linear combination fitting (LCF) of sample spectra was performed with reference spectra of relevant metal species using SIXpack and Athena software packages for the copper and silver samples, respectively. The fitting range was -10 to +175 eV with relation to the copper foil edge and -25 to +100 eV to the silver foil edge. A list of the reference compounds used for this analysis is provided in the Table C.1

(Appendix C). The fitting procedure found the best single component fit and proceeded to add more reference compounds until the R-factor (goodness-of-fit) was not improved by 10%. No attempt to remove the signal from the background copper in the sediment was made as it was expected to be less than 10% of the total signal in most cases. To allow easier interpretation of the XANES fitting, similar reference compounds were referred to as the type of species (Cu-Humic acid and Cu-Histidine were called Cu-O-R while Cu-Cysteine and Cu-Glutathione were called Cu-S-R).

4.3. Results

4.3.1 Nanoparticle Characterization

Silver and silver sulfide nanoparticles were confirmed to be metallic silver and acanthite (Ag_2S) by XRD analysis (Appendix C, Figure C.3A). XRD peak broadening was identified in both samples but appeared more pronounced in the metallic Ag NPs suggesting a smaller crystal domain for these particles. Number-weighted DLS measurements indicated the majority of the particles in DI water averaged 25nm and 34nm diameter for the Ag^0 and Ag_2S NPs. However, the samples were polydisperse and intensity-weighted distributions are higher at 160nm and 94nm for Ag^0 and Ag_2S NPs, respectively, due to the presence of larger particles or aggregates (Appendix C, Table C.2). Characterization of these particles in filtered mesocosm water indicates aggregation of Ag^0 and Ag_2S NPs to 113nm and 61nm (number-average), respectively; while this characterization data has been presented elsewhere[41] it is reproduced in Table C.3 and the data relevant to the present study are summarized in Table 4.1. The TEM image (Figure 4.1) for Ag^0 NPs confirms the presence of mostly smaller particles, with some larger particles

present. The Ag_2S particles appear more aggregated than the Ag^0 NPs but still remain as spherical particles.

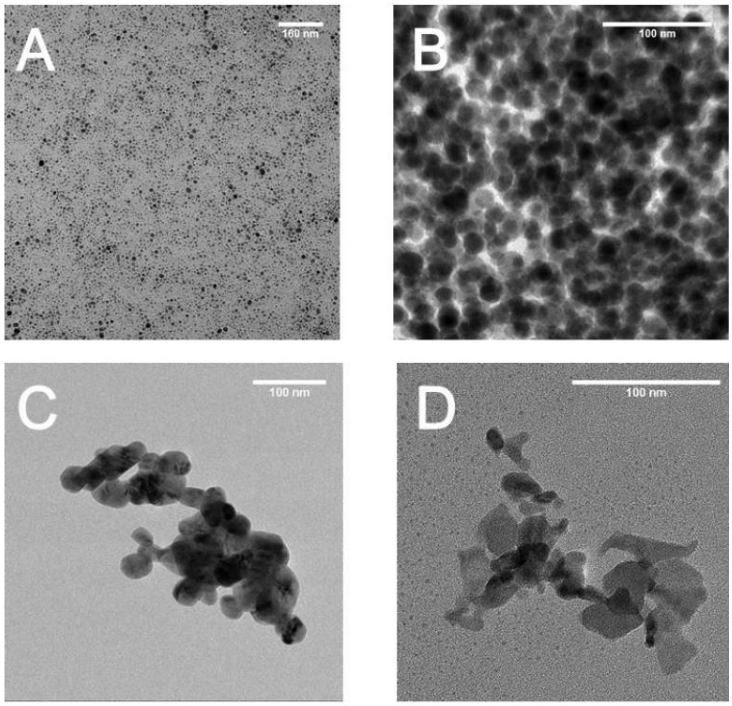

Figure 4.1. TEM images of Ag^0 NPs [A], Ag2S NPs [B], CuO NPs [C] and CuS NPs [D] reproduced from Moore et. al. 2016.[41] Additional TEM images showing different morphology of CuS NPs can be found in Figure C.4.

The gum arabic coated copper oxide NPs were identified by XRD as primarily tenorite (CuO) although a copper carbonate hydroxide phase was also identified (Figure C.3B). The uncoated and dry particles obtained from Sigma Aldrich did not contain this copper carbonate hydroxide phase suggesting this may have been a result of dispersing them in water to coat them with gum arabic. The sulfidized copper NPs were identified by XRD as a mixture of covellite (CuS) and brochantite ($Cu_4SO_4(OH)_6$). TEM imaging of the sulfidized Cu particles identified two distinct morphologies of particles, one appears to be aggregates of acicular rods, likely

brochantite, and the other is large aggregates of spherical particles, likely CuS (Figure C.3). The size of these sulfidized particles is approximately 15-20 nm for the spherical morphology and 50-100 nm long rods with widths on the order of 15-20 nm although they appear to have aggregated. DLS measurements in mesocosm pore water suggest the CuO and CuS nanoparticles indeed aggregate into larger clusters on the order of hundreds of nanometers (Table 4.1).

Table 4.1. Nanomaterial characterization summary of particles dispersed in mesocosm porewater reproduced from Moore et. al. 2016.[41] Values shown are the mean (standard deviation). Zeta potential is calculated from the electrophoretic mobility data using the Smoluchowski equation. The pH ranged from 7.0 to 7.3 for these porewater samples while the specific conductance ranged from 70 to 114 μS/cm.

	TEM	DLS	EPM
	primary particle diameter (nm)	hydrodynamic radius (nm)	Zeta Potential (mV)
	DI water	mesocosm porewater	mesocosm porewater
Ag0	4.67 (1.4)	113 (9.4)	-22.2 (1.5)
Ag2S	18.1 (3.2)	61 (0.4)	-25.8 (2.5)
CuO	31.1 (12)	236 (11)	-25.2 (1.4)
CuS	12.4 (4.1)	185 (11)	-21.6 (0.7)

4.3.2 Mesocosm Characterization

Seasonal temperature changes were observed along with periods of freezing during the early part of the year (Appendix C, Figure C.5). Water temperatures measured during sampling events correlate with seasonal temperature changes (Figure 4.2). Additional pH, DO and ORP measurements collected during sampling events show a gradual decrease in pH observed in each mesocosm. The dissolved oxygen levels and ORP in the water column were highest during the coldest sampling event, and lowest in the hottest months, consistent with expectation. Oxygen profiles analyzed on one inch wide soil cores collected at the three month sampling event show dissolved oxygen concentrations decreasing rapidly in the first 1 to 1.4 centimeter for all

treatments (Appendix C, Figure C.6), which is also consistent with expectations based on similar measurements in an earlier work.[46]

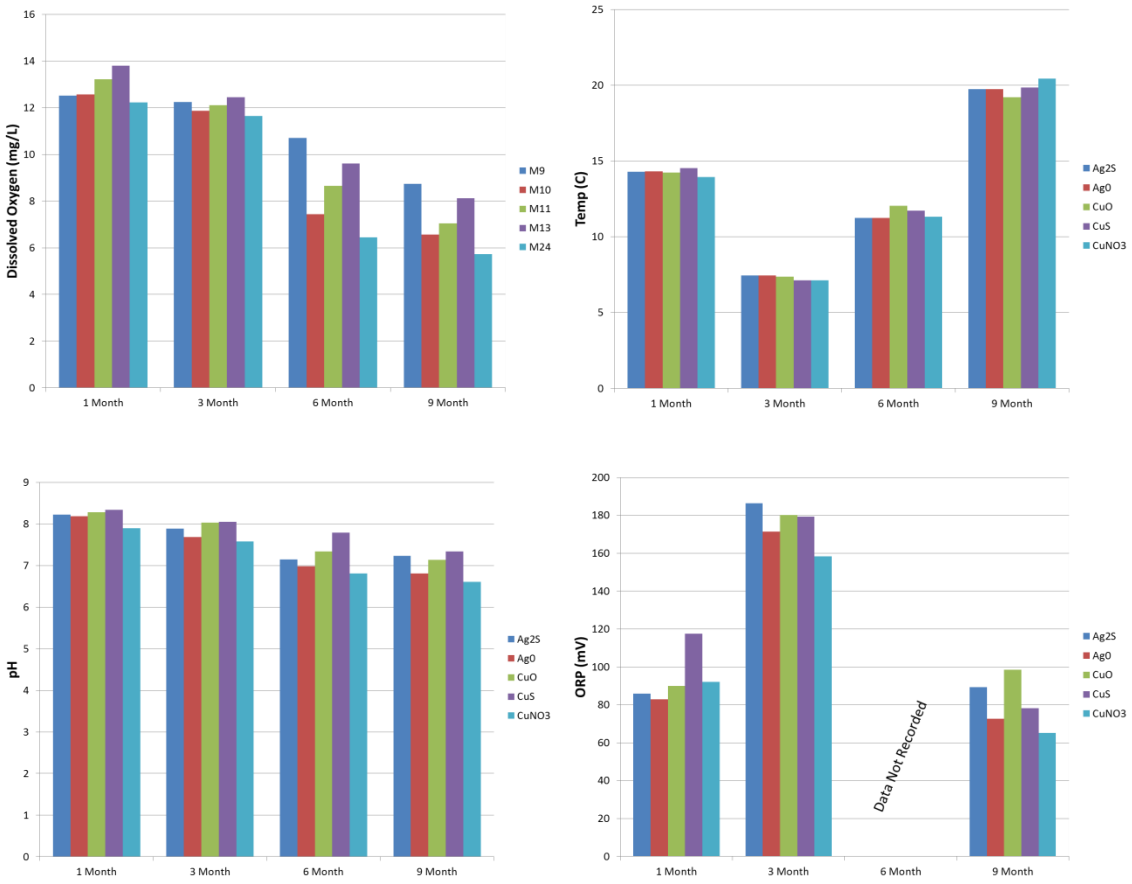

Figure 4.2. Dissolved oxygen, water temperature, pH and ORP measurements collected in the water column of the mesocosm during sampling events.

4.3.3 Metal Concentrations

Copper concentration in the surficial sediment samples collected from the shallow portion of the mesocosm boxes are shown in Figure 4.3A. Generally, the target concentration of approximately 100 ppm Cu to facilitate X-ray characterization was achieved for all three doses.

For all three doses, the copper concentration appears to decrease over the nine month sampling interval and this decrease over time is consistent with trends seen in previous mesocosm studies.[45] A student's t-test indicated there is a significant difference between Ag concentration in the 1 month and 9 month sampling for CuO NPs and $CuNO_3$, but not for CuS. This decline of copper on the surficial sediment suggests that the copper is either migrating along the slope of the mesocosm boxes to deeper depths as was previously shown for Ag NPs in these mesocosms,[46] or becoming buried and diluted with stirred-up sediment and decaying plant material which have lower concentrations of copper. There are large standard deviations for most samples suggesting a large degree of heterogeneity of copper concentration. This variability may be explained by the non-uniform deposition of NPs into the surficial sediment due to the *Egeria densa* plants "shading" the sediment in many regions and preventing even deposition of NPs. The CuS NP exposed sediment shows the most variability over time, which suggests that CuS NPs are quite labile. This is a result of the presence of brochantite or potentially, by microbial activity in this surficial sediment layer,[41] or through oxidative dissolution as was observed in more controlled laboratory experiments.[33] Although background concentrations of Cu in the sediment were measured to be approximately 25ppm, less than 10ppm Cu was found in the surficial sediment layer of the boxes exposed to Ag which suggests this layer was diluted with organic matter containing less copper.

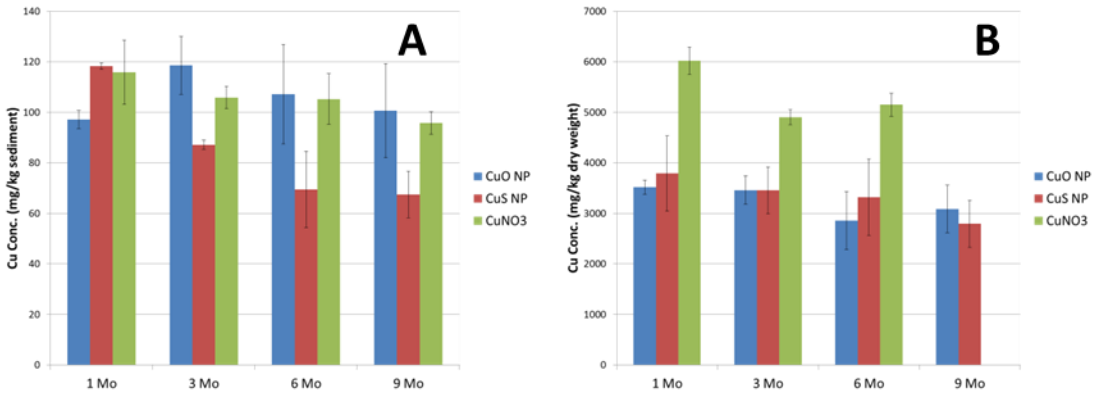

Figure 4.3. Copper concentrations in the surficial sediment (A) and dried plant tissue (B) of duplicate samples collected at each sampling event. Standard deviations for the two measurements are shown as error bars. Copper in a control box (Ag dosed box) was 5-10 mg/kg in sediment and about 10-20 mg/kg in dried plant tissue.

The copper concentrations in the *Egeria densa* samples collected for each sampling event are shown in Figure 4.3B. Relatively high Cu concentration in the plant tissues compared to the sediment is a result of the drying process and is consistent with previous studies.[45] The plant tissue exposed to $CuNO_3$ was found to have more copper than either of the nanoparticle exposed tissues indicating that copper is more readily taken up in the ionic form. The *Egeria* plants exposed to $CuNO_3$ were visibly affected by the dosing which caused many of the leaves to detach from the stems and the 3 month and 6 month sampling contained mostly the stems of the plants. *Egeria* plants were not present by the final sampling event and were not collected. Nanoparticle additions at the same nominal Cu dose did not cause any observable toxicity to the plants, consistent with the lower concentration of Cu in the plant tissues compared to $Cu(NO_3)_2$. The plants exposed to CuO and CuS had similar concentrations of copper suggesting that deposition/attachment/uptake rates were similar for both types of particles. This is consistent with the particles having similar properties in terms of size, charge, and coating type. The

Egeria tissues from the boxes exposed to silver had very low Cu concentrations (10-20 ppm Cu) compared to the Cu dosed samples (>1000 ppm). Although there is a decrease in copper over time, there remained elevated concentrations of copper relative to background. Since the plant tissues collected and analyzed were from new growth, the Cu apparently remains bioavailable to *Egeria* and/or mobile in the plant tissue throughout the nine month study. However, reduced growth due to the toxicity of Cu may have resulted in sampling sections at later time points which were originally exposed during dosing. Based upon rough estimates of the total Egeria biomass being 250-500g dry plant weight and average Cu concentrations being ~3000ppm (dry weight), approximately 25-50% of the total copper dosed as ENMs was associated with plant tissue.

Similar trends were found in the silver concentrations in the surficial sediments and dried *Egeria* tissue (Figure 4.4) exposed to Ag_2S and Ag^0 NPs compared with the Cu exposed samples. Similar to Cu, there is a gradual decline in the Ag concentration over time in the surficial sediment. A student's t-test indicated there is a significant difference between Ag concentration in the 1 month and 9 month sampling. Again this may be explained through the dilution of the surficial sediment with decaying plant material, bioturbation, or gradual migration down the slope of the mesocosm boxes.

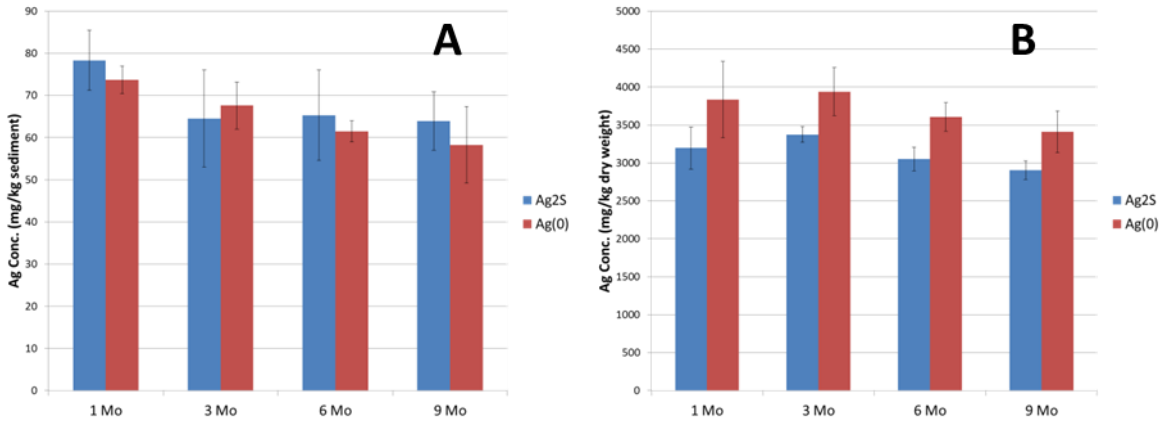

Figure 4.4. Silver concentrations in the surficial sediment (A) and dried plant tissue (B) of duplicate samples collected at each sampling event. Standard deviations for the two measurements are shown as error bars.

The silver concentration in the *Egeria* plant tissue also remained fairly constant throughout the experiment for both exposures. The Ag^0 NP exposed plant were visibly more affected than the Ag_2S NP exposed causing detachment of some leaves, although the visually observable effects of the Ag^0 NPs were small compared to the $CuNO_3$ treatment. At all of the time points sampled, the Ag^0 NP exposed samples contained more Ag than the Ag_2S NP exposed plants, indicating greater bioavailability. The Ag^0 NPs may have attached more readily than the Ag_2S NPs, or were generally more labile due to their greater solubility. The elevated concentrations of Ag in new growth of the plants over the course of the study indicate that the Ag remains bioavailable despite being transformed to Ag_2S which has low solubility. The plants are either able to solubilize the Ag_2S NPs, take up Ag_2S NPs, or potentially to mobilize the Ag in the plant tissue once it has been taken up. Additional research is needed to distinguish between these possibilities.

4.3.4 Cu Speciation in Sediments

A summary of the Cu XANES fitting for the surficial sediments are shown in Table 4.2 and the fits are shown in Figure 4.5. Several important conclusions can be drawn from the Cu speciation over time in the three different treatments, CuO, CuS, and $CuNO_3$. First, the sediment exposed to CuO NPs did not show the presence of the initial CuO material in any samples indicating that the CuO was completely transformed in the sediment on a timescale less than one week. This is consistent with a recent study indicating a relatively high solubility of CuO NPs in these same freshwater mesocosms.[48] Second, the speciation of Cu in all treatments is generally found to be a mixture of Cu-S bound (organic and inorganic Cu-sulfides) and Cu-O-R bound (Cu bound to organic matter) copper rather than just present as the added CuO or CuS NPs), indicating that the Cu derived from these NPs is labile in the sediment regardless of its initial form. Interestingly, the Cu in collected sediments for all three treatments was found to be 100% Cu-O-R at the winter sampling point. The predominance of Cu-O-R in surficial sediment during winter is consistent with the quiescent and highly oxidizing environment during this time period. The predominance of the Cu-organic matter species is likely from the large influx of organic matter from the senescence prior to winter. It is important to note that this speciation is for copper present in the surficial sediment only, and some CuS is likely to present in the deeper sediments given the rapid reduction in oxygen saturation during the first 1.5 centimeter of sediment at that sampling time (Appendix C, Figure C.6). The method of surficial sediment sampling may have introduced heterogeneity into the samples. Although the vacuuming technique attempted to collect the top layer of sediment and be consistent with sampling depth and amount of sediment collected; the amount of heterogeneity this type of sampling introduced was not quantified.

Even though the copper speciation was similar for the treatments, some differences between treatments were identified depending on the type of particles that was added to the mesocosm. For example, only CuO NPs resulted in formation of low amounts of metallic copper, which has a distinct white line in the XANES spectra. The presence of humic acid in anoxic and reducing conditions with large copper loadings has been found to produce metallic copper.[49] The sediment became anoxic from microbial activity within the first cm of sediment in soil cores collected at the 3 month sampling event (Appendix C, Figure C.6). However, it is unclear why metallic Cu was formed only in the CuO NP dosed mesocosm. The CuS dosed mesocosm tended to have greater fractions of inorganic CuS in the fits (Appendix C, Table C.4), compared to the other treatments. The fluctuations between Cu-O-R and Cu-S character in the surficial sediment samples, even for the CuS dosed mesocosm, indicated that the dosed CuS is labile. This is likely due to oxidative dissolution of the added CuS phase (Ma et al., 2014), as well as the CuS phases formed during the warmer months with greater biological activity in the sediment.

Table 4.2. Summary of the Cu XANES fits for the surficial sediment samples. The initial speciation was assumed to be that of the initially dosed particle and was not fit.

CuO NP	CuO NP	Cu-S	Cu-O-R	Cu^0
Initial	100%	-	-	-
1 Month	-	39%	46%	15%
3 Month	-	-	100%	-
6 Month	-	41%	45%	13%
9 Month	-	48%	52%	-
CuS NP	CuO NP	Cu-S	Cu-O-R	Cu^0
Initial	-	100%	-	-
1 Month	-	74%	24%	-
3 Month	-	-	100%	-
6 Month	-	74%	24%	-
9 Month	-	6%	94%	-
$CuNO_3$	CuO NP	Cu-S	Cu-O-R	Cu^0
Initial	-	-	-	-
1 Month	-	24%	76%	-
3 Month	-	-	100%	-
6 Month	-	24%	75%	-
9 Month	-	6%	95%	-

4.3.5 Cu Speciation in *Egeria densa*

The copper speciation in the *Egeria densa* plant tissue exposed to CuO NPs was unexpectedly found to persist as CuO (tenorite) for up to six months (Table 4.3). The Cu speciation one month after the initial does was a mixture of CuO and Cu bound to inorganic and organic sulfur and organic matter suggesting the CuO NPs may be ad/absorbing into the plant tissue. The plant tissue appears to be protecting the NPs from completely transforming as was observed in the sediment. However, a fraction of the Cu is becoming associated with plant proteins and organic matter produced by the plants. The Cu speciation remains a mixture of Cu bound to organic matter, Cu bound to thiols and CuO. The absence of CuO in the 9 month samples suggests a relatively slow transformation/dissolution, but this trend needs to be

confirmed. A minor fraction of the Cu in most samples across all treatments appears to be Cu-S-R which is consistent with other studies involving Cu uptake in tomatoes where Cu is bound to glutathione or cysteine as the plant respond to dissolved Cu ions.[50]

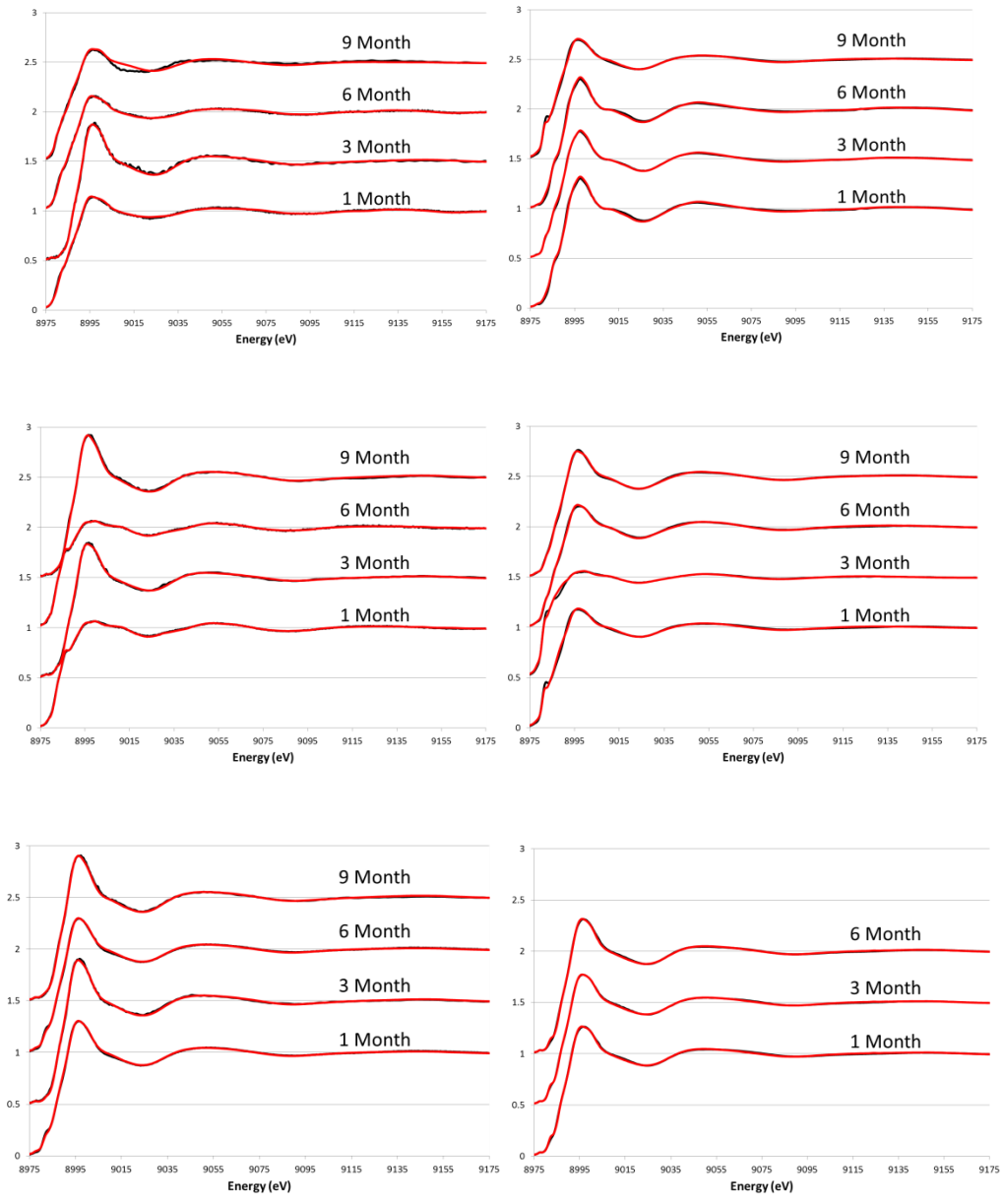

Figure 4.5. Normalized Cu XANES spectra (black) and fits (red) for CuO exposed sediment (top left) and plant tissue (top right), CuS NP exposed sediment (middle left) and plant tissue (middle right) and $CuNO_3$ exposed sediment (bottom left) and plant tissue (bottom right).

The copper speciation in the *Egeria* exposed to CuS NPs also shows CuS persisting in plant tissues throughout the experiment. The one month speciation shows Cu bound to organic matter and sulfur as a mixture of the CuS starting material and Cu-S-R bound. This suggests that CuS NPs have associated with the plant tissue and undergone some degree of dissolution and association with plant proteins. The fraction of Cu associated with inorganic sulfur remains higher than for the CuO and $CuNO_3$ exposed samples which is understandable considering that plants were exposed to CuS NPs.

The $CuNO_3$ exposed plant tissue had a similar Cu speciation at all time points, showing a mixture of Cu bound to thiols and organic matter. In contrast to added NPs (CuO and CuS), no inorganic CuS phase was formed in plants when $CuNO_3$ was used as the copper source. Reasons for this are unclear, but it suggests that CuO NPs can undergo solid state sulfidation without dissolution as has been previously reported for CuO NPs in cell cultures.[40] The $CuNO_3$ treatment appeared to cause significant harm to the Egeria plant eliminating all the plants by the 9 month sampling event. Although ecological endpoints were not monitored, the toxicity of the $CuNO_3$ treatment can be observed in the images of the boxes (Appendix C Figure C.7) showing detachment of the leaves, lack of flowering and no plants after 9 months. The copper speciation in *Egeria* exposed to $CuNO_3$ remains fairly consistent over time which may be a result of overwhelming the plant defense response. The growth of the plants and their ability to transform copper may have been affected due to the increased toxicity compared to the nanoparticulate forms.

Table 4.3. Summary of the Cu XANES fits for the *Egeria densa* samples. The initial speciation was assumed to be that of the initially dosed particle and was not fit.

CuO NP	CuO NP	Cu-S	Cu-O-R	Cu-S-R
Initial	100%	-	-	-
1 Month	42%	22%	35%	-
3 Month	35%	-	33%	31%
6 Month	42%	19%	35%	3%
9 Month	-	19%	51%	30%
CuS NP	CuO NP	Cu-S	Cu-O-R	Cu-S-R
Initial	-	100%	-	-
1 Month	-	19%	47%	35%
3 Month	-	48%	17%	35%
6 Month	-	35%	52%	12%
9 Month	-	28%	71%	-
$CuNO_3$	CuO NP	Cu-S	Cu-O-R	Cu-S-R
Initial	-	-	-	-
1 Month	-	-	86%	14%
3 Month	-	-	82%	18%
6 Month	-	-	91%	9%

4.3.6 Ag Speciation in Sediments

The Ag speciation for the surficial sediment and *Egeria densa* samples exposed to Ag^0 and Ag_2S NPs is summarized in Table 4.4. The Ag speciation in the surficial sediment exposed to Ag^0 NPs one month after the initial dose (and one week after the final dose) is a mixture of Ag_2S and Ag bound to thiol with a very small fraction (4%) remaining as metallic Ag, indicating that Ag^0 NPs rapidly transform into silver sulfide in the surficial sediment. The speciation remains fairly consistent with the primary species being Ag_2S and a minor Ag-thiol species present. Thus, once transformed into Ag_2S the silver remains largely as inorganic silver sulfide. This transformation to silver sulfide is more rapid than previously reported, with other studies showing 15% remaining as remaining as metallic silver after 28 days in marine sediments[51] while another study shows 18% remaining as metallic Ag after 18 months.[46] Although the short timescale of transformation may be attributed to the small size of the Ag0 NPs, the overall result of silver rapidly transforming and stabilizing as silver sulfide in sediments is consistent with other studies.

The silver speciation in the surficial sediment exposed to silver sulfide in all samples is also a mixture of Ag_2S and Ag bound to thiol suggesting the Ag_2S NPs are relatively stable over time. Therefore, there appears to be little difference in Ag speciation for the Ag^0 and Ag_2S dosed mesocosms because of the rapid transformation and the high stability of the product, Ag_2S. However, the presence of some small fraction of Ag-thiol species suggests that the Ag_2S NPs are not completely inert, and may remain bioavailable over the 9 month experiment. This could explain why new growth of *Egeria* continues to contain elevated levels of metals.

4.3.7 Ag Speciation in *Egeria densa*

The Ag speciation in the tissue of *Egeria* plants in mesocosms dosed with Ag^0 NPs was a mixture of Ag^0, Ag_2S and Ag bound to thiol suggesting either a portion the Ag^0 NPs were sorbed into/onto the plant tissue and persisting as NPs or they were dissolving and undergoing ion-uptake followed by reductive precipitation of Ag^0 NPs which has been shown to occur in many other plants exposed to ionic Ag.[52,53] The speciation remains fairly consistent throughout the study suggesting the *Egeria* is protecting the Ag^0 in the tissues from becoming sulfidized on a long term basis or there is a pseudo-steady state achieved between the dissolved and nanoparticulate silver species within the plants. Although the Ag^0 treatment was observed to cause toxicity to the Egeria in the initial months (Appendix C, Figure C.7), the plants appear to rebound from this chemical assault in the later sampling events supporting the finding that the Ag had transformed into the less toxic form, Ag_2S.

Table 4.4. Summary of XANES fitting for Ag^0 and Ag_2S exposed surficial sediment and *Egeria.*

Sediments				Egeria			
Ag^0 NP	Ag^0	Ag-Thiol	Ag_2S	Ag^0 NP	Ag^0	Ag-Thiol	Ag_2S
Initial	100%	-	-	Initial	100%	-	-
1 Month	4%	12%	83%	1 Month	19%	25%	56%
3 Month	-	-	98%	3 Month	13%	-	86%
6 Month	-	18%	81%	6 Month	-	24%	66%
9 Month	-	39%	59%	9 Month	24%	10%	65%
Ag_2S NP	Ag^0	Ag-Thiol	Ag_2S	Ag_2S NP	Ag^0	Ag-Thiol	Ag_2S
Initial	-	-	100%	Initial	-	-	100%
1 Month	-	29%	70%	1 Month	-	25%	74%
3 Month	-	13%	85%	3 Month	-	2%	97%
6 Month	-	13%	86%	6 Month	-	19%	80%
9 Month	-	13%	86%	9 Month	-	35%	63%

The Ag speciation in the *Egeria* tissue exposed to Ag_2S NPs for all sample times is quite similar to that for Ag^0. However, there is no evidence of elemental silver in the plants taken from mesocosms dosed with Ag_2S. Since many plant species are known to synthesize metallic silver NPs after being exposed to silver ions, the absence of Ag^0 in the samples exposed to Ag_2S NPs may be a result of the lower ion concentrations expected for Ag_2S compared to Ag^0. The Ag_2S NP treatment did not show signs of toxicity to the *Egeria* in any of the sampling times (Appendix C, Figure C.7).

4.4. Implications

Although these mesocosm experiments were not replicated, the findings of this case study have many important implications concerning the fate of ENMs in natural wetlands and freshwater ecosystems. Although the initial form of metal dosed was found to affect the distribution and the metal speciation in the sediment and plant tissue even after nine months, all treatments appear to be converging and becoming incorporated in the biogeochemical cycling of metals. These findings suggest the metal ENMs tested are fairly labile and differences between treatments will be erased over time.

This study provides relative timescales of transformations which can impact ENM fate models by showing copper sulfide ENMs are more labile than silver sulfide ENMs which indicates all metal sulfides do not behave the same. The initial weeks (perhaps days) after dosing were found to be the most important timeframe to study transformations of pristine ENMs in sediments. Although the pristine materials transform rather rapidly, longer lasting effects on the water quality and health of the mesocosm can be observed at the 9 month sampling events. Differences in the toxicity between treatments suggest sulfidized ENMs are less toxic than their

pristine counterparts or dissolved ions. Additionally, with transformation in plant and sediments being very different from each other, the seasonal decay of plant materials may reintroduce ENMs to the sediments and lead to a longer term exposure risk than previously modeled.

Plants can slow transformation rates, and produce different transformation products compared with the sediments. This suggests if ENMs are taken into plant tissue, they are a more persistent pollutant than previously thought. This highlights the importance of understanding the uptake of ENM into plants and relative amount of plant biomass to assess the impact of ENMs on natural systems and predict their environmental fate.

The uptake and persistence of ENMs into plant tissues has implications concerning the use of aquatic plants as tools to phyto-remediate contaminated wetlands. Both labile and more inert ENMs are shown to be taken into plant tissues in significant quantities. This result provides further evidence supporting the use of aquatic plants for the remediation purposes even in the cases involving nearly insoluble ENMs.

References

1. Sun, T. Y.; Conroy, G.; Donner, E.; Hungerbuhler, K.; Lombi, E.; Nowack, B., Probabilistic modelling of engineered nanomaterial emissions to the environment: a spatio-temporal approach. *Environmental Science: Nano* **2015,** *2*, (4), 340-351.

2. Gottschalk, F.; Sonderer, T.; Scholz, R. W.; Nowack, B., Modeled environmental concentrations of engineered nanomaterials (TiO(2), ZnO, Ag, CNT, Fullerenes) for different regions. *Environ. Sci. Technol.* **2009,** *43*, (24), 9216-9222.

3. Kaegi, R.; Voegelin, A.; Sinnet, B.; Zuleeg, S.; Hagendorfer, H.; Burkhardt, M.; Siegrist, H., Behavior of metallic silver nanoparticles in a pilot wastewater treatment plant. *Environ. Sci. Technol.* **2011,** *45*, (9), 3902-3908.

4. Mehrazar, E.; Rahaie, M.; Rahaie, S., Application of nanoparticles for pesticides, herbicides, fertilisers and animals feed management. *International Journal of Nanoparticles* **2015,** *8*, (1), 1-19.

5. Agrawal, S.; Rathore, P., Nanotechnology pros and cons to agriculture: A review. *Int. J. Curr. Microbiol. App. Sci* **2014,** *3*, (3), 43-55.

6. Solanki, P.; Bhargava, A.; Chhipa, H.; Jain, N.; Panwar, J., Nano-fertilizers and Their Smart Delivery System. In *Nanotechnologies in Food and Agriculture*, Rai, M.; Ribeiro, C.; Mattoso, L.; Duran, N., Eds. Springer International Publishing: Cham, 2015; pp 81-101.

7. Dale, A. L.; Casman, E. A.; Lowry, G. V.; Lead, J. R.; Viparelli, E.; Baalousha, M., Modeling Nanomaterial Environmental Fate in Aquatic Systems. *Environ. Sci. Technol.* **2015,** *49*, (5), 2587-2593.

8. Praetorius, A.; Scheringer, M.; Hungerbühler, K., Development of Environmental Fate Models for Engineered Nanoparticles—A Case Study of TiO2 Nanoparticles in the Rhine River. *Environ. Sci. Technol.* **2012,** *46*, (12), 6705-6713.

9. Hendren, C. O.; Badireddy, A. R.; Casman, E.; Wiesner, M. R., Modeling nanomaterial fate in wastewater treatment: Monte Carlo simulation of silver nanoparticles (nano-Ag). *Sci. Total Environ.* **2013,** *449*, 418-425.

10. Thwala, M.; Klaine, S. J.; Musee, N., Interactions of metal-based engineered nanoparticles with aquatic higher plants: A review of the state of current knowledge. *Environ. Toxicol. Chem.* **2016**, n/a-n/a.

11. Lalau, C.; Mohedano, R.; Schmidt, É.; Bouzon, Z.; Ouriques, L.; dos Santos, R.; da Costa, C.; Vicentini, D.; Matias, W., Toxicological effects of copper oxide nanoparticles on the growth rate, photosynthetic pigment content, and cell morphology of the duckweed Landoltia punctata. *Protoplasma* **2015,** *252*, (1), 221-229.

12. Farrag, H. F., Evaluation of the Growth Responses of Lemna gibba L. (Duckweed) Exposed to Silver and Zinc Oxide Nanoparticles. *World Applied Sciences Journal* **2015,** *33*, (2), 190-202.

13. Carpenter, S. R.; Lodge, D. M., Submerged Macrophytes: Carbon Metabolism, Growth Regulation and Role in Macrophyte-Dominated Ecosystems Effects of submersed macrophytes on ecosystem processes. *Aquatic Botany* **1986,** *26*, 341-370.

14. Perreault, F.; Popovic, R.; Dewez, D., Different toxicity mechanisms between bare and polymer-coated copper oxide nanoparticles in Lemna gibba. *Environ. Pollut.* **2014,** *185*, 219-227.

15. Levard, C.; Hotze, E. M.; Colman, B. P.; Dale, A. L.; Truong, L.; Yang, X. Y.; Bone, A. J.; Brown, G. E.; Tanguay, R. L.; Di Giulio, R. T.; Bernhardt, E. S.; Meyer, J. N.; Wiesner, M. R.; Lowry, G. V., Sulfidation of Silver Nanoparticles: Natural Antidote to Their Toxicity. *Environ. Sci. Technol.* **2013,** *47*, (23), 13440-13448.

16. Shi, J.; Abid, A. D.; Kennedy, I. M.; Hristova, K. R.; Silk, W. K., To duckweeds (Landoltia punctata), nanoparticulate copper oxide is more inhibitory than the soluble copper in the bulk solution. *Environ. Pollut.* **2011,** *159*, (5), 1277-1282.

17. Maurer, F.; Christl, I.; Fulda, B.; Voegelin, A.; Kretzschmar, R., Copper Redox Transformation and Complexation by Reduced and Oxidized Soil Humic Acid. 2. Potentiometric Titrations and Dialysis Cell Experiments. *Environ. Sci. Technol.* **2013,** *47*, (19), 10912-10921.

18. Reidy, B.; Haase, A.; Luch, A.; Dawson, A. K.; Lynch, I., Mechanisms of Silver Nanoparticle Release, Transformation and Toxicity: A Critical Review of Current Knowledge and Recommendations for Future Studies and Applications. *Materials* **2013,** *6*, (6).

19. Wang, P.; Menzies, N. W.; Lombi, E.; Sekine, R.; Blamey, F. P.; Hernandez-Soriano, M. C.; Cheng, M.; Kappen, P.; Peijnenburg, W. J.; Tang, C.; Kopittke, P. M., Silver sulfide nanoparticles (AgS-NPs) are taken up by plants and are phytotoxic. *Nanotoxicology* **2015**, 1-9.

20. Larue, C.; Castillo-Michel, H.; Sobanska, S.; Cécillon, L.; Bureau, S.; Barthès, V.; Ouerdane, L.; Carrière, M.; Sarret, G., Foliar exposure of the crop Lactuca sativa to silver nanoparticles: Evidence for internalization and changes in Ag speciation. *J. Hazard. Mater.* **2014,** *264*, 98-106.

21. Rico, C. M.; Majumdar, S.; Duarte-Gardea, M.; Peralta-Videa, J. R.; Gardea-Torresdey, J. L., Interaction of Nanoparticles with Edible Plants and Their Possible Implications in the Food Chain. *Journal of Agricultural and Food Chemistry* **2011,** *59*, (8), 3485-3498.

22. López-Moreno, M. L.; de la Rosa, G.; Hernández-Viezcas, J. A.; Castillo-Michel, H.; Botez, C. E.; Peralta-Videa, J. R.; Gardea-Torresdey, J. L., Evidence of the Differential Biotransformation and Genotoxicity of ZnO and CeO2 Nanoparticles on Soybean (Glycine max) Plants. *Environ. Sci. Technol.* **2010,** *44*, (19), 7315-7320.

23. Gardea-Torresdey, J. L.; Gomez, E.; Peralta-Videa, J. R.; Parsons, J. G.; Troiani, H.; Jose-Yacaman, M., Alfalfa Sprouts: A Natural Source for the Synthesis of Silver Nanoparticles. *Langmuir* **2003,** *19*, (4), 1357-1361.

24. Ma, R.; Levard, C.; Judy, J. D.; Unrine, J. M.; Durenkamp, M.; Martin, B.; Jefferson, B.; Lowry, G. V., Fate of Zinc Oxide and Silver Nanoparticles in a Pilot Wastewater Treatment Plant and in Processed Biosolids. *Environ. Sci. Technol.* **2013,** *48*, (1), 104-112.

25. Lombi, E.; Donner, E.; Taheri, S.; Tavakkoli, E.; Jämting, Å. K.; McClure, S.; Naidu, R.; Miller, B. W.; Scheckel, K. G.; Vasilev, K., Transformation of four silver/silver chloride nanoparticles during anaerobic treatment of wastewater and post-processing of sewage sludge. *Environ. Pollut.* **2013,** *176*, (0), 193-197.

26. Lombi, E.; Donner, E.; Tavakkoli, E.; Turney, T. W.; Naidu, R.; Miller, B. W.; Scheckel, K. G., Fate of Zinc Oxide Nanoparticles during Anaerobic Digestion of Wastewater and Post-Treatment Processing of Sewage Sludge. *Environ. Sci. Technol.* **2012,** *46*, (16), 9089-9096.

27. Kim, B.; Park, C.-S.; Murayama, M.; Hochella, M. F., Discovery and characterization of silver sulfide nanoparticles in final sewage sludge products. *Environ. Sci. Technol.* **2010,** *44*, (19), 7509-7514.

28. Thalmann, B.; Voegelin, A.; von Gunten, U.; Behra, R.; Morgenroth, E.; Kaegi, R., Effect of Ozone Treatment on Nano-Sized Silver Sulfide in Wastewater Effluent. *Environ. Sci. Technol.* **2015,** *49*, (18), 10911-10919.

29. Bondarenko, O.; Juganson, K.; Ivask, A.; Kasemets, K.; Mortimer, M.; Kahru, A., Toxicity of Ag, CuO and ZnO nanoparticles to selected environmentally relevant test organisms and mammalian cells in vitro: a critical review. *Arch. Toxicol.* **2013,** *87*, (7), 1181-1200.

30. Thalmann, B.; Voegelin, A.; Sinnet, B.; Morgenroth, E.; Kaegi, R., Sulfidation Kinetics of Silver Nanoparticles Reacted with Metal Sulfides. *Environ. Sci. Technol.* **2014,** *48*, (9), 4885-4892.

31. Khaksar, M.; Jolley, D. F.; Sekine, R.; Vasilev, K.; Johannessen, B.; Donner, E.; Lombi, E., In Situ Chemical Transformations of Silver Nanoparticles along the Water–Sediment Continuum. *Environ. Sci. Technol.* **2015,** *49*, (1), 318-325.

32. Li, L.; Hu, L.; Zhou, Q.; Huang, C.; Wang, Y.; Sun, C.; Jiang, G., Sulfidation as a Natural Antidote to Metallic Nanoparticles Is Overestimated: CuO Sulfidation Yields CuS Nanoparticles with Increased Toxicity in Medaka (Oryzias latipes) Embryos. *Environ. Sci. Technol.* **2015**.

33. Ma, R.; Stegemeier, J.; Levard, C.; Dale, J. G.; Noack, C. W.; Yang, T.; Brown, G. E.; Lowry, G. V., Sulfidation of copper oxide nanoparticles and properties of resulting copper sulfide. *Environmental Science: Nano* **2014,** *1*, (4), 347-357.

34. Yu, S.; Yin, Y.; Zhou, X.; Dong, L.; Liu, J., Transformation kinetics of silver nanoparticles and silver ions in aquatic environments revealed by double stable isotope labeling. *Environmental Science: Nano* **2016,** *3*, (4), 883-893.

35. Yu, S.-j.; Yin, Y.-g.; Liu, J.-f., Silver nanoparticles in the environment. *Environmental Science: Processes & Impacts* **2013,** *15*, (1), 78-92.

36. Stegemeier, J. P.; Schwab, F.; Colman, B. P.; Webb, S. M.; Newville, M.; Lanzirotti, A.; Winkler, C.; Wiesner, M. R.; Lowry, G. V., Speciation Matters: Bioavailability of Silver and Silver Sulfide Nanoparticles to Alfalfa (*Medicago sativa*). *Environ. Sci. Technol.* **2015,** *49*, (14), 8451-8460.

37. Sekine, R.; Brunetti, G.; Donner, E.; Khaksar, M.; Vasilev, K.; Jämting, Å.; Scheckel, K. G.; Kappen, P.; Zhang, H.; Lombi, E., Speciation and lability of Ag-, AgCl- and Ag2S-nanoparticles in soil determined by X-ray absorption spectroscopy and Diffusive Gradients in Thin Films. *Environ. Sci. Technol.* **2014**.

38. Choi, O.; Cleuenger, T. E.; Deng, B. L.; Surampalli, R. Y.; Ross, L.; Hu, Z. Q., Role of sulfide and ligand strength in controlling nanosilver toxicity. *Water Res.* **2009,** *43*, (7), 1879-1886.

39. Devi, G. P.; Ahmed, K. B. A.; Varsha, M. K. N. S.; Shrijha, B. S.; Lal, K. K. S.; Anbazhagan, V.; Thiagarajan, R., Sulfidation of silver nanoparticle reduces its toxicity in zebrafish. *Aquat. Toxicol.* **2015,** *158*, 149-156.

40. Wang, Z.; von dem Bussche, A.; Kabadi, P. K.; Kane, A. B.; Hurt, R. H., Biological and Environmental Transformations of Copper-Based Nanomaterials. *ACS Nano.* **2013,** *7*, (10), 8715-8727.

41. Moore, J. D.; Stegemeier, J. P.; Bibby, K.; Marinakos, S. M.; Lowry, G. V.; Gregory, K. B., Impacts of Pristine and Transformed Ag and Cu Engineered Nanomaterials on Surficial Sediment Microbial Communities Appear Short-Lived. *Environ. Sci. Technol.* **2016,** *50*, (5), 2641-2651.

42. Yin, L. Y.; Cheng, Y. W.; Espinasse, B.; Colman, B. P.; Auffan, M.; Wiesner, M.; Rose, J.; Liu, J.; Bernhardt, E. S., More than the Ions: The Effects of Silver Nanoparticles on Lolium multiflorum. *Environ Sci Technol* **2011,** *45*, (6), 2360-2367.

43. Djokovic, V.; Krsmanovic, R.; Bozanic, D. K.; McPherson, M.; Van Tendeloo, G.; Nair, P. S.; Georges, M. K.; Radhakrishnan, T., Adsorption of sulfur onto a surface of silver nanoparticles stabilized with sago starch biopolymer. *Colloids Surf B Biointerfaces* **2009,** *73*, (1), 30-5.

44. Reinsch, B. C.; Levard, C.; Li, Z.; Ma, R.; Wise, A.; Gregory, K. B.; Brown, G. E.; Lowry, G. V., Sulfidation of Silver Nanoparticles Decreases Escherichia coli Growth Inhibition. *Environ. Sci. Technol.* **2012,** *46*, (13), 6992-7000.

45. Colman, B. P.; Espinasse, B.; Richardson, C. J.; Matson, C. W.; Lowry, G. V.; Hunt, D. E.; Wiesner, M. R.; Bernhardt, E. S., Emerging Contaminant or an Old Toxin in Disguise? Silver Nanoparticle Impacts on Ecosystems. *Environ. Sci. Technol.* **2014,** *48*, (9), 5229-5236.

46. Lowry, G. V.; Espinasse, B. P.; Badireddy, A. R.; Richardson, C. J.; Reinsch, B. C.; Bryant, L. D.; Bone, A. J.; Deonarine, A.; Chae, S.; Therezien, M.; Colman, B. P.; Hsu-Kim, H.; Bernhardt, E. S.; Matson, C. W.; Wiesner, M. R., Long-Term Transformation and Fate of Manufactured Ag Nanoparticles in a Simulated Large Scale Freshwater Emergent Wetland. *Environ. Sci. Technol.* **2012,** *46*, (13), 7027-7036.

47. Webb, S. M., SIXpack: a graphical user interface for XAS analysis using IFEFFIT. *Phys. Scr.* **2005,** *T115*, 1011-1014.

48. Vencalek, B. E.; Laughton, S. N.; Spielman-Sun, E.; Rodrigues, S. M.; Unrine, J. M.; Lowry, G. V.; Gregory, K. B., In Situ Measurement of CuO and Cu(OH)2 Nanoparticle Dissolution Rates in Quiescent Freshwater Mesocosms. *Environmental Science & Technology Letters* **2016**.

49. Fulda, B.; Voegelin, A.; Maurer, F.; Christl, I.; Kretzschmar, R., Copper Redox Transformation and Complexation by Reduced and Oxidized Soil Humic Acid. 1. X-ray Absorption Spectroscopy Study. *Environ. Sci. Technol.* **2013,** *47*, (19), 10903-10911.

50. Ryan, B. M.; Kirby, J. K.; Degryse, F.; Harris, H.; McLaughlin, M. J.; Scheiderich, K., Copper speciation and isotopic fractionation in plants: uptake and translocation mechanisms. *New Phytol.* **2013,** *199*, (2), 367-378.

51. Wang, H.; Ho, K. T.; Scheckel, K. G.; Wu, F.; Cantwell, M. G.; Katz, D. R.; Horowitz, D. B.; Boothman, W. S.; Burgess, R. M., Toxicity, Bioaccumulation, and Biotransformation of Silver Nanoparticles in Marine Organisms. *Environ. Sci. Technol.* **2014,** *48*, (23), 13711-13717.

52. Marchiol, L.; Mattiello, A.; Poscic, F.; Giordano, C.; Musetti, R., In vivo synthesis of nanomaterials in plants: location of silver nanoparticles and plant metabolism. *Nanoscale Res. Lett.* **2014,** *9*, (1), 101.

53. Haverkamp, R. G.; Marshall, A. T., The mechanism of metal nanoparticle formation in plants: limits on accumulation. *J. Nanopart. Res.* **2008,** *11*, (6), 1453-1463.

Chapter 5

Conclusions

5.1 Summary

This dissertation highlighted the key differences between how pristine ENMs and their sulfidized counterparts interact with plant tissue and behave in aquatic environments. These significant findings were accomplished by conducting two laboratory-based exposures of Ag^0 and Ag_2S ENMs to a terrestrial plant and an aquatic plant species, and a simulated fresh water mesocosm exposure of CuO, CuS, Ag^0 and Ag_2S ENMs. Comparisons with metal ion exposures were made to determine the novel behaviors of nanoparticulate species of these metals compared to ionic forms of the metals. This research utilized synchrotron based high powered X-ray imaging and speciation techniques conducted at two national laboratories to provide high resolution information on the distribution and speciation of metals in the plant tissues. The findings from these studies provide novel insights into the environmental fate of silver and copper ENMs.

The primary objectives of this dissertation consisted of two parts. Part 1 quantified the differences in silver uptake from three forms of silver (Ag+, Ag^0-NPs, and Ag_2S-NPs) in hydroponically-grown alfalfa (*Medicago sativa*) and the duckweed species *Landoltia punctata*, along with a qualitative elucidation and comparison of the mechanisms of uptake of these silver forms. Part 2 determined the relative time scales of transformation for the introduced nanomaterials (Ag^0-NPs, Ag_2S-NPs, CuO-NPs and CuS-NPs) in both the sediment and plant

tissue, characterized the metal uptake and speciation in the aquatic plant *Egeria densa* exposed to each of these nanoparticle species or to ions, and identified the impact of the initial chemical form of ENM dosed on the final metal speciation after nine months.

5.2 Conclusions

The following is a summary of the major conclusions of this research, as they relate to the objectives stated above.

5.2.1 Part 1

The pristine (metallic silver) and transformed (silver sulfide) ENMs distribute and interact differently with plant tissues suggesting there are two mechanisms governing the uptake of silver into plant tissue.

- The silver distribution in the roots of terrestrial and aquatic plants exposed to silver sulfide ENMs were found to be in discrete clusters and not uniformly throughout the root tissue suggesting the more insoluble ENMs primarily adhered onto the root surface and the ENMs were taken up as intact nanoparticles.
- The distribution of silver in the roots from plants exposed to metallic silver ENMs shows both discrete clusters and ubiquitous silver throughout the roots suggesting the silver is likely being taken up through two routes: 1) adsorption of ENMs onto the root surface followed by direct ENM uptake and 2) dissolution of ENM and uptake of soluble silver throughout the root tissue.

- The silver distribution in the roots exposed to ionic silver only show ubiquitous silver throughout the root tissue without discrete clusters indicating the presence of ubiquitous silver throughout the roots is a result of the uptake of dissolved silver.

The attachment and uptake of ENM is not governed only by available metal ions suggesting the less soluble and less reactive sulfidized ENM are as bioavailable as their pristine counterparts.

- Total metals associated with the plant tissue exposed to the pristine and transformed (sulfidized) ENMs showed comparable silver and copper concentrations. Although the distribution of metals was shown to be different, the overall amount of metal associated with the plant tissue was found to be similar; indicating the attachment of these ENM is governed by the ENM properties such as the surface coating, surface charge and size rather than the solubility of the ENM. Factors that influence attachment of the NPs to roots may have more influence on uptake by plants than solubility of the NPs.
- Direct evidence of nanomaterials was observed in the alfalfa root cells exposed to Ag^0 and Ag_2S indicating both types of ENM are bioavailable to the plants and become incorporated into the root cell walls. Although other studies have shown comparable particles in plant cells, the possibility of biosynthesized particles from dissolved silver casts uncertainty on their findings. This research has shown direct evidence that the less soluble ENMs are found in similar regions of the plant cells as their pristine counterparts strongly suggesting that both are being taken up directly as intact ENMs.

The speciation of silver associated with the duckweed tissue depended on the type of silver dosed and there was more metallic silver associated with the plants exposed to $AgNO_3$ than the metallic Ag^0 ENM.

- The silver from the $AgNO_3$ exposed duckweed transformed into metallic silver, likely through an in-vivo bio-reduction process observed in many different plant species exposed to ionic silver. Surprisingly, the silver from the Ag^0 ENM exposed duckweed was found to be a mixture of Ag_2S, Ag^0 and Ag bound thiols. This may be a result of a common plant response to heavy metals and a slower release of Ag+ ions associated with the ENM treatment compared to the $AgNO_3$.
- The silver from the Ag_2S ENM exposed duckweed remained primarily as silver sulfide suggesting very little dissolution occurred and any silver internalized was likely taken up as Ag_2S NPs.

5.2.2 Part 2

Transformations in the surficial sediment of pristine ENMs (CuO and Ag^0) are rapid, on the order of days to weeks. Transformations of sulfidized ENMs are slower than pristine ENMs, on the order of weeks to months.

- No CuO characteristic was found in the sediment one month after dosing and only a small fraction (4%) of the initial Ag^0 remained as metallic at the one month sampling indicating these pristine ENMs are very labile in the sediment.
- The majority (>70%) of the Ag_2S ENMs remained as silver sulfide through the nine month exposure while the CuS ENM was completely transformed after three months.

Silver sulfide is less labile than CuS suggesting that the availability of nanoparticulate metal sulfides will be strongly dependent on the cation metal.

Transformations of ENMs in plant tissues are much slower than in surficial sediments indicating uptake of ENMs by plants may create a more persistent and long-term contamination risk than previously assumed.

- The presence of CuO speciation was found in the plant tissues of the mesocosm up to six months after dosing, indicating particles which associate with plant tissues are significantly more persistent than if they were to settle onto surficial sediment.
- Although all silver species rapidly transform into silver sulfide, the presence of metallic silver in the Egeria exposed to Ag^0 ENMs throughout the study indicate the plants are preserving Ag^0.
- Silver sulfide ENMs primarily remain as silver sulfide in the plant tissue with minor transformations into thiolated silver species.

Although the speciation of copper and silver is generally converging over time, the initial form of the ENMs dosed was found to affect the speciation of silver and copper in the sediment and plant tissue and the health of the mesocosm throughout the nine month study.

- Differences in the speciation of copper and silver was observed in both the sediment and plant tissue nine months after exposure for the pristine and sulfidized ENMs. In the surficial sediment, there were more copper sulfides and silver sulfides associated with the 9 month exposure to sulfidized ENMs compared to the pristine ones.

- The copper speciation in the sediment and plant tissues were found to be fairly labile and generally converging, suggesting the copper is entering the biogeochemical cycling process and will eventually converge to a similar speciation.
- There are differences in the speciation of silver in the plants and sediment samples after nine months: 1) the plants exposed to Ag^0 ENM still show metallic silver and 2) the sediment exposed to Ag_2S ENMs have more Ag_2S than the Ag^0 exposed. The difference in silver speciation in the sediment and plant tissues indicates silver is partially labile. However, seasonal cycling was not observed suggesting the sulfidation of silver is less reversible than copper sulfidation.
- High turbidity and increased plant mortality were observed for the pristine and ionic treatments throughout the 9 months suggest the water quality and health of the Egeria plants were less impacted by the sulfidized ENMs.

The most significant findings of this research are contained in the several original contributions included in this dissertation. The most important finding is that, although Ag^0 and Ag_2S ENMs have dramatically different chemical properties, the total amount of Ag uptake of silver into plants is similar and likely employs two different uptake pathways (direct NP uptake and absorption of solubilized NPs). The association of these ENMs with plants was not governed only by soluble silver for hydroponic exposures. The uptake may have been driven by the properties which were similar between the particles such as surface coating, charge or particle size. This study has also shown that although the initial speciation of the ENMs does affects the fate of silver and copper in natural freshwater environments, the association of these metals with plant tissue slows their transformation and may result in a longer persistence.

5.3 Future Research Needs

Although this research has provided important understanding concerning the fate of pristine and transformed ENMs in plants and fresh water ecosystems there remain several gaps in knowledge requiring future research to fully understand and accurately model the fate of ENMs in the environment.

The higher-than-expected persistence of ENMs in plant tissues, as identified by this study, increases the importance of further research on the mechanisms by which these ENMs are being passed onto other organisms, and potentially entering the food web, through trophic transfer. Such research should be designed to improve understanding of the transfer of these ENM internalized by plants into other organisms which feed on them. The long-term persistence of ENMs in plant tissue suggests these ENMs will be able to be transferred throughout the food web. Trophic level experiments should be conducted to test the hypothesis that these ENMS will transfer between organism and provide a better understanding of risks imposed by these ENMs on the environment and the food webs.

This research has shown the association of copper and silver from ENMs with plant tissues does not appear to be governed by the solubility of the ENMs. With these results suggesting the attachment of ENMs onto plant tissues is likely governed by surface charge, coating and particle size, additional studies should be conducted to test this hypothesis. The attachment and distribution of ENMs with different sizes and coating should be investigated using XRF mapping, nano-computed tomography and TEMs imaging to determine what is governing the attachment and uptake of the ENMs.

This research has highlighted the importance of investigating the both the pristine, as manufactured, ENMs and potential transformation products which will likely be introduced to the environment. It is evident that speciation must be considered because it can affect the uptake, distribution and fate of ENMs in the environment. Accordingly, the lack of knowledge regarding the increasing number of commercial ENMs which can transform and generate a vast array of products is troubling. The transformed ENMs have been shown to be less toxic due to increased stability leading to longer persistence in the environment. Assuming the initial speciation will affect the toxicity, fate and transport of ENMs in the environment; future studies should investigate all relevant transformed species to sufficiently understanding of how these materials behave in the environment. Many previously conducted studies involving toxicity, mobility, transformations and fate of ENMs should be reinvestigated with focus on the most relevant transformation products.

Although many studies have investigated how ENMs behave in laboratory systems, the understanding of how ENMs behave in complex environments remains limited. A large amount of research has investigated the uptake of ENMs into plants through hydroponic exposures, which are expected to overestimate the toxicity and bioavailability compared with soil-based or complex mesocosm-scale exposures. Further studies utilizing environmentally relevant soil media should be conducted to determine how ENMs behave in relevant agricultural scenario.

Further mesocosm-level experiments with more frequent sampling intervals, especially during the first weeks and months, are needed to produce accurate transformation rates in both sediments and surficial sediments which will ultimately be utilized in ENM fate models. Additionally, the transition between the anoxic and aerobic zones of the surficial sediments

should be further investigated to better understand how the transformations are occurring as a function of sediment depth. Synchrotron-based XRF mapping and speciation techniques should be utilized on frozen sediment cores to produce speciation profiles and better characterize the transformations in the surficial sediment layer.

Investigations concerning the long term environmental persistence of other ENMs, including more labile (ZnO) and more inert (CeO_2, AlO_3, TiO_2 and SiO_2) ENMs using mesocosm scale studies would help our understanding of the risks these ENM pose to the environment. Mesocosm scale studies which can bridge the controlled laboratory exposure studies and the complexities of real environmental exposure are particularly valuable. Many water quality and chemistry parameters (e.g. metal concentration, turbidity, presence of ENMs etc.) should be carefully monitored to more fully understand the complex environment in mesocosm experiments. Many types of mesocosms should be explored (flowing rivers, coastal estuaries, oceans etc.) to better characterize how ENMs will behave in the different environments they will likely encounter. Additional studies in realistic mesocosm and soil-based exposure of ENMs to plant should be conducted to test the hypothesis that, although hydroponic and laboratory experiments can provide valuable insight into the interactions between ENMs and plants, realistic exposure scenario are needed to accurately model the complexities of natural systems.

Chapter 6

Appendices

6.1 Appendix A. Supporting Information for Chapter 2

Figure A.1 : Photograph of the alfalfa plants in their holders. Notice the increased mortality and stunted growth in nano-Ag(0) and $AgNO_3$ compared to other treatments with lower filterable silver concentrations. Hormesis (increased growth) can be observed in the supernatant.

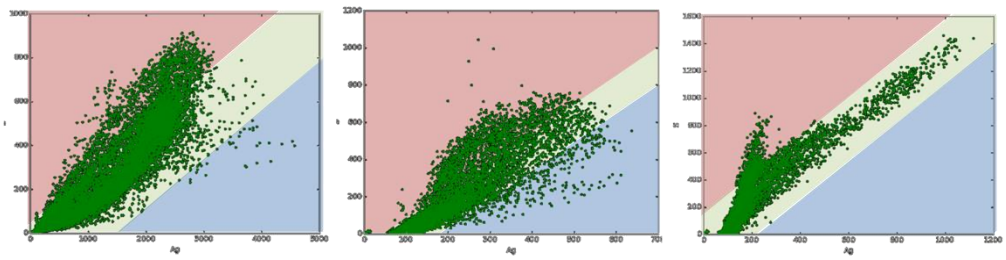

Figure A.2: Silver (X axis) vs Sulfur (Y axis) fluorescence count correlation plots for the samples exposed to $AgNO_3$ (left), nano-Ag(0) (middle) and nano-Ag_2S (right), with populations identified as high (blue) medium (green) and low (red) Ag:S ratio.

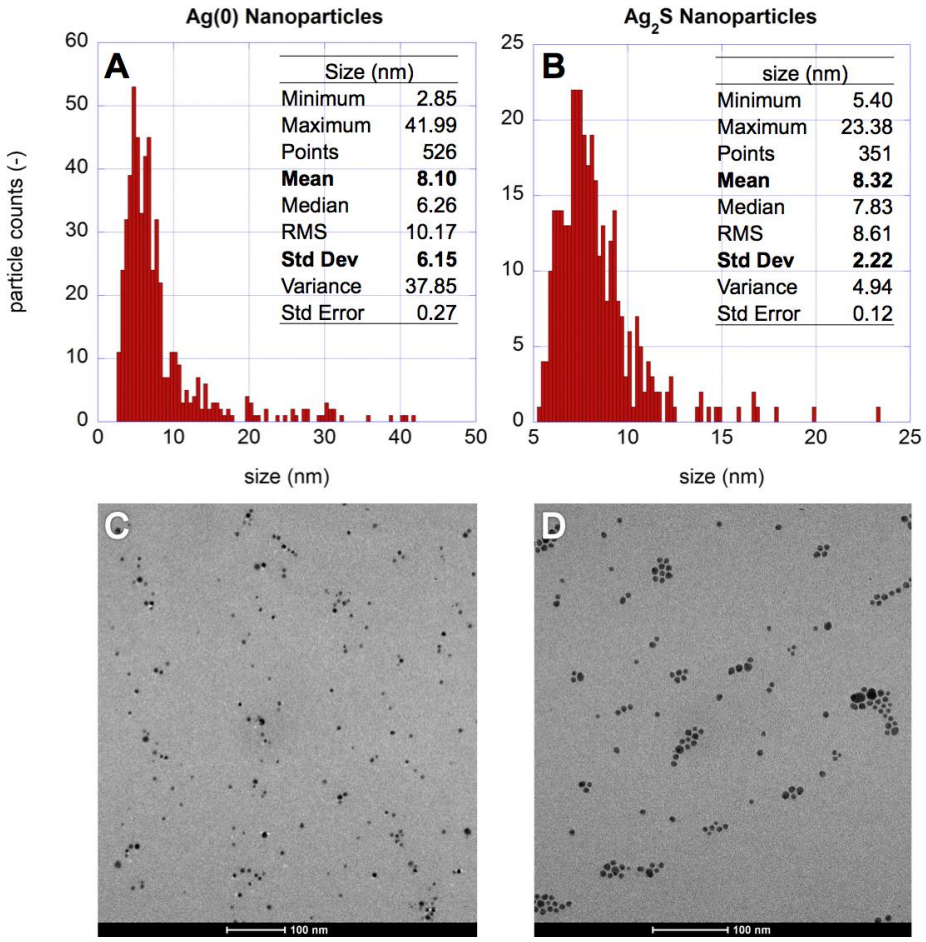

Figure A.3: Diameter size distribution of freshly synthesized nano-Ag(0), A; and nano-Ag_2S nanoparticles, B. The diameter of the particles was determined by quantitative image analysis (software: ImageJ 1.0) of transmission electron micrographs as shown in C, nano-Ag(0); and D, nano-Ag_2S. The particles analyzed here were taken from a suspension in half strength Hoagland's medium.

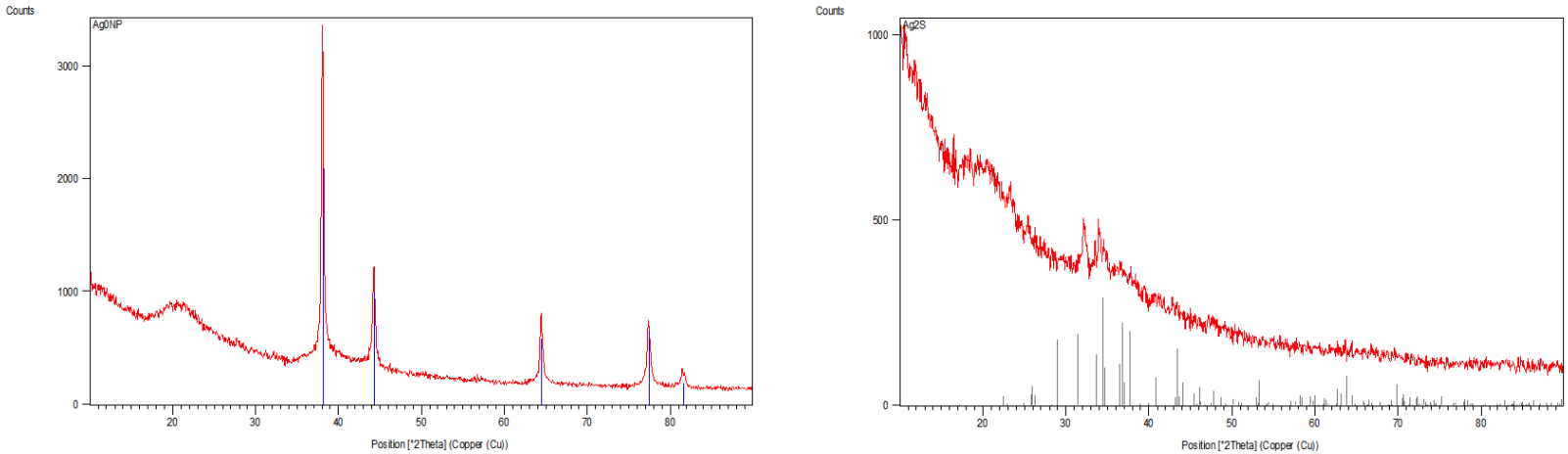

Figure A.4 :Nano-Ag(0) (left) and nano-Ag_2S (right) X-ray powder diffraction spectra after drying at 50C with fitted to the reference spectra of metallic silver and acanthite (Ag_2S) .

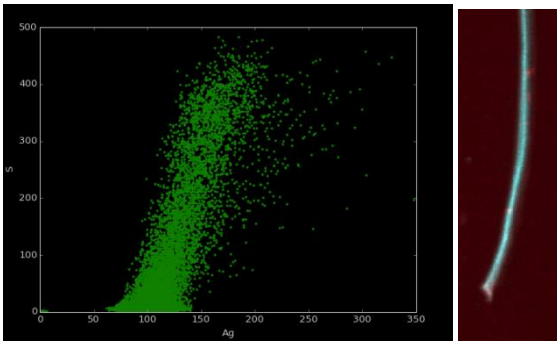

Figure A.5: Control alfalfa root tip with Ag/S correlation plot with bi color, which shows potential auto-correlation. The background silver signal, attributed to the fluorescence of argon, is on the order of 100 counts per sec and remains similar for the plant tissue analyzed, suggesting no silver is present in the tissue of control plants.

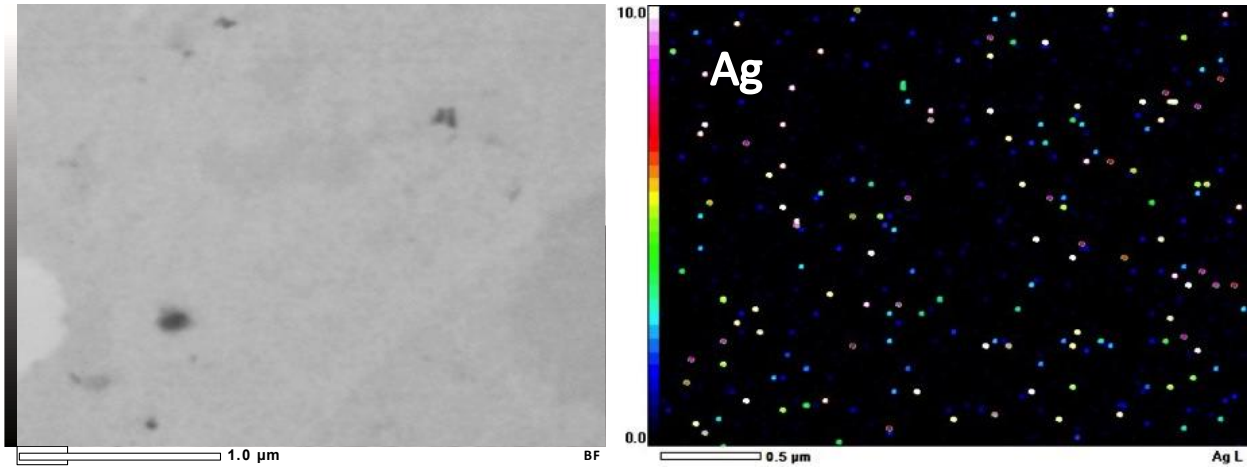

Figure A.6: Map of Ag in the cytoplasm of alfalfa exposed to nano-Ag_2S. Left: Transmission electron microscopy image. Right: Same area mapped by energy dispersive X-ray spectroscopy showing evenly distributed Ag hotspots between 1-10 wt%.

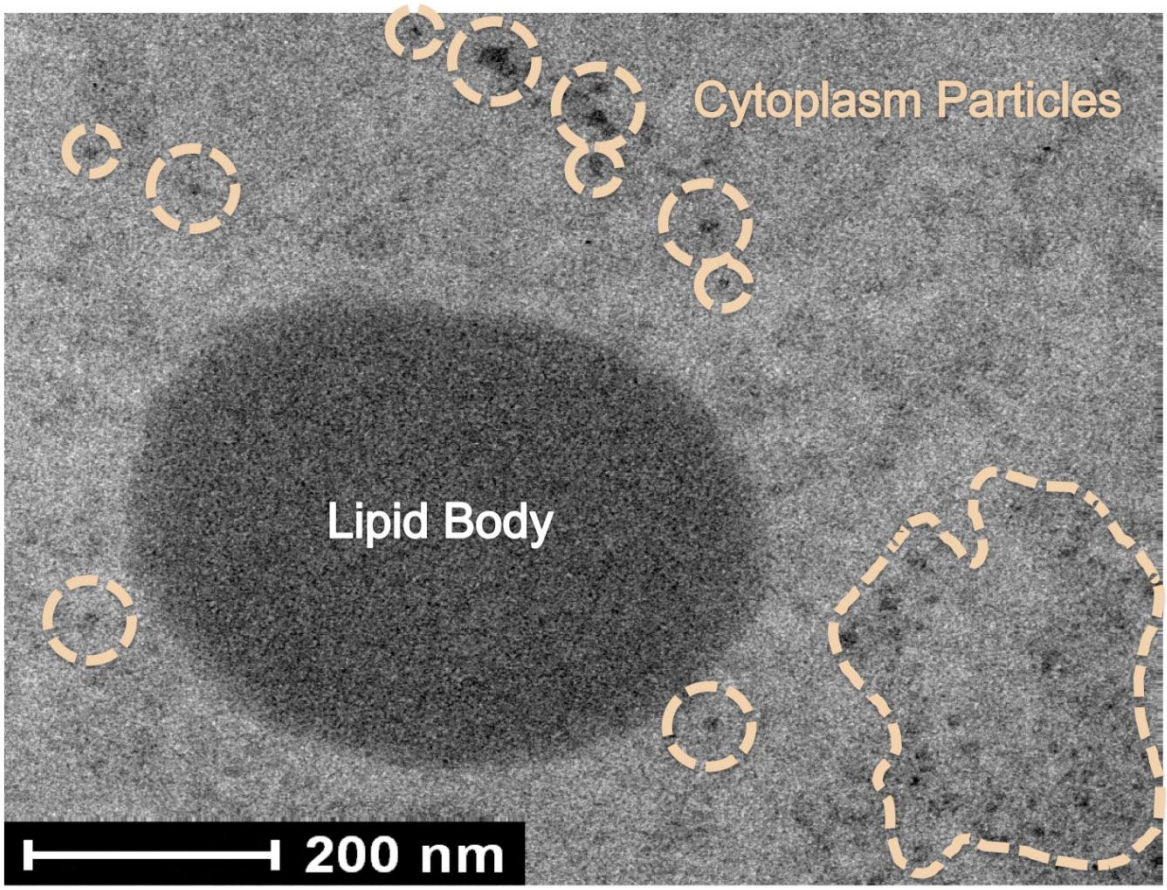

Figure A.7: Transmission electron microscopy micrograph showing a magnified lipid body of a control root cell of Alfalfa (*Medicago sativa*). The spherical electron dense (i.e. dark) region outlines the structure of the lipid body. Note the highly electron dense particles in the cytoplasm (highlighted by peach broken lines, likely Si as observed by energy dispersive X-ray spectroscopy in comparable regions of the cytoplasm).

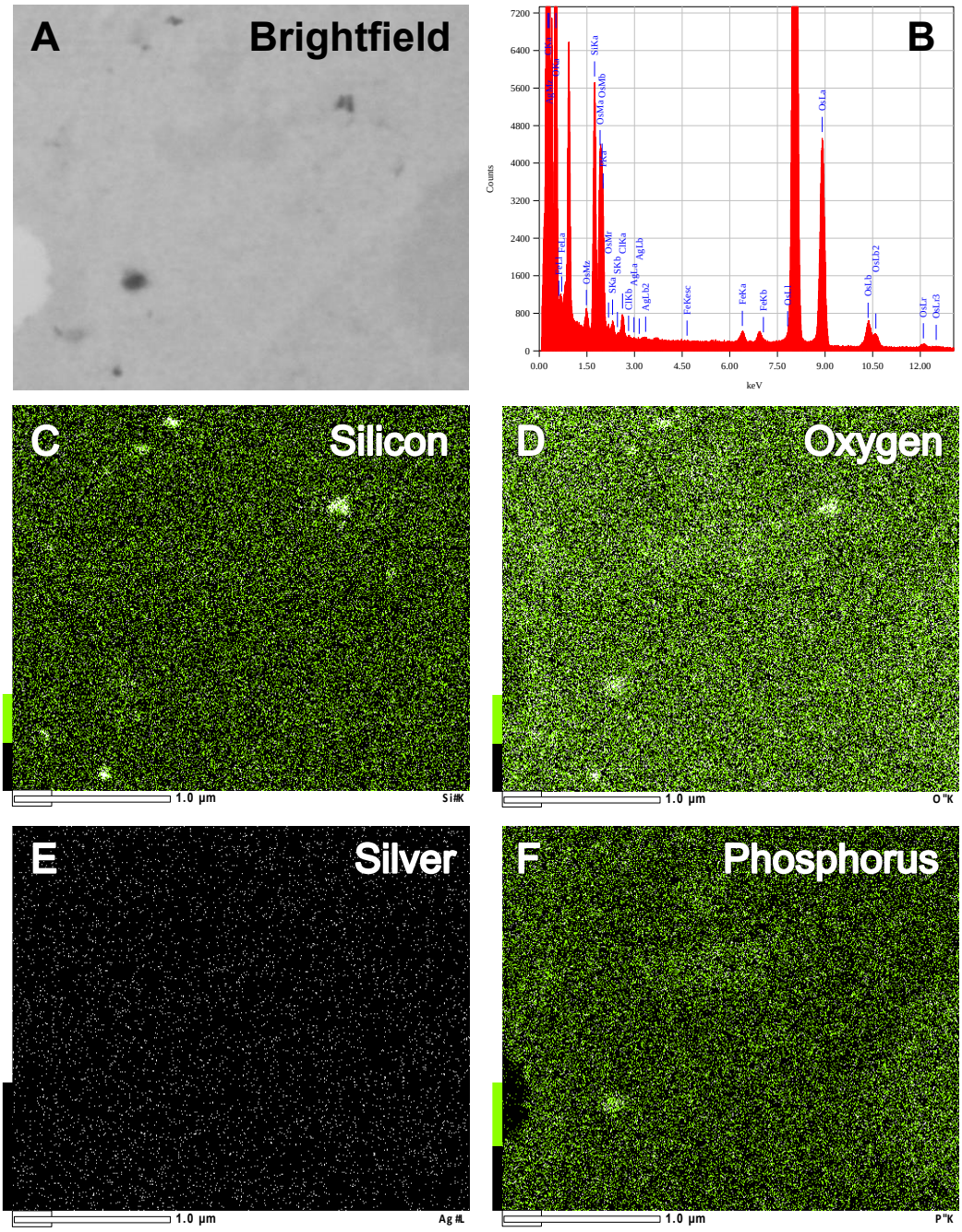

Figure A.8: Transmission electron microscopy (TEM) coupled with energy dispersive X-ray spectroscopy (EDS) of particles in the cytoplasm of alfalfa exposed to nano-Ag_2S nanoparticles. A: Phase contrast image of aggregates in the cytoplasm. The aggregates can be seen in the phase contrast image as dark spots. The line scan shows elevated signals of Si and O. B: The energy spectrum of the same region as in A shows a strong Si peak. C: Mapping shows that Si is concentrated on all but one aggregate in the cytoplasm, whereas no aggregates of Ag are visible. D: Oxygen is concentrated, too, on the nano-sized aggregates, confirming the presence of Si in the form of nano-Si_yO_X.

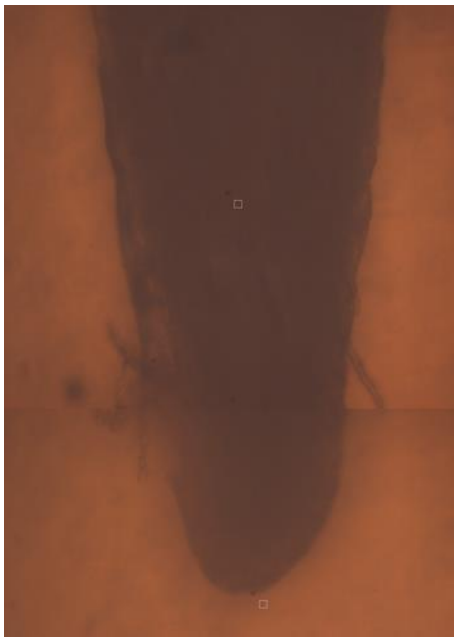

Figure A.9: Light micrograph image of root tip used to generate the outline in figure 2.

40

Table A.1 (continued next page): Size distribution of the particles in suspension as determined by dynamic light scattering (DLS, continuation next page). The particles were suspended in half strength Hoagland's medium. Only the peaks with maximal intensity are shown.

	Filtered[a]	n^b (-)	Size	±	Stdev	Intensity (%)
100 nm size standard[c]	yes	1	96	±	23	100.0
ultrapure water	yes	1	-	±	-	-
Hoagland's medium[d]	yes	1	(727	±	130)	(100.0)
nano-Ag(0)	no	3	11.6	±	4.4	92.0
	yes	3	11.6	±	2.9	93.1
nano-Ag_2S	no	3	(12.8	±	3.7)	(97.9)
	yes	3	16	±	13	100.0

[a]Filtered through a 0.45 µm polytetrafluorethylene (PTFE) filter. [b]Number of replicated measurements. [c]Certified latex standard (Izon, USA) to validate instrument performance. [d]Half strength. [e]Measurements with a polydispersity >0.35 are shown in brackets because highly polydisperse samples, especially if unfiltered, are not accurately measurable using DLS.

41

Table A.1 continuation: Size distribution of the particles in suspension as determined by dynamic light scattering (DLS). The particles were suspended in half strength Hoagland's medium.

	Filtered[a]	n^b (-)	Diffusion Coefficient (μ^2/s)	Count Rate (kcps)	Derived Count Rate[f] (kcps)	PdI (-)
100 nm size standard[c]	yes	1	4.75	415	9,438	0.01
ultrapure water	yes	1	-	-	-	-
Hoagland's medium[d]	yes	1	(0.41)	(167)	(1,506)	(0.52)
nano-Ag(0)	no	3	4.19	248	68,670	0.28
	yes	3	6.52	405	32,117	0.31
nano-Ag_2S	no	3	(1.17)	(473)	(473)	(0.42)
	yes	3	7.10	469	469	0.26

[a]Filtered through a 0.45 µm polytetrafluorethylene (PTFE) filter. [b]Number of replicated measurements. [c]Certified latex standard (Izon, USA) to validate instrument performance. [d]Half strength. [e]Measurements with a polydispersity >0.35 are shown in brackets because highly polydisperse samples, especially if unfiltered, are not accurately measurable using DLS. [f]Note that the derived count rate is a function of the particle type and therefore only proportional to particle concentration for particles of the same kind.

42

Table A.2: Diameters of electron dense particles and aggregates measured by transmission electron microscopy in different cell compartments of the root tip. Underlined values were significantly different from the same particle type in the control (One-way analysis with unequal variances, Levene statistics $p<0.001$, Dunnett's C post-hoc analysis at a 95% significance level). Italicized values are particles that were exclusively present in exposed plant cells.

Treatment	Particle Morphology	*N*	Diameter (nm)				
			Average	Median	Stdev	Min	Max
Control	Cytoplasm Particles	52	7.9	7.1	3.1	2.9	15.3
	Vacuole Aggregates	45	61	39	53	10	243
AgNO3	Cytoplasm Particles	66	7.9	8.0	3.9	1.5	17.9
	Cytoplasm Aggregates	49	*33*	29	18	12	90
	Cytoplasm + Vacuole Round Particles	41	*102*	77	61	32	278
nano-Ag(0)	Border Cell Adsorbed Particles	62	*74*	72	17	33	133
	Cell Wall Particles	46	*2.52*	2.43	0.83	1.25	4.78
	Cytoplasm Particles	63	9.9	9.2	4.9	1.0	30.1
	Cytoplasm Aggregates	8	*55*	51	17	32	86
	Vacuole Aggregates	26	74	54	48	22	209
nano-Ag_2S	Border Cell Adsorbed Particles	68	84	76	34	32	205
	Cell Wall Particles	81	*2.54*	2.55	0.77	0.93	4.94
	Cytoplasm Particles	38	17.2	14.7	7.8	6.6	36.9
	Cytoplasm Aggregates	17	*96*	112	35	49	164
	Vacuole Aggregates	44	230	187	189	17	794

Table A.3: Maximum x-ray count attributed to Ag for K-edge XRF map (Figure 2) and attributed to Ag and S the L-edge Ag XRF map (Figure 3).

	Fig 2 Ag Counts	Fig 3 Ag counts	Fig 3 S counts
Ag(0)	1837	637	1042
Ag_2S	3406	1117	1459
$AgNO_3$	N/A	4571	914

6.2 Appendix B. Supporting Information for Chapter 3

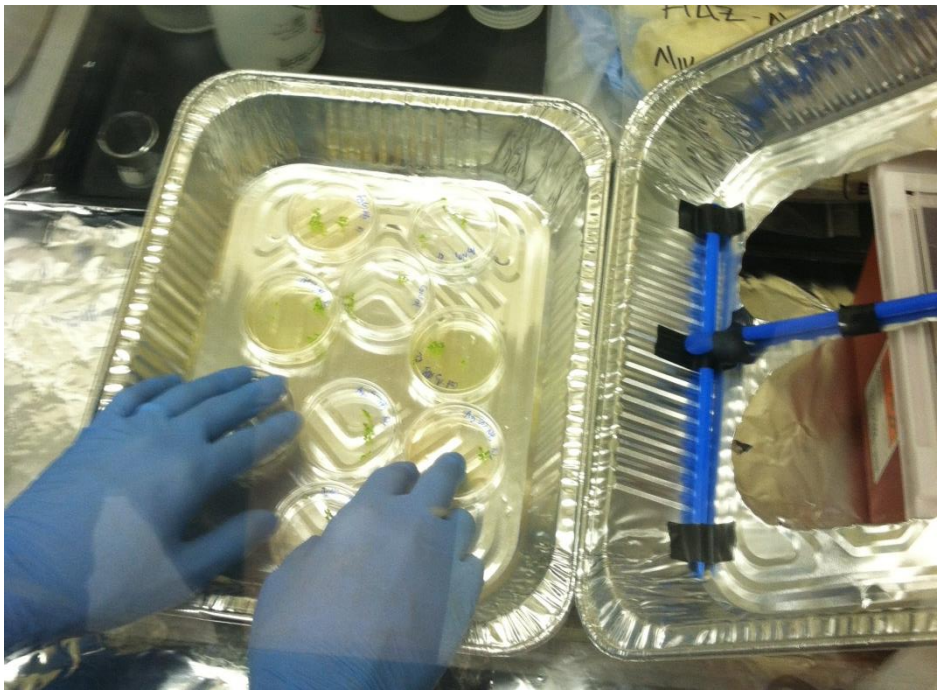

Figure B.1. Duckweed cultures being exposed to NP suspensions in an aluminum tray inside a standard fume hood. Holes in the cover pan on the right are for cool fluorescent lights (not shown). The blue tubes are disposable spatula inserted as structural supports.

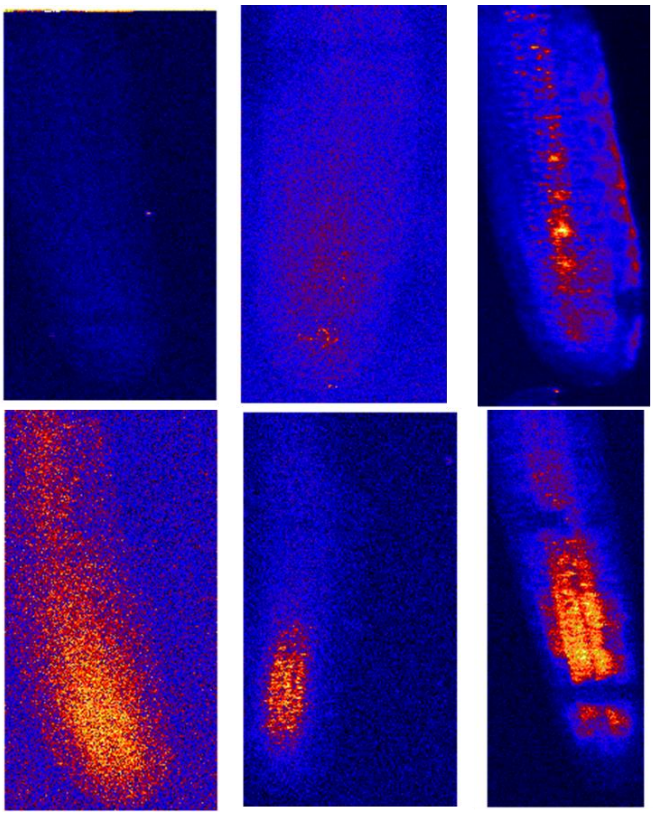

Figure B.2. Zinc specific XRF maps of 24h (top) and 60h (bottom) duckweed roots exposed to $AgNO_3$ (left), Ag^0-NPs (middle) and Ag_2S NPs (right). Please note the scale was internally calibrated.

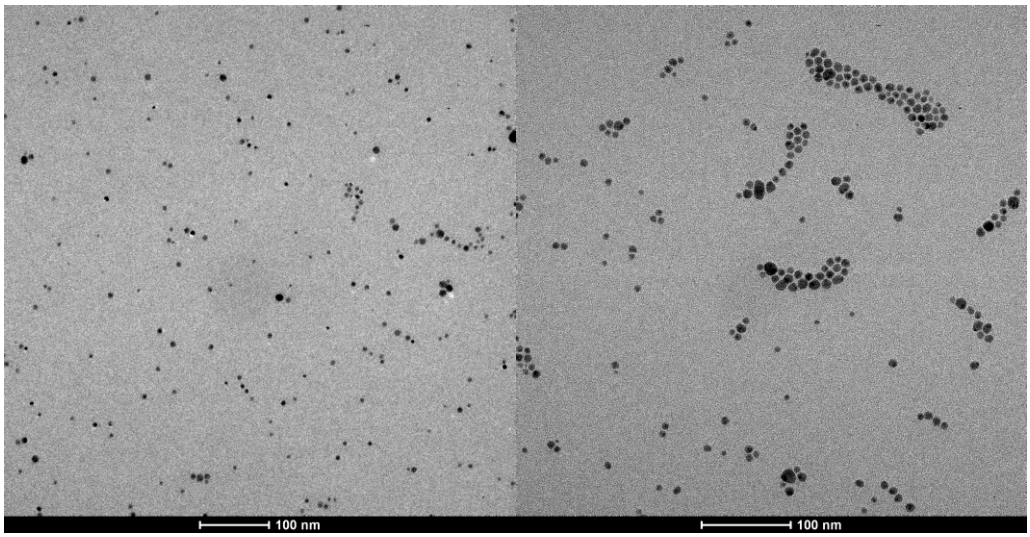

Figure B.3: Transmission electron microscopy (TEM) images of the first batch of the silver nanoparticles (Ag^0-NPs) under investigation. Left: polyvinylpyrrolidone coated Ag^0-NPs. Right: Sulfidized Ag_2S-NPs.

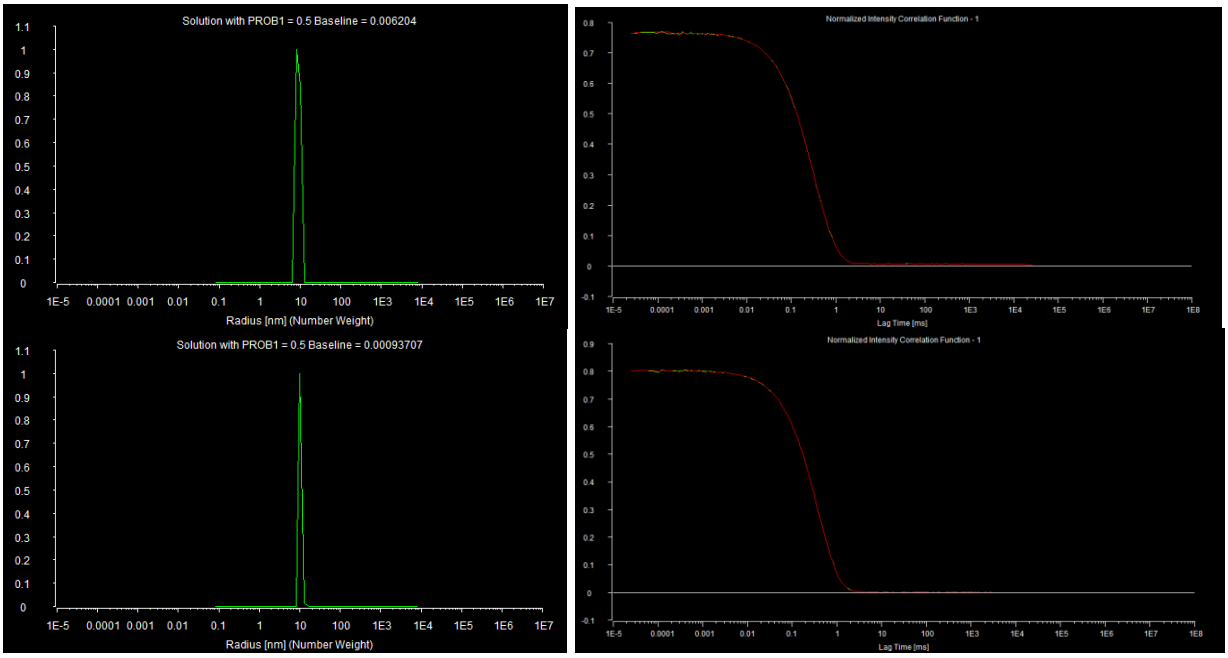

Figure B.4. Number-weighted size distributions and autocorrelation functions for the Ag_2S NPs in ½ strength hutners media after 0h (top) and 48 hours (bottom).

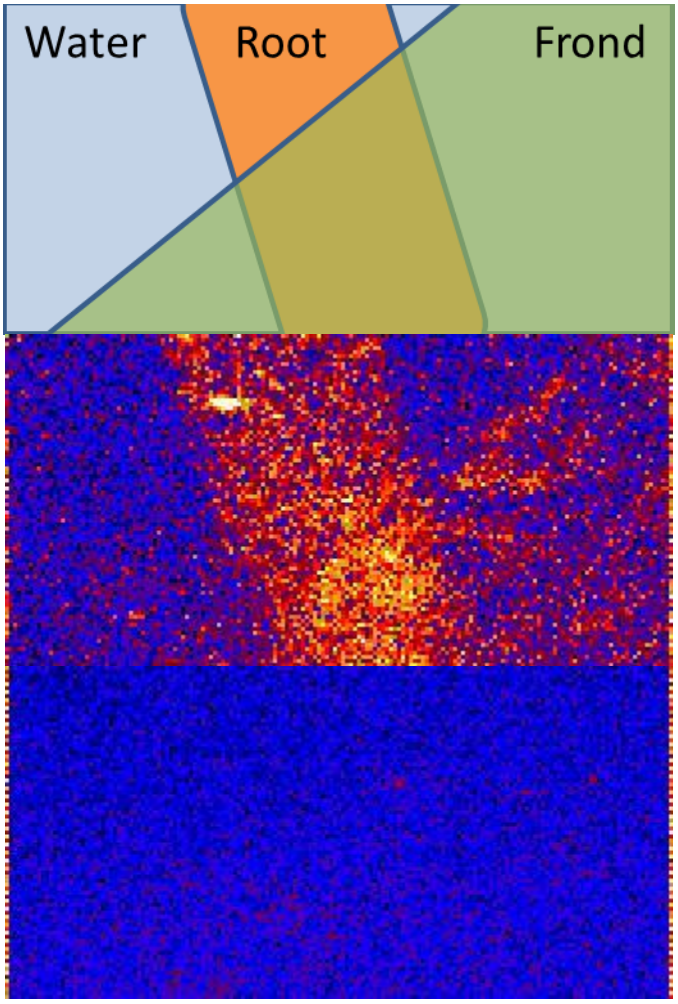

Figure B.5. A cartoon of the region of interest in the Ag2S exposed duckweed sample (top), the Zn specific map for comparison and orientation (middle) and the silver specific map (bottom) showing very little silver on the frond or in the upper root.

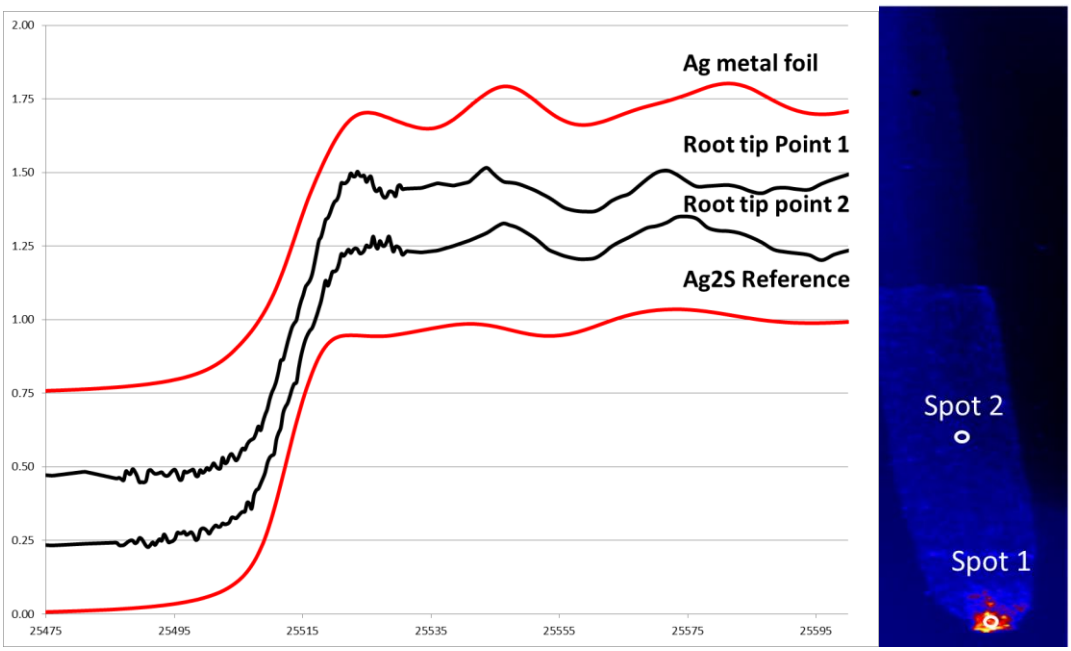

Figure B.6. Micro-XANES mapping of two spots on the Ag_2S-NPs exposed root sample. Spectra generally confirm the presence of Ag_2S, but there is also some evidence of Ag^0 on root tip spot 1 as noted by the elevated signal at ~25,545 eV. Note that the possibility of photo-reduction by the beam cannot be completely ruled out for this map (taken at room temperature).

Table B.1. Model Compounds used for XAS analysis

Ag^0	Ag_2CO_3	AgBr
Ag_2S	Ag-Acetate	AgCl
Ag-Cysteine	$AgPO_4$	AgI
AgO	Ag_2O	

Table B.2. Maximum fluorescence count associated with Ag (min and **max** count used for scaling)

	$AgNO_3$	Ag^0	Ag_2S
24 hours	**5906**	**9256**	**19646**
	116	2228	1475
60 hours	**8897**	**3246**	**714**
	74	39	83

Note that the maximum counts is more affected by the distribution of Ag in the plants rather than the total mass of Ag taken up. For example, the presence of clusters of Ag_2S nanoparticles leads to a larger maximum count than either $AgNO_3$ or Ag^0-NPs even though there is more total silver in the $AgNO_3$.

6.3 Appendix C. Supporting Information for Chapter 4

Figure C.1. Image of surficial sampling device using a modifidied falcon tube and two tubes.

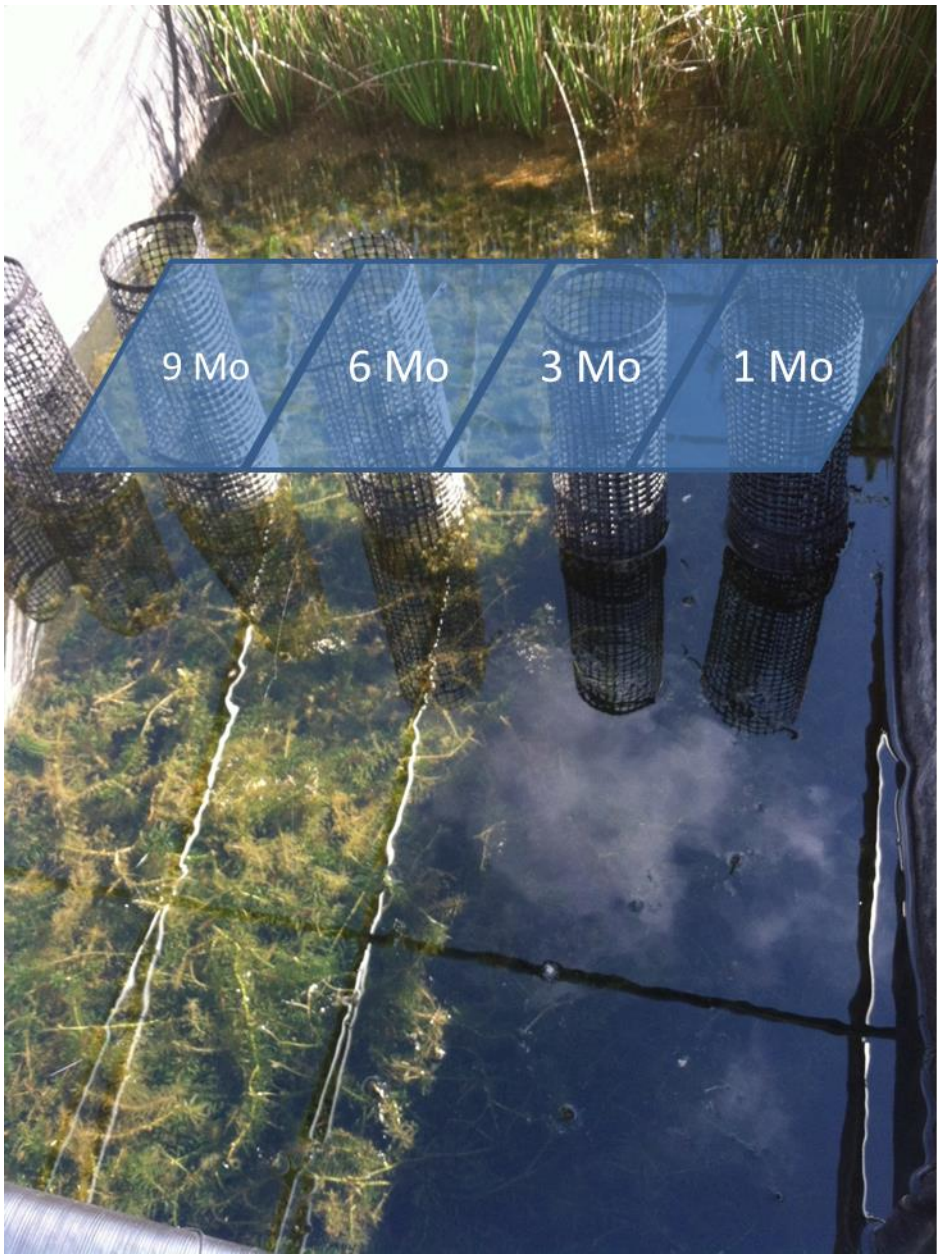

Figure C.2. Depiction of sampling locations of surficial sediment

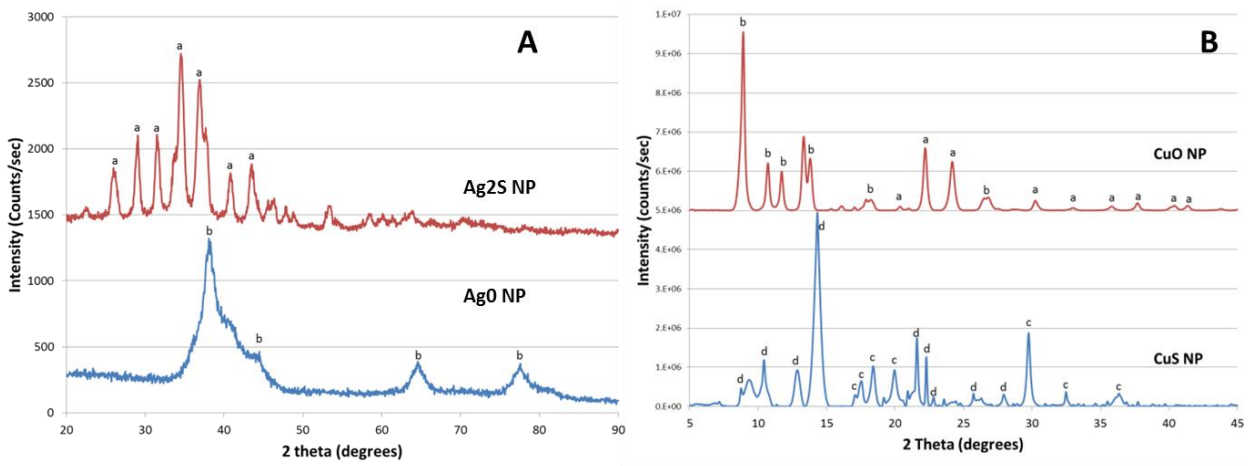

Figure C.3.A) XRD spectra of Ag2S NPs and Ag^0 NPs. Collected using a Cu-anode with indicators for peaks matching (a): acanthite (Ag_2S) and (b): metallic silver (Ag^0) . B) XRD spectra of CuO and CuS NPs collected at SSRL's 11-3 and indicators for peaks matching to (a): tenorite (CuO), (b): copper carbonate hydroxide ($CuCO_3OH$), (c): Covellite (CuS) and (d): Brochantite ($Cu_4SO_4(OH)_6$)

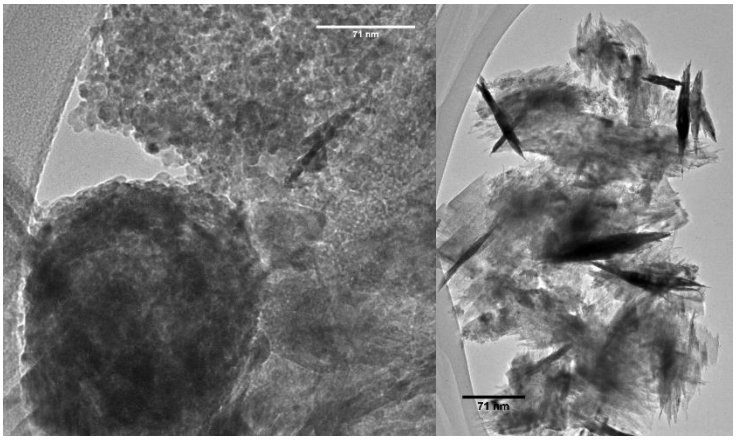

Figure C.4. Additional TEM images showing spherical and rod-like particle morphologies found in the CuS particles.

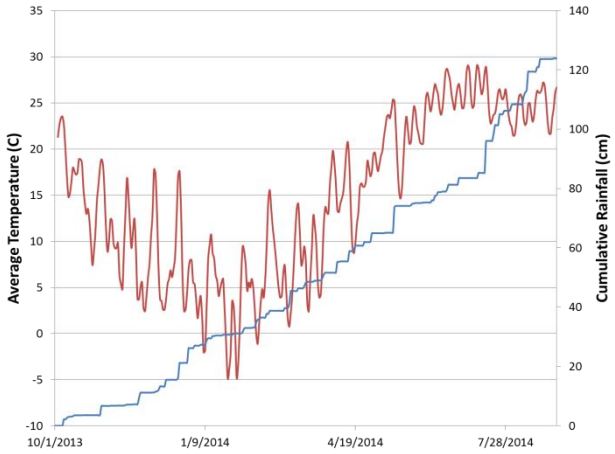

Figure C.5. Historical weather data for Durham, NC obtained from weather underground, showing 3 day floating average temperature in C (red) and cumulative rainfall in cm (blue).

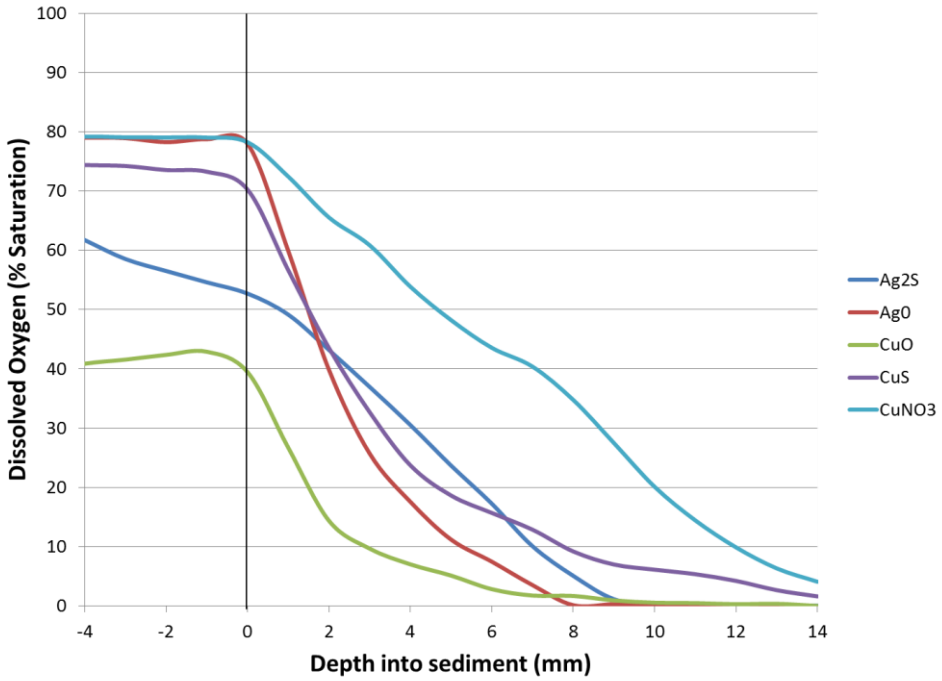

Figure C.6. Oxygen profiles measured on sediment cores collected during the 3 month sample event using a microprobe within 1 hour of sampling.

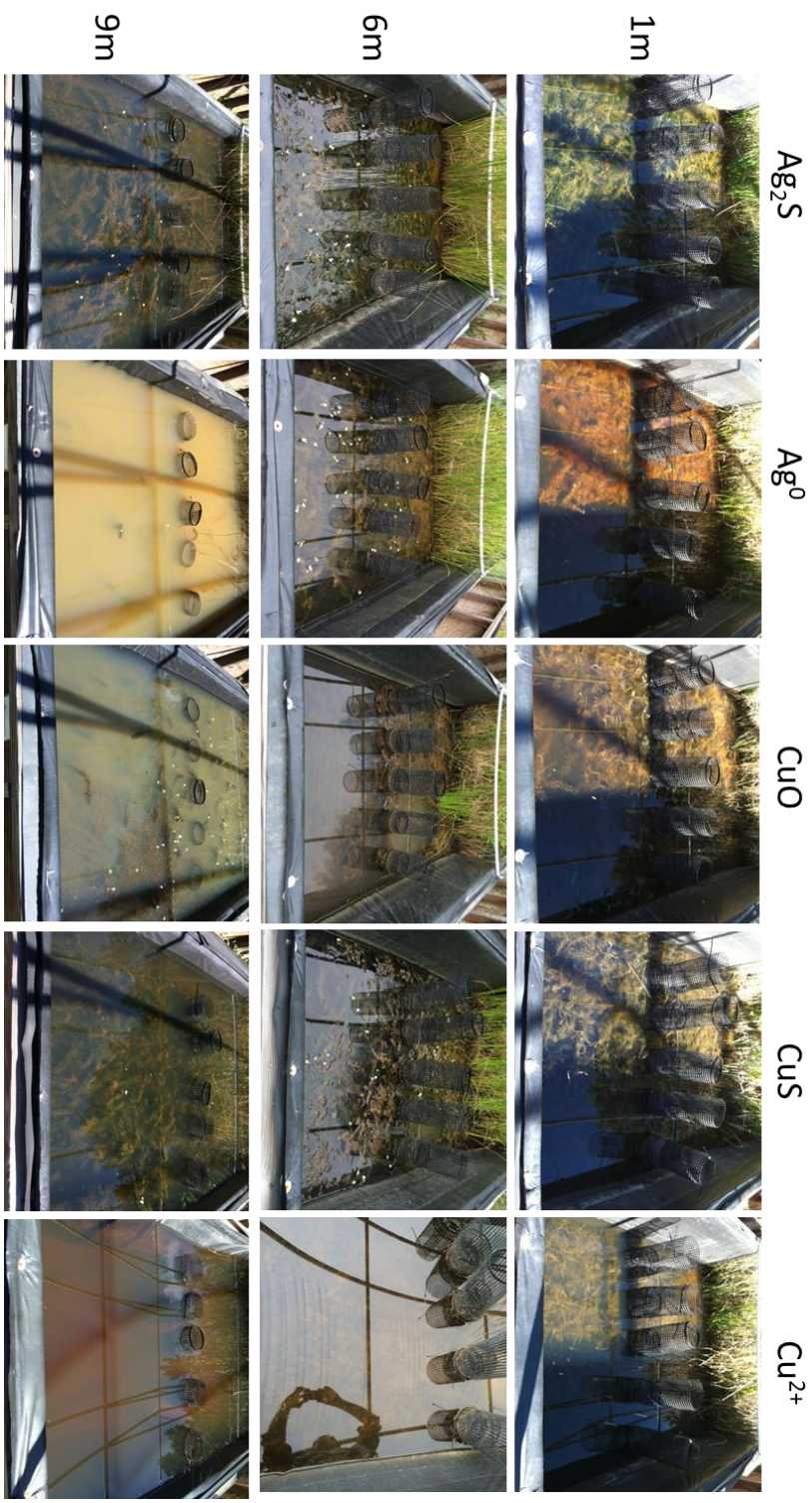

Figure C.7. Images of mesocosm boxes taken at the 1 month, 6 month and 9 month sampling events. Notice the deterioration of the *Egeria* in the $CuNO_3$, CuO and Ag^0 boxes as well as the lack of plants in the 9 month exposed to $CuNO_3$.

Table C.1. Summary of model compounds used for XANES fitting along with the simplified bonding environment used for explaination of fits.

Silver Reference	Simplified	Copper Reference	Simplified	Copper Reference	Simplified
Ag^0 NP	Ag^0	Cu^0	Cu^0	$CuNO_3$	$CuNO_3$
Ag_2S NP	Ag_2S	CuS NP	Cu-S	$Cu_3(PO_4)_2$	$Cu_3(PO_4)_2$
Ag-Cysteine	Ag-Thiol	Covelite	Cu-S	$CuSO_4$	$CuSO_4$
AgO	AgO	Chalcosite	Cu-S	$CuCO_3(OH)$	$CuCO_3(OH)$
Ag_2CO_3	Ag_2CO_3	Cu-Cysteine	Cu-S-R	Azurite	CuCO3(OH)
Ag-Acetate	Ag-Acetate	Cu-Glutathione	Cu-S-R	Malachite	CuCO3(OH)
$AgPO_4$	$AgPO_4$	CuO NP	Cu-O	CuCl	CuCl
Ag_2O	Ag_2O	Cu-Humic Acid	Cu-O-R	Chalcopyrite	Cu-O-Fe
AgBr	AgBr	Cu-Histidine	Cu-O-R	Cu_2O	Cu_2O
AgCl	AgCl	Cu-FeOOH	Cu-O-R		
AgI	AgI				

Table C.2. DLS characterization of Ag0 and Ag2S NPs in DI water.

Conc for ZP, Mob, Cond, pH	200 ppm	200 ppm
avg Z-ave diameter (nm)	104.07	71.54
Z-ave std dev	2.69	0.84
avg PdI	0.334	0.252
PdI std dev	0.055	0.009
avg Int-weighted dia (nm)	160.37	93.79
Int-weighted std dev	4.50	1.94
avg Vol-weighted diameter (nm)	54.97	51.21
Vol-weighted std dev	8.11	1.81
avg Num-weighted diameter (nm)	24.89	34.28
Num-weighted std dev	1.37	1.77

Table C.3. Table of DLS and Zeta potential characterization in filtered mesocosm porewater reproduced from Moore et. al. (Moore, Stegemeier et al. 2016).

Table 1. Nanomaterial Suspension in Filtered Mesocosm Porewater Characterization and DLS and Zeta Potential (ZP) Characterization[a]

ENM	pH	specific conductance (μS/cm)	estimated I (mM)	primary particle diameter (nm)	hydrodynamic diameter (nm)	zeta potential (mV)
Ag^0	7.3	114 ± 1.4	1.6	4.67 ± 1.4	113 ± 9.4	−22.2 ± 1.5
Ag_2S	7.2	101 ± 0.82	1.4	18.1 ± 3.2	61.5 ± 0.37	−25.8 ± 2.5
CuO	7.0	70.8 ± 0.16	1.0	31.1 ± 12	236 ± 11	−25.2 ± 1.4
CuS	7.1	74.8 ± 0.21	1.1	12.4 ± 4.1	185 ± 11	−21.6 ± 0.70

[a]Values are expressed as mean ± one standard deviation (SD). Ionic strength (I) is estimated from specific conductance according to the approach described by Marion & Babcock for mixed salt solutions.[54] ZP was calculated from measured EPM data using the Smoluchowski equation.

Table C.4. Cu XANES fitting results for Egeria and surficial sediments. Presented with the R-factor (goodness-of-fit) parameter for fits from -25 to +100 ev of the edge.

Egeria								
CuO NP	Covelite	Chalcosite	Cu-GSH	Cu-Cyst	Cu-Humic	Cu-Hist	CuO-NP	R factor
1 month	22%				35%		42%	7.41E-05
3 month				31%	33%		35%	4.20E-05
6 month	19%			3%	35%		42%	7.38E-05
9 month		19%	30%		51%			7.12E-05
CuS NP								
1 month		19%	35%		47%			9.11E-05
3 month		48%	35%		17%			7.89E-05
6 month	35%		12%		52%			3.15E-05
9 month	28%				38%	32%		2.64E-05
CuNO3								
1 month				14%	19%	68%		2.63E-05
3 month				18%	30%	53%		2.70E-05
6 month				9%	39%	52%		2.85E-05

Sediments							
CuO NP	Chalcosite	CuS		Cu-Humic	Cu-Histidine	Cu-Metal	R factor
1 month	39%			13%	33%	15%	4.91E-05
3 month				57%	43%		8.91E-05
6 month	41%			22%	24%	13%	3.25E-05
9 month	17%	31%			52%		0.000308
CuS NP	Chalcosite	CuS	Covelite	Cu-Humic	Cu-Histidine		
1 month			74%		24%		1.98E-05
3 month				35%	65%		4.29E-05
6 month	14%		60%		24%		2.25E-05
9 month	6%			94%			6.15E-05
CuNO3	Chalcosite	CuS	Covelite	Cu-Cyst	Cu-Humic	Cu-Histidine	Cu-FeOOH	
1 month	13%			12%	61%	14%		2.83E-05
3 month					71%	30%		3.76E-05
6 month	13%			11%	58%	17%		2.82E-05
9 month	6%				85%		10%	4.30E-05